Role of nitrite and endothelium-derived vasodilators in blood flow

Julie Laterreur

A Thesis

in

The department

of

Chemistry and Biochemistry

Presented in Partial Fulfillment of the Requirements
for the Degree of Master of Science (Chemistry) at
Concordia University
Montreal, Quebec, Canada

March 2007

Your file Votre référence
ISBN: 978-0-494-28879-5
Our file Notre référence
ISBN: 978-0-494-28879-5

Abstract

The role of nitrite and endothelium-derived vasodilators in blood flow

Julie Laterreur

It has been shown that infusion of nitrite into humans results in vasodilation. The goal of this study was to investigate the mechanism of nitrite-induced vasodilation, which may be due to NO production on nitrite reduction by deoxyhemoglobin (deoxyHb). We found that nitrosylhemoglobin (nitrosylHb) and methemoglobin (metHb) are formed in anaerobic deoxyHb/nitrite incubates and S-nitrosohemoglobin is produced on aeration. The efficiency of NO transfer from the heme to Cysβ93 of hemoglobin varies with the initial deoxyHb/nitrite ratio and with the amount of metHb present. Higher S-nitrosohemoglobin (HbSNO) yields were observed at close to the physiological nitrite to heme ratio and the yield decreased with increasing metHb. Also, hydrogen peroxide depressed the HbSNO yield whereas antioxidant enzymes promoted NO transfer from the heme to Cysβ93. These results indicate that NO transfer requires that Hb undergo its T→R allosteric transition, that oxygen be present presumably as an oxidant and HbSNO formation is inhibited by metHb.

Sequential extraction, HPLC/fluorescence and HPLC/MS/MS methods were developed to detect nitrite, adenosine and epoxyeicosatrienoic acids (EETs) in human interstitial fluid with high sensitivity, precision and accuracy. These methods were used to determine the interactions and compensatory responses amongst these endothelium-derived vasodilators. Nitrite and adenosine were found to increase with exercise level but EETs were below the level of detection (10 nM). Blockade of nitric oxide and prostaglandin formation resulted in diminished nitrite levels but the adenosine levels remain unchanged.

Acknowledgements

I would like to thank my supervisor, Dr. Ann M. English, for giving me the opportunity to work in her laboratory and on these interesting projects. Also, I would like to thank her for her guidance and support during my Masters degree.

Also, I would like to thank Dr. Robert Boushel for providing me with the interstitial fluid samples and for the opportunity to work on a very interesting project. I thoroughly enjoyed all our conversations because of his enthusiasm and his millions of ideas. Thanks to Dr. Cameron Skinner, a member of my research committee member, and the Graduate Program Director in the Department of Chemistry and Biochemistry, for his helpful comments and suggestions.

Special thanks to Jean-François Roy, Dr. Michelle Chrétien, and Line Ste- Marie for all their help and stimulating discussions, but most of all for every pleasant and amusing moment. Also, thanks to Ernesto Moran, Dr. Qadir Timerghazin, Meng Wei Ye, Dr. Heng Jiang and Biao Shen, my lab colleagues. Thanks to Dr. Angelo Filosa from AstraZeneca for his time and help in developing the adenosine detection method, and for letting me use his mass spectrometer.

Je voudrais remercier mes parents pour leur constant soutien et leur amour inconditionnel. Merci de m'avoir toujours encouragé dans tous mes projets de vie. Je voudrais aussi dire merci à Jean-Christophe pour tout son amour, sa compréhension, ses encouragements et surtout d'être toujours là pour moi.

Table of contents

List of Figures

List of Scheme

List of Tables

List of Abbreviations

ACN	acetonitrile
AE1	anion exchange Protein 1
AMP	adenosine monophosphate
ATP	adenosine triphosphate
cAMP	cyclic adenosine monophosphate
CD	circular dichroism
cGMP	cyclic guanosine monophosphate
COX	cyclooxygenase
CuZnSOD	Cu,Zn superoxide dismutase
DAN	2,3-diaminonaphthalene
deoxyHb	deoxygenated hemoglobin; $HbFe^{II}$
DHET	dihydroepoxyeicosatrienoic acids
2,3-DPG	2,3-diphosphoglycerate
DTPA	diethylenetriamine pentaacetic acid
EETs	epoxyeicosatrienoic acids
ESI	electrospray ionization
Fe^{II}-heme	ferrous heme
Fe^{IV}-heme	ferryl heme
GSNO	*S*-nitroso-*L*-glutathione
Hb	hemoglobin
HbSNO	*S*-nitrosohemoglobin; $SNOHbFe^{II}O_2$

HPLC	high-performance liquid chromatography
HT	high tension
ICG	indocyanine green
L-NAME	*N*-nitroso-*L*-arginine Methyl Ester
LOD	limit of detection
metHb	oxidized hemoglobin; $HbFe^{III}$
MeOH	methanol
MGCM	2'-O-(*N*-methylanthraniloyl)guanosine 3'-5'cyclic monophosphate salt
MLCK	myosin light chain kinase
MRFA	*L*-methionyl-arginyl-phenylalanyl-alanine acetate
MRM	multiple reaction monitoring
MS	mass spectrometry
NAT	2,3-naphthotriazole
NeOTF	2-(2,3-naphthalimino)ethyltrifluoromethanesulfonate
nitrosylHb	nitrosylated hemoglobin; $HbFe^{II}NO$
nitrosylmetHb	nitrosylated methemoglobin; $HbFe^{III}NO$
NIRS	near-infrared spectroscopy
NO	nitric oxide
NO_2^-	nitrite
NOS	nitric oxide synthase
O_2	oxygen
$O_2^{\cdot-}$	superoxide
oxyHb	oxygenated hemoglobin; $HbFe^{II}O_2$

PGs	prostaglandins
PKA	protein kinase-A
R	relaxed state of hemoglobin
RBC	red blood cell
ROS	reactive oxygen species
RSD	relative standard deviation
RSNO	S-nitrosothiol
SPE	solid phase extraction
SIM	single ion monitoring
T	tense state of hemoglobin
TCA	trichloroacetic acid
TMB	3,3',5,5'-tetramethylbenzidine
TOF	time of flight
W	watts

1.0 General introduction

1.1 Metabolic mechanisms of vasodilation

During exercise there is an increase in the metabolic demand for oxygen (O_2) by muscle tissue that leads to an increase in blood flow (Figure 1.1). This requires an increase in the internal diameter of blood vessels, which occurs on relaxation of smooth muscle by vasodilators from endothelial cells, the red blood cells (RBCs), and substances released by skeletal muscle. The mechanism by which blood flow matchs O_2 delivery to meet the metabolic demand of tissue is not precisely known, especially during exercise. This is of importance in the understanding of cardiovascular diseases where there is impaired O_2 and nutrient supply to tissues.

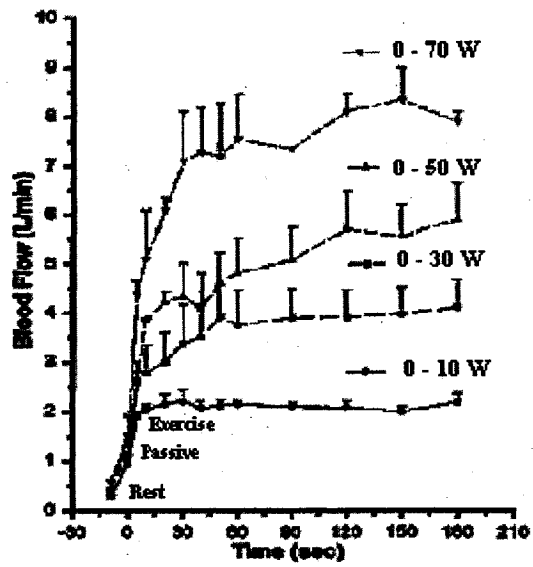

Figure 1.1. Blood flow measured with ultrasound Doppler in the femoral artery. At rest, during passive movement of the knee-extensor muscle group (movement of a joint without participation or effort on the part of the subject), and when exercising at up to 70 W output during knee extension of one leg (1).

In this thesis, different mechanisms that could cause an increase in blood flow are investigated. The results obtained provide some insight into the physiological regulation of blood flow during exercise. The thesis is separated into two parts. In Chapters 2 to 4, the mechanism of nitrite-induced vasodilation in RBCs is probed. In Chapters 5 and 6, possible interactions amongst the vasodilators from endothelial cells are examined.

1.2 Red blood cells

Erythrocytes, or RBCs, mainly contain hemoglobin (Hb), the primary role of which is to transport O_2 from the lungs to the muscles and to carry CO_2 back from the tissues to the lungs. Recently, RBCs have been ascribed an unique role in dilating blood vessels, which requires O_2-regulated binding and bioactivation of nitric oxide (NO) by Hb and also by ATP release from the RBCs when oxygen saturation is low (2-5).

1.2.1 Hemoglobin

Hb is the major component in RBCs (5 mM) and the most important respiratory protein in vertebrates. This tetrameric protein is composed of two α–chains and two β–chains, with each chain containing one noncovalently bound heme. The Hb tetramer has two quaternary structures. The quaternary configuration of low affinity, deoxygenated Hb (deoxyHb; $HbFe^{II}$) is known as the tense (T) state. Conversely, the quaternary structure of the fully oxygenated, high affinity form of Hb (oxyHb; $HbFe^{II}O_2$) is known as the relaxed (R) state. In the artery, Hb is approximately 96% saturated with O_2 while only 64% saturated in the vein (6). At rest, 21% of O_2 from the blood is released to the tissues whereas > 65% O_2 is released during exercise (Figure 1.2). Thus, most O_2 is

released when needed. Hypoxic vasodilation of blood vessels occurs around 40-60% O_2 saturation of Hb (7).

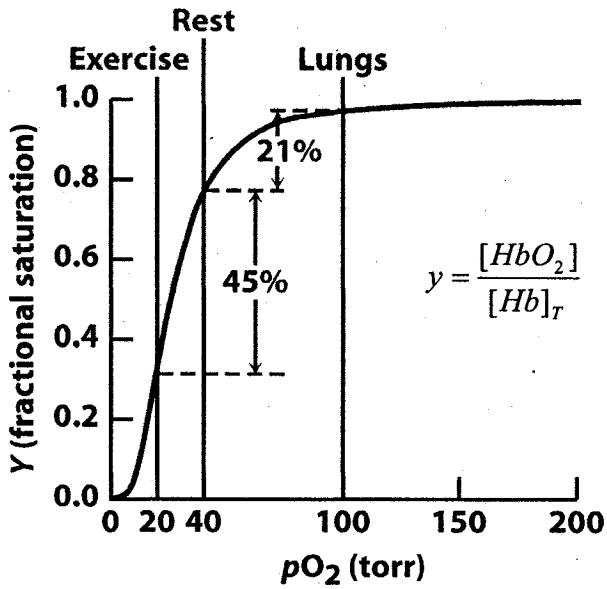

Figure 1.2. Oxygen-Hb dissociation curve. (Source: Berg JM, Tymoczk JL, Stryer L, Biochemistry, sixth edition: 2006; Chapter 7; W. H. Freeman and Company, New York)

The transition between the R and T states of Hb is triggered by changes in the partial pressures of O_2, hydrogen, and carbon dioxide (6). The two structures differ in the arrangement of the four subunits (quaternary structure) and in the conformation of the subunits (tertiary structure). The quaternary R ↔ T transition consists of a 12-15° rotation of the $\alpha_1\beta_1$ dimer relative to the $\alpha_2\beta_2$ dimer, and 0.8 Å translation of one dimer relative to the other (Figure 1.3) (6). In the T-state, the heme group iron is five-coordinate, high spin and about 0.5 Å displaced from the plane of the porphyrin towards His-F8 (Figure 1.4). The ferrous heme is constrained by salt bridges between the C-terminal of the four subunits. In the R quaternary state, the salt bridges are broken, the

iron is six-coordinate, low spin and it moves into the plane of the porphyrin (6). The addition of a ligand such as NO or O_2 to deoxyHb brings about the T → R transition (6).

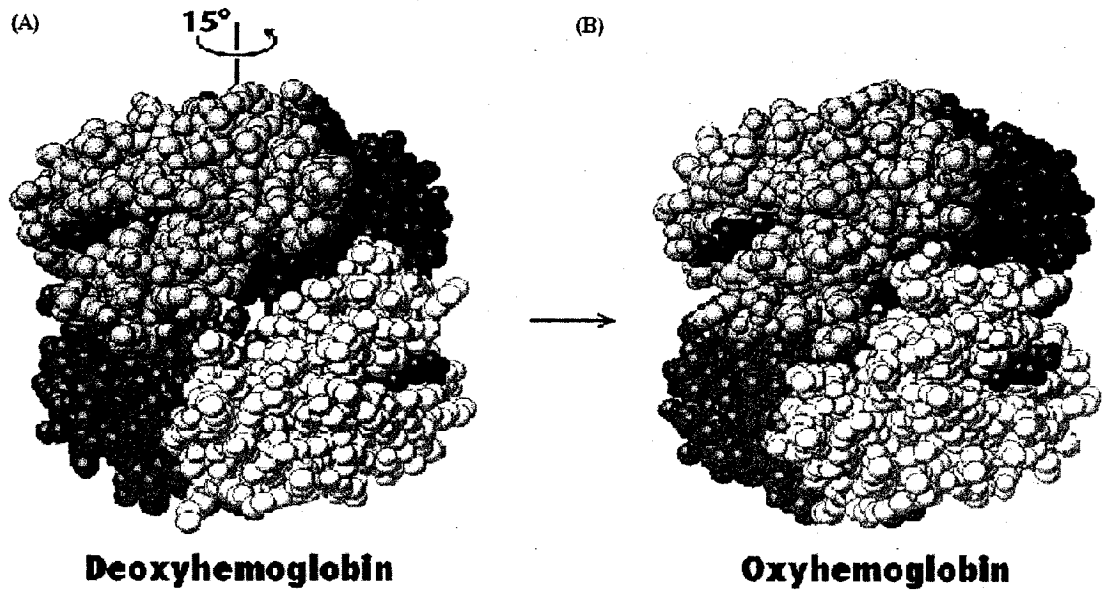

Figure 1.3. R and T-state of human Hb. (A) T-state of Hb, (B) R-state of Hb. (Source: Berg JM, Tymoczk JL, Stryer L, Biochemistry, sixth edition: 2006; Chapter 7; W. H. Freeman and Company, New York)

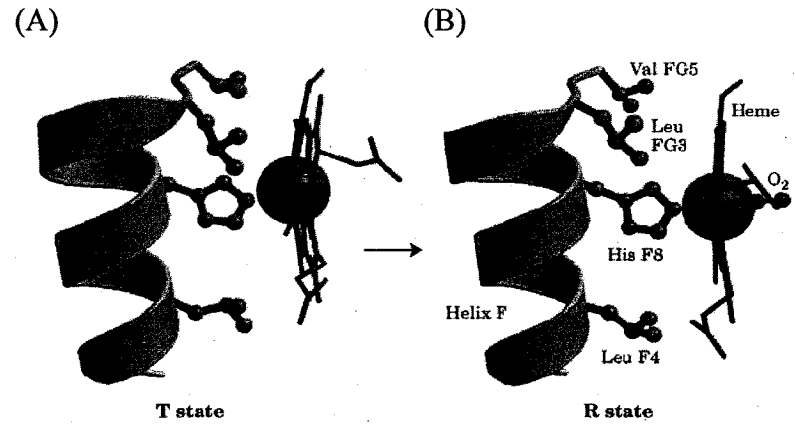

Figure 1.4. Position of heme in the two state of Hb. (A) T-state of Hb, (B) R-state of Hb (Source: Nelson D, Cox MM. Lehninger: Priciple of Biochemistry, Third edition: 2000; Chapter 7: 213)

1.2.2 Nitric oxide

NO is a potent vasodilator formed by the oxidation, in the presence of oxygen, of *L*-arginine to *L*-citrulline by the enzyme nitric oxide synthase (NOS) (Figure 1.5) (6).

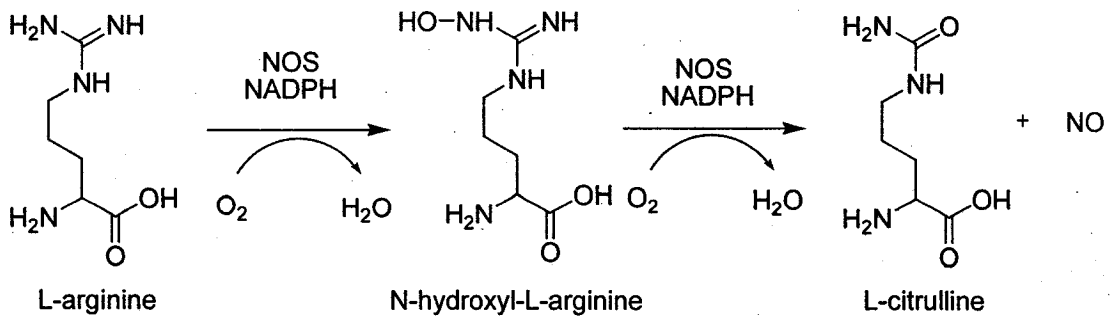

Figure 1.5. Nitric oxide formation. Oxidation of *L*-arginine to *L*-citrulline with the formation of NO by nitric oxide synthase.

NO has a half-life of a few seconds under physiological conditions (8). There are many possible fates of NO in the body; for example, it may oxidized by O_2 resulting in the formation of nitrite (NO_2^-) or it may be taken up by RBCs. Nitrite is present in plasma at a concentration ranging from 0.3 to 3.5 μM (9-11) and is stable in blood compared to NO and *S*-nitrosothiols (RSNOs) as it is less readily oxidized or reduced (12). Several groups have suggested that nitrite could be a storage form of NO (3, 7, 9, 12-15).

1.2.3 Nitrite

Since the 1920s, sodium nitrite has been used in dye, rubber chemicals and pharmaceuticals manufacture, as a corrosion inhibitor, in heat-transfer salts in meat curing, and several other applications (16). In the 1950s, nitrite was found to be present at ~ 40 μM in saliva (17). Given this high level of nitrite *in vivo*, different groups became interested in the emerging biology of this anion. There are at least three sources of nitrite

in vivo: it is formed as an oxidation product of NO, it may be ingested with food and it is generated from bacteria in the digestive system as a result of nitrate reduction. Nitrite likely has a distinct and important signalling role in mammalian biology. For example, it has been shown to affect cyclic guanosine monophosphate (cGMP) production, cytochrome P450 activities, and the expression of heat shock protein 70 and heme oxygenase-1 in a variety of tissues (18). Most of these effects are related to the reduction of nitrite to NO, which can proceed by different mechanisms. Under acidic conditions, nitrite is converted to nitrous acid followed by spontaneous decomposition to NO and NO_x (eq. 1.1 to 1.3).

$$NO_2^- + H^+ \leftrightarrow HNO_2 \qquad (1.1)$$

$$2\ HNO_2 \rightarrow N_2O_3 + H_2O \qquad (1.2)$$

$$N_2O_3 \rightarrow NO + NO_2 \qquad (1.3)$$

In vivo, NO_2^- reduction is more complex and happens mostly in the stomach where the pH is very low (19, 20). The formation of NO in the stomach has been shown to increase mucous barrier thickness and gastric blood flow (21). Xanthine oxidase, which is located in the endothelium of blood vessels in the heart, catalyzes the reduction of nitrite to NO (22, 23). This is enhanced at low oxygen tensions and acidic conditions such as those seen during ischemia. The NO produced has a cardioprotective effect and reduces the size of the infarct (24).

Since NO formation from nitrite was thought to require extremely low oxygen tension and low pH, some doubt was raised regarding the role of nitrite as a vasodilator. However, Gladwin and coworkers have shown that infusion of nitrite into humans results

in vasodilation through the reduction of nitrite to NO by Hb (Figure 1.6). Based on these results they have proposed that nitrite could be the largest intravascular storage pool of NO (12). The mechanism proposed for the conversion of nitrite to NO by deoxyHb remains unclear and will be discussed in Chapters 2, 3, and 4.

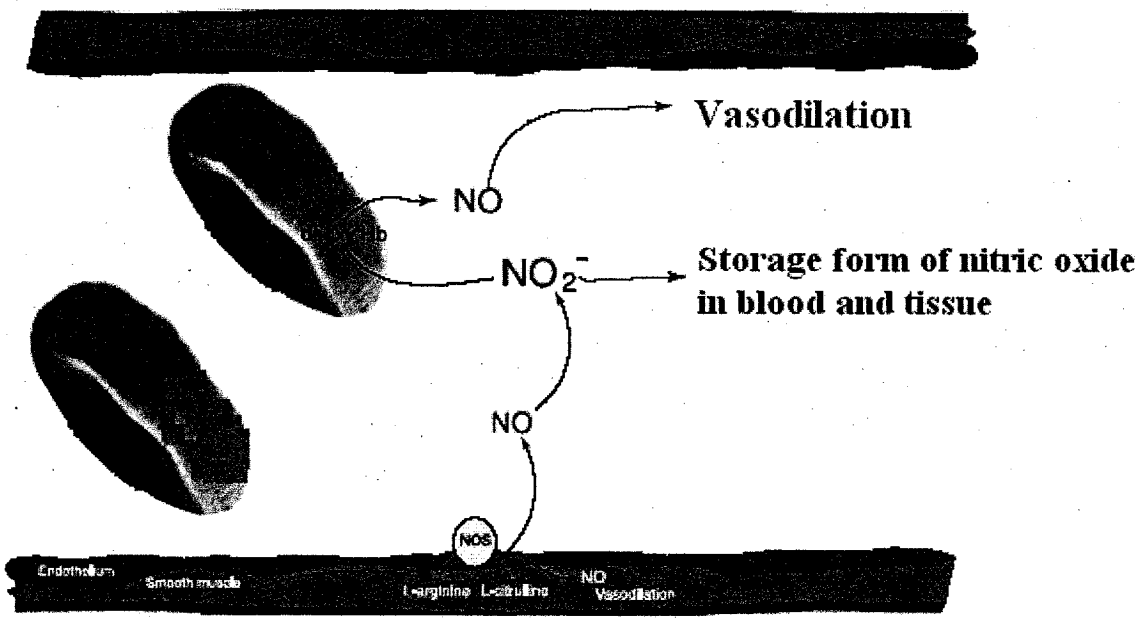

Figure 1.6. Reduction of nitrite to NO by deoxyHb.

1.2.4 Reactions between nitrite and Hb

Reactions between nitrite and Hb have been studied since the middle 1800s. The first report by Arthur Gamgee in 1868 showed that the exposure of blood to an atmosphere of nitrite changed its color from red to brown (25). Later, spectroscopic analysis revealed that this observation reflects the reaction of oxyHb with nitrite to form nitrate and methemoglobin (metHb; $HbFe^{III}$) (26). It has also been shown that the reaction of nitrite with metHb results in the formation of a reversible $HbFe^{III}NO_2^-$ complex (27).

Since the reaction of nitrite with metHb or oxyHb results in the loss of NO bioactivity, oxyHb and metHb do not seem to be involved in nitrite-induced vasodilation.

However, the reaction of excess deoxyHb with nitrite results in the formation of nitrosylhemoglobin (nitrosylHb; $HbFe^{II}$-NO) and metHb. In this reaction, nitrite is first reduced by deoxyHb to form metHb and NO. The NO released then rapidly binds to another ferrous heme (Fe^{II}-heme) to form nitrosylHb. Because Fe^{II}-hemes bind NO tightly, nitrosylHb was generally considered a dead-end for NO bioactivity until NO transfer to Cysβ93 on oxygenation of partially nitrosylated Hb was reported (28). The destabilization of the cysteine-bound NO of *S*-nitrosohemoglobin (HbSNO) during Hb deoxygenation was assumed to facilitate the transfer of NO to low-molecular-weight and membrane-associated thiols such as those in anion exchange protein 1(AE1), resulting in increased availability of NO for vasodilation (Figure 1.7) (7, 12).

$$NO_2^- + HbFe^{II} + H^+ \rightarrow HbFe^{III} + NO + OH^- \quad (1.4)$$

$$NO + HbFe^{II} \rightarrow HbFe^{II}NO \quad (1.5)$$

$$HbFe^{II}NO + O_2 \rightarrow oxyHbSNO \quad (1.6)$$

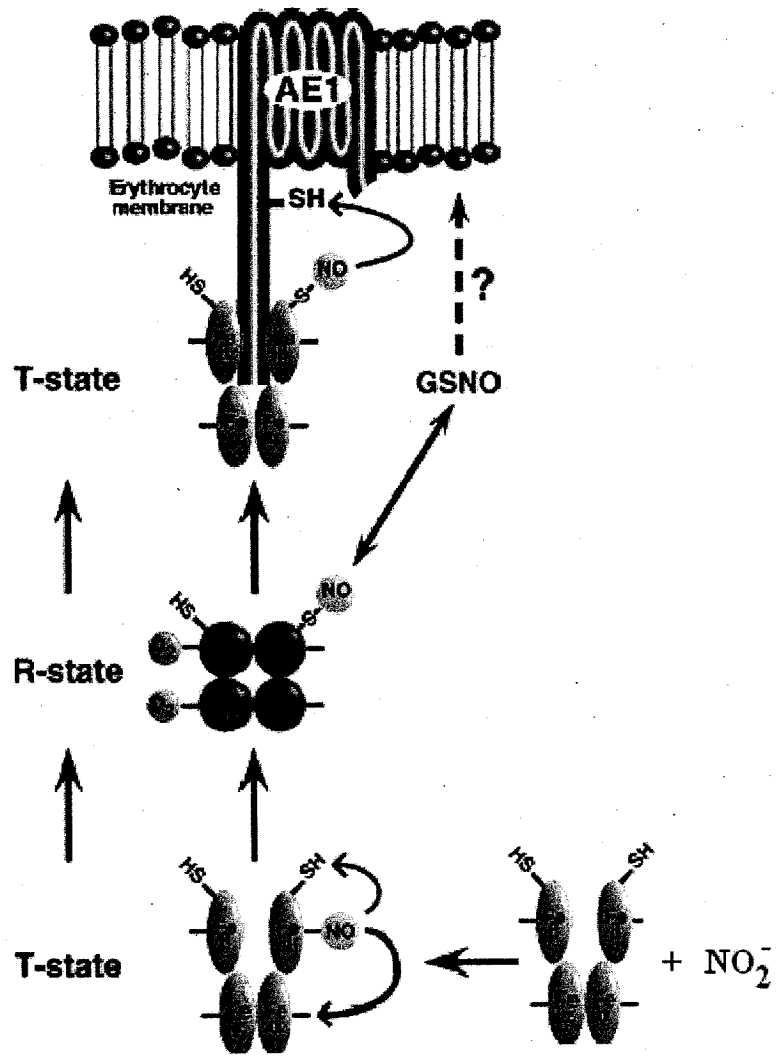

Figure 1.7. Proposed mechanism for NO transfer from the heme to Cysβ93. Nitrite reacts with excess deoxyHb to form nitrosylHb. Following oxygenation the NO is transferred to Cysβ93. Deoxygenation of HbSNO promotes NO transfer from Cysβ93 to AE1. Adapted from reference (7).

We have investigated the mechanism of NO transfer from the heme to Cysβ93 and these results will be discussed in Chapters 2, 3, and 4.

1.3 Endothelial cells

Endothelial cells line the surface of blood vessels throughout the entire circulatory system, from the heart to the smallest capillaries (29). These cells are involved in many

aspects of vascular biology such as vasodilation, vasoconstriction, blood clotting, and inflammation. Possible mediators of muscle vasodilation during exercise, such as adenosine, NO, prostaglandins (PGs), and epoxyeicosatrienoic acids (EETs), are produced in endothelium cells (30). These compounds are thought to be the vasodilators that maintain and increase blood flow during exercise.

1.3.1 Adenosine

Adenosine is a nucleoside comprising one adenine molecule linked to a *D*-ribose sugar molecule (Figure 1.8A). Adenosine is formed mostly in endothelial cells by the degradation of adenosine monophosphate (AMP) through the enzyme 5'nucleotidase (30). Recently, it has been shown that the adenosine concentration increases in interstitial fluid during exercise (31-33). Adenosine is proposed to induce vasodilation by binding to adenosine receptors on the smooth muscle cell. As shown in Figure 1.8B, this binding increases the formation of cyclic adenosine monophosphate (cAMP) from adenosine triphosphate (ATP) followed by the activation of protein kinase A (PKA). Subsequently, myosin light chain kinase (MLCK) is phosphorylated by PKA resulting in a decrease in the affinity of PKA for Ca^{2+}–calmodulin kinase, which is needed for smooth muscle contraction (30). There is also a pathway involving the activation of PKA by cAMP that induces vasodilation by the formation of NO (Figure 1.8B) (30).

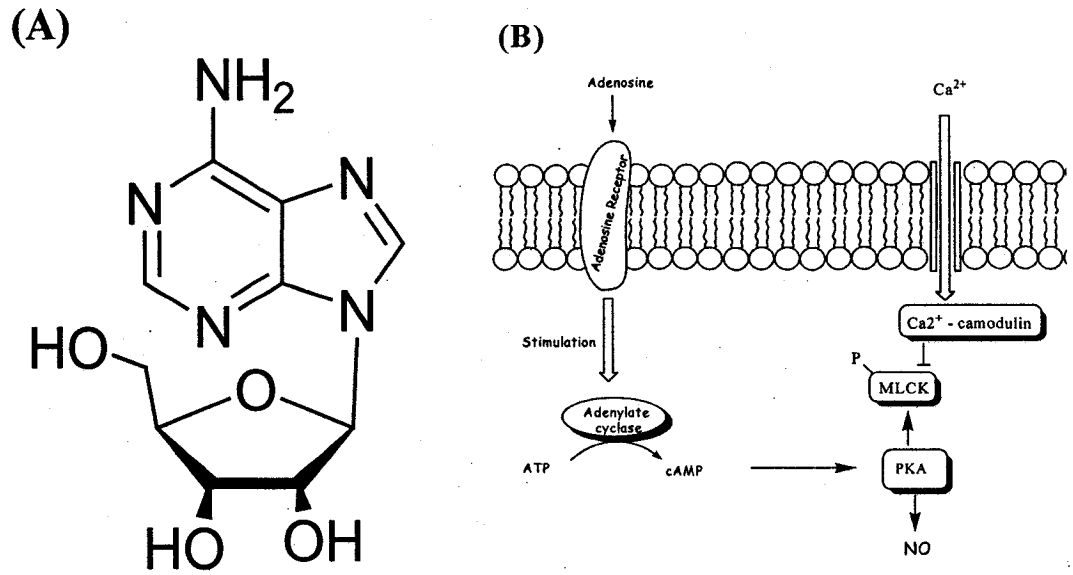

Figure 1.8. Adenosine-induced vasodilation. (A) Structure of adenosine (B) Mechanism of adenosine-induced vasodilation.

1.3.2 Nitric oxide

NO, a highly reactive, diffusible, and unstable radical, plays an important role in the regulation of a wide range of physiological processes, including cellular immunity, angiogenesis, neurotransmission, vasodilation, and platelet aggregation (34-37). NO is produced by vascular endothelium, smooth muscle, cardiac muscle, and many other cell types. During exercise, NO production by endothelial NOS (Figure 1.5) is increased. In the NO-cGMP pathway, the NO formed binds to a heme moiety on soluble guanylyl cyclase which increases the production of cGMP. The increased cGMP activates the protein kinase that inhibits calcium influx into the smooth muscle cell and decreases Ca^{2+}-calmodulin stimulation of MLCK (Figure 1.9). This results in a decrease in smooth

muscle tension and vasodilation (38). In NO- and adenosine-mediated vasodilation decrease in Ca^{2+} causes vasodilation.

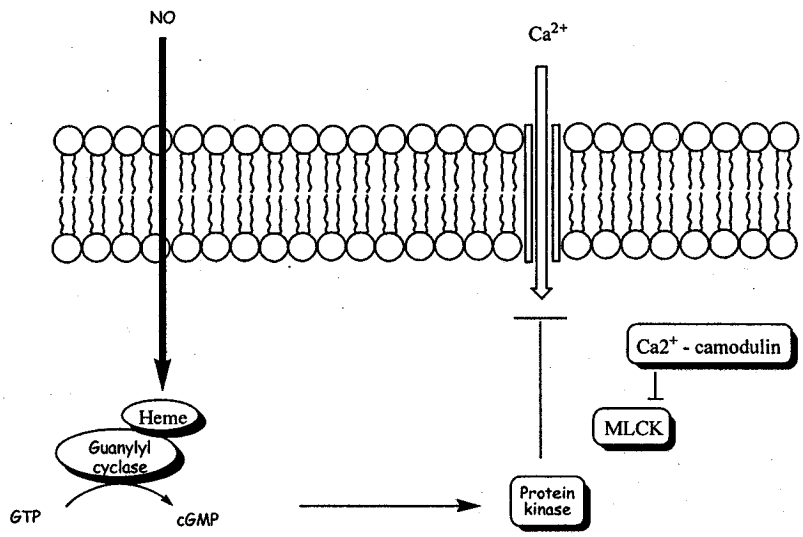

Figure 1.9. Mechanism of nitric oxide-induced vasodilation.

1.3.3 Epoxyeicosatrienoic acids

Members of a class of arachidonic acid derivatives, the EETs have been found to mediate vasodilation. Arachidonic acid, one of the most abundant unsaturated fatty acids in mammals, is metabolized by cytochrome P-450 (CYP 2C) to four geometric EET isomers that differ in the position of the epoxide group (Figure 1.10A). 14,15-EET and 11,12-EET are the most abundant of the EET isomers in human (39). EETs play roles in regulating cellular proliferation, inflammation, peptide hormone secretion, and various cellular signal pathways relevant to cardiovascular and renal functions (40, 41). They are produced in the endothelium and relax the vascular smooth muscle by opening potassium channels, decreasing calcium influx, and hyperpolarizing smooth muscle cells (Figure 1.10B) (42).

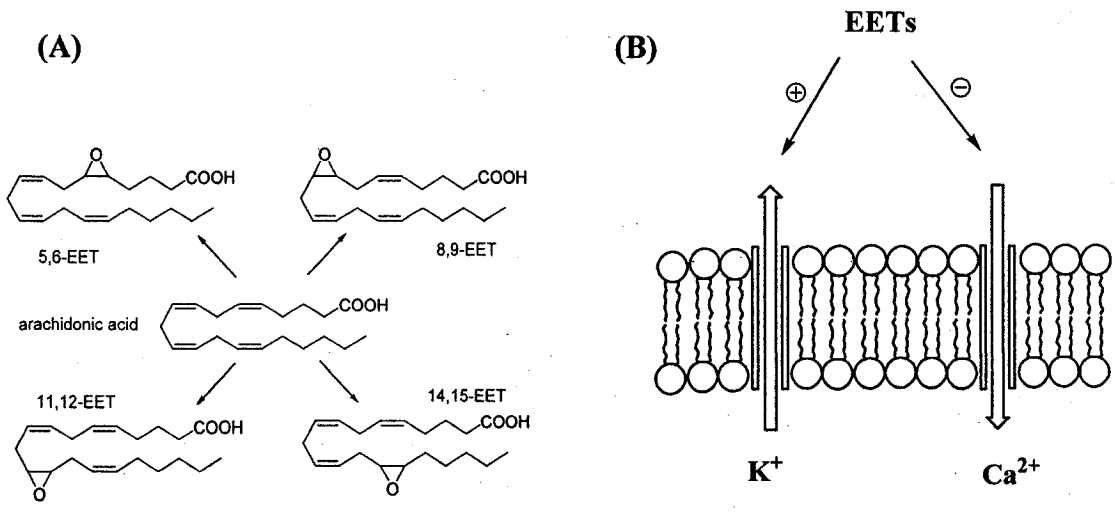

Figure 1.10. EET-induced vasodilation. (A) Formation of EETs from arachidonic acid. (B) Mechanism of EET-induced vasodilation.

1.3.4 Prostaglandins

PGs are formed mostly in the endothelium cell by the action of cyclooxygenases (COX-1 and COX-2) on arachidonic acid. They mediate a wide range of physiological functions, including control of blood pressure, contraction of smooth muscle, and modulation of inflammation (43, 44). Prostacyclin (PGI_2, Figure 1.11A), a member of the PGs, has been shown to increase cAMP levels and decrease phospholipase-C activity, which results in a decrease in intracellular calcium, thereby relaxing smooth muscle (Figure 1.11B) (30).

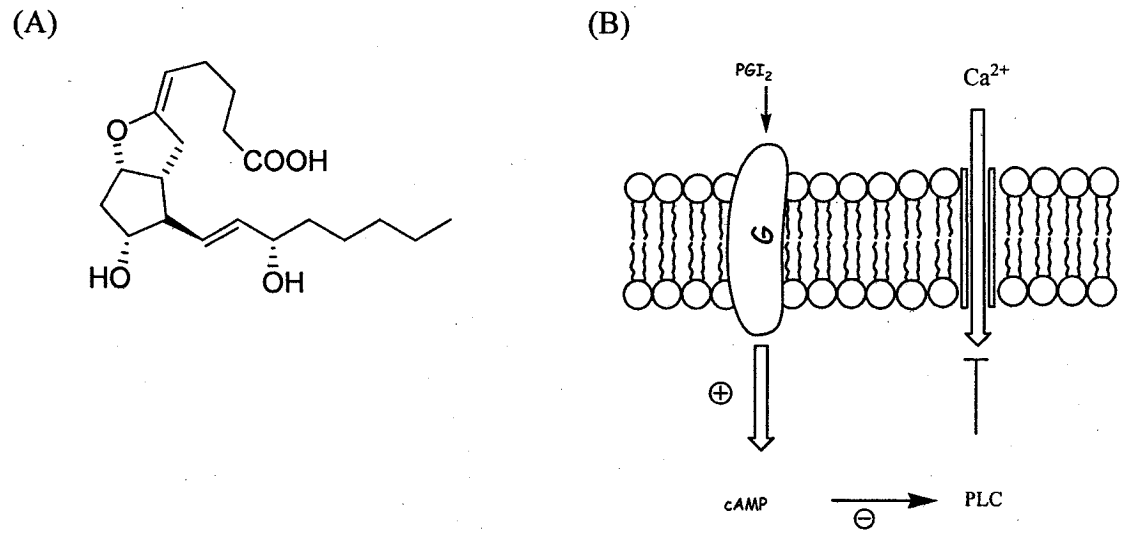

Figure 1.11. Prostaglandin-induced vasodilation. (A) Prostacyclin structure. (B) Mechanism of prostacyclin-induced vasodilation.

1.3.5 Metabolic control of muscle blood flow during exercise in humans

Endothelium cells produce several vasodilators but the redundant, synergistic interactions and compensatory responses between them remain unclear. The elucidation of their relative importance and interactions is critical in understanding the pathophysiological basis of impaired oxygen and nutrient supply in cardiovascular disease and how these dilators are altered under environmental influences such as exercise. Due to the existence of redundant mechanisms, blockade of one vasodilator is unlikely to elicit changes in muscle blood flow during exercise. Combined blockade offers the potential to uncover important interactions and control mechanisms. The influence of multiple vasodilator blockades on muscle blood flow and on vasodilator concentrations at rest and during exercise in human muscle interstitial fluid obtained by microdialysis was investigated and will be discussed in Chapters 5 and 6.

1.4 Outline of thesis

In Chapter 2, reactions between nitrite and different forms of Hb at physiological concentrations were investigated. UV-vis and circular dichroism (CD) spectroscopies were used to probe environmental changes at the heme group.

In Chapter 3, a modified Saville assay using solid-phase extraction and HPLC/UV/MS was developed to detect S-nitrosoHb. The extent of Cysβ93 *S*-nitrosation on exposure of deoxyHb/nitrite incubations to air was monitored with this new method. The products obtained were compared with those obtained on nitrosylHb ($HbFe^{II}NO$) oxygenation.

In Chapter 4, the mechanism of NO transfer from the heme to Cysβ93 was investigated by examining deoxyHb/nitrite incubations under different conditions.

In Chapter 5, methodology for the sequential extraction, separation and detection of nitrite, adenosine, and EETs in interstitial fluid was developed. This methodology was applied to the analysis of human microdialysates collected from healthy volunteers during knee-extension exercise.

In Chapter 6, the methodology developed in Chapter 5 was applied in the analysis of 90 microdialysates from five healthy volunteers collected during knee-extension exercise at different probe positions. Samples with and without the inhibition of NO synthase by *N*-nitroso-*L*-arginine methyl ester (*L*-NAME), and the inhibition of PG production by indomethacin were investigated to establish the effects of the combined pharmacological blockade on vasodilator levels in tissues.

Conclusions and suggestions for future studies are presented in Chapter 7.

2.0 Spectroscopic analysis of the reaction between nitrite and hemoglobin at physiological concentrations

2.1 Introduction

In the past several years, the interaction between nitrite and Hb has become the subject of much interest. Nitrite is present in plasma at a concentration ranging from 0.3 to 3.5 μM (10, 13) and is comparatively stable with respect to NO.

Different mechanisms have been proposed for the reaction of nitrite with Hb. Most studies to date were performed under very dilute conditions (≤ 50 μM Hb compare to the 5 mM Hb in RBC) (27, 45, 46). Under these conditions the Hb tetramer is dissociated into dimers (k_d = 2.9 x 10^{-6} M) (47), which could alter its reactions with ligands (47, 48). Our group has shown different behavior at dilute versus physiological concentrations of oxyHb in its reaction with *S*-nitroso-*L*-glutathione (GSNO) (48). We have provided evidence that the reaction of oxyHb at physiological concentrations with GSNO in the presence of Cu,Zn-superoxide dismutase (CuZnSOD) resulted in the formation of HbSNO within a putative oxyHb-CuZnSOD encounter complex (48, 49). The proposed mechanism for CuZnSOD-catalyzed NO transfer from GSNO to Cysβ93 is given in reactions 2.1-2.3. NO targeting to Cysβ93 by CuZnSOD is insignificant in dilute Hb solutions and only metHb is formed from the NO released in reaction 2.2

$$\text{oxyHbSH} + \text{Cu}^{\text{II}}\text{ZnSOD} \rightarrow \text{oxyHbS}^{\cdot} + \text{Cu}^{\text{I}}\text{ZnSOD} + \text{H}^{+} \qquad (2.1)$$

$$\text{GSNO} + \text{Cu}^{\text{I}}\text{ZnSOD} + \text{H}^{+} \rightarrow \text{GSH} + {}^{\cdot}\text{NO} + \text{Cu}^{\text{II}}\text{ZnSOD} \qquad (2.2)$$

$${}^{\cdot}\text{NO} + \text{oxyHbS}^{\cdot} \rightarrow \text{oxyHbSNO} \qquad (2.3\ a)$$

$${}^{\cdot}\text{NO} + \text{oxyHb} \rightarrow \text{metHb} + \text{NO}_3^{-} \qquad (2.3\ b)$$

In this study, our primary focus was on the reaction of nitrite with deoxyHb because of its possible relevance *in vivo*. It has been proposed that nitrite is first reduced by deoxyHb to form metHb (12, 50). The NO released would then rapidly bind another ferrous heme (7, 12, 28, 51) and it is proposed that subsequent transfer of NO to Cysβ93 of the β–chain of Hb to form HbSNO occurs on reoxygenation of Hb (7, 12). The subsequent destabilization of the Cys-NO bond during Hb deoxygenation is assumed to facilitate the transfer of NO to low-molecular-weight thiol and anion exchange protein 1 AE1 (Figure 1.6) resulting in increased availability of NO for vasodilation (7, 12). The relevant reactions are given in the following equations:

$$NO_2^- + HbFe^{II} + H^+ \rightarrow HbFe^{III} + {}^{\cdot}NO + OH^- \qquad (2.4)$$

$${}^{\cdot}NO + HbFe^{II} \rightarrow HbFe^{II}NO \qquad (2.5)$$

$$HbFe^{II}NO + O_2 \rightarrow oxyHbSNO + O_2^{-\cdot} \qquad (2.6)$$

Other groups have proposed that most of the NO-bound Hb is in form of nitrosylmetHb ($HbFe^{III}NO$) rather than nitrosylHb (52, 53). They concluded that the accumulation of the nitrosylmetHb intermediate during nitrite reduction is explained by the relatively slow conversion of nitrosylmetHb to nitrosylHb, despite the very high affinity of deoxyHb for NO. The resultant accumulation of nitrosylmetHb produces a pool of labile, potentially bioactive NO (k_{off} $HbFe^{III}NO$ = 1.5 s^{-1}) (51, 52). In fact, Stamler and coworkers have proposed that nitrosylmetHb is a HbSNO precursor rather than nitrosylHb (53). These reactions are given in the following equations:

$$NO_2^- + HbFe^{II} + H^+ \rightarrow HbFe^{III} + \cdot NO + OH^- \quad (2.7)$$

$$\cdot NO + HbFe^{III} \rightarrow HbFe^{III}NO + O_2 \rightarrow oxyHbSNO \quad (2.8)$$

In this chapter, we have investigated the reactions of nitrite with 3 mM oxyHb, metHb and deoxyHb which are close to the physiological concentrations (~ 5 mM) to compare the results with those in the literature where more dilute solutions (5 – 50 μM) of Hb were used (27, 50, 51, 54, 55). To reproduce the physiological conditions, an FTIR-type cell with a 6-μm path length was used to allow measurements of the visible absorption of 12 mM heme. The effect of adding CuZnSOD on the reaction between nitrite and oxyHb, and the effect of oxygen on the reaction of nitrite with deoxyHb were investigated.

2.2 Materials and methods

2.2.1 Materials

Bovine Hb and 3,3',5,5'-tetramethylbenzidine (TMB) were purchased from Sigma. A rabbit polyclonal antibody developed against bovine CuZnSOD was purchased from Santa Cruz Biotechnology and a goat anti-rabbit horseradish-peroxidase conjugated antibody was obtained from Bio-Rad. Bovine erythrocyte CuZnSOD was obtained from Roche Molecular Biochemicals. NAP-10 columns and Q-Sepharose anion exchange resin (100 μm particule size) were obtained from Amersharm Bioscience. Sodium dithionate ($Na_2S_2O_4$) and sodium phosphate salts were obtained from Fisher Scientific. Sodium nitrite was obtained from Anachemia. Nanopure water (specific resistance, 18 MΩ-cm)

obtained from a Millipore Simplicity water purification system was used for all reactions, which were carried out in 200 mM sodium phosphate buffer, pH 7.2 (NaPi). N_2 gas was purchased from Praxair. A Model 3 stirred cell (3-mL) and PM30 ultrafiltration discs were purchased from Millipore.

2.2.2 Hb purification

A solution of metHb was prepared by addition of small portions of the lyophilized solid to NaPi followed by repeated agitation and centrifugation in order to completely dissolve the protein. After 2 min of centrifugation at 12 000 rpm at room temperature, the precipitate was discarded and the supernatant stored at 4°C prior to use. To remove CuZnSOD impurity from the Sigma Hb preparation, the solution was loaded onto a 1.6x10-cm Q-Sepharose column equilibrated with NaPi and Hb was eluted with the same buffer. The eluant was concentrated to ~3 mM Hb in the 3-mL ultrafiltration cell with a 30-kDa cut-off PM30 membrane by applying nitrogen at a pressure of 65 psi directly into the ultrafiltration cell. Purified Hb was used to prepare all Hb forms in this chapter.

2.2.3 Western blotting and SOD-activity assay

Complete removal of CuZnSOD from the Hb solution was investigated by Western blot analysis and SOD-activity assay (49). Western blotting was performed on a 1.5 mM Hb sample using the anti-CuZnSOD antibody diluted to 0.4 μg/mL. The blot was probed with a goat anti-rabbit-HRP secondary antibody (1:3000) and the presence of CuZnSOD was detected by colorimetric method with TMB. SOD activity was performed using a modified procedure described previously (56). Briefly, 10 μL of 37.5 μM Hb was

added to 990 mL of Tris-cacodylate buffer, with or without CuZnSOD, in a 1.5-mL quartz cuvette with a 1-cm pathlength. Pyrogallol (5 mL) was added to a final concentration of 200 mM and the absorbance at 320 nm was read every 15 s over 3 min.

2.2.4 DeoxyHb and oxyHb preparation

DeoxyHb was prepared in a glove box (MBraun, Model MB-OX-SE1) by addition of sodium dithionate (50 mg) to metHb (1 mL of ~ 5 mM) followed by removal of the low molecular weight reagents on a NAP-10 column preconditioned with NaPi. DeoxyHb was eluted from the column with NaPi. OxyHb was prepared from deoxyHb by vortexing in air for 5 min. All Hb solutions were used within 3 days after their preparation and stored at 4°C prior to use.

2.2.5 DeoxyHb/nitrite incubations

A stock solution of $NaNO_2$ in NaPi was prepared, degassed under nitrogen, and inserted into the glove box. DeoxyHb (12 mM heme) was incubated with 12 mM nitrite for 5 min at room temperature inside the glove box. The UV/visible spectra of the incubations were recorded prior to aeration. The samples were removed from the glove box, vortexed in air for 10 min, and the spectra were recorded again.

2.2.6 OxyHb/nitrite and metHb/nitrite incubations

OxyHb (10 mM heme) with and without CuZnSOD (5 μM) was incubated at room temperature with 10 mM $NaNO_2$ in NaPi for 5, 10 and 15 min. Also, metHb (10 mM heme) was incubated with 10 mM $NaNO_2$ in NaPi for 5 min at room temperature.

2.2.7 UV/visible analysis of the Hb incubations

The heme Soret and visible bands of Hb were used to probe its reaction with nitrite. The bands monitored are essentially porphyrin π-π^* transitions and yield information on the environment of the heme group. To record the Soret and visible absorption spectra, 10 μL of each Hb incubation was loaded by syringe onto the 13x2-mm CaF_2 window of a demountable FTIR cell (Harrick). Incubations containing deoxyHb were loaded inside the glove box and the incubations containing oxyHb or metHb were loaded outside the glove box. The FTIR cell was immediately assembled using a 6-μm Teflon spacer (Harrick) and placed in a custom-made bracket in a Beckman DU 800 UV-visible spectrophotometer. Each spectrum was recorded with a scan rate of 1200 nm/min and a bandwidth of 1 nm. As mentioned in Section 2.1, use of an FTIR-type cell allowed the protein concentration in the Hb/nitrite incubations measured at close to physiological values (~ 20 mM heme).

2.2.8 CD analysis of Hb incubations

To record the Soret band, 20 μL of the Hb incubation was loaded by syringe into the FTIR cell as described in Section 2.2.7. The cell was immediately assembled using a 50-μm Teflon spacer (Harrick) and placed in a JASCO CD 710 spectropolarimeter. Each spectrum represents an average of 5 scans with a resolution of 0.2 nm, a response time of 2 s, a scan speed of 20 nm/min and a bandwidth of 1 nm. Contributions from the buffer and $NaNO_2$ were subtracted from the spectra using the JASCO CD software. Data analysis was performed using Sigma Plot and Microsoft Excel software.

2.3 Results

2.3.1 Western blotting and SOD-activity analysis

SOD activity was measured using the pyrogallol autoxidation method (49). Rates of pyrogallol oxidation were determined from the linear portion of the plots of $A_{320\ nm}$ *vs* time (Figure 2.1 A). Addition of 0.375 μM Hb tetramer, purified as described in Section 2.2.2, resulted in the same rate of pyrogallol autoxidation compared to that in buffer alone. Addition of 3.0 nM CuZnSOD monomer (ε_{258nm} = 5.15 $mM^{-1}cm^{-1}$ per monomer) to the Hb solution decreased the rate of pyrogallol oxidation due to competition for the superoxide (Figure 2.1A). Analysis of samples containing 0.375 μM untreated Hb tetramer revealed 0.64±0.16 nM CuZnSOD present in the sample. When normalized for 5 mM Hb tetramer, the concentration of CuZnSOD monomer present is 13±1 μM. This value is close to the reported value of 20 μM CuZnSOD monomer in adult RBCs (48).

Western-blot analysis of untreated Hb revealed a band at 16 kDa, which correspond to the CuZnSOD monomer. However, this band was not detected in purified Hb (Figure 2.1B), indicating that the purification technique (Section 2.2.2) removed most of the CuZnSOD present in untreated Sigma Hb.

(A)

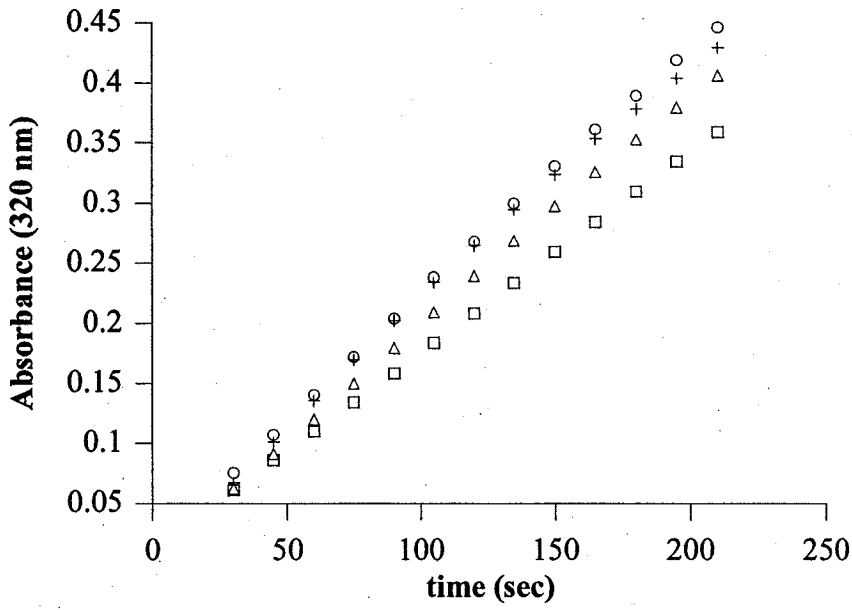

(B)

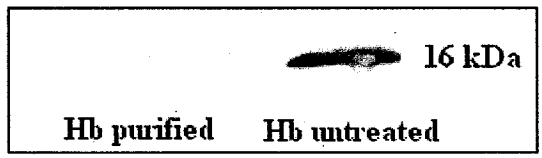

Figure 2.1. SOD activity and Western-blot analysis of CuZnSOD. (A) Time course of absorbance change at 320 nm following addition of 200 μM pyrogallol to buffer (+), purified Hb (o), purified Hb + 3 nM CuZnSOD (□), and untreated Hb (Δ) (n = 3). (B) Western-blot analysis of purified Hb and untreated Hb with anti-CuZnSOD (n = 3).

2.3.2 UV/visible absorption analysis of Hb

It has been clearly shown that the optical absorption of heme in Hb is affected by the quaternary structure of the globin and by tertiary structural changes (47). UV/visible spectroscopy was used in this project to probe the binding of ligands to the heme group that are known to cause change in the quaternary structure of the protein (T → R).

Previously recorded basis spectra of metHb, deoxyHb, nitrosylHb, nitrosylmetHb and oxyHb forms in the literature were used to confirm the results obtained (27, 46-48, 57).

2.3.3 UV/visible absorption spectra of oxyHb/nitrite incubations without CuZnSOD

The incubation of 2.5 mM oxyHb with nitrite at a 1:1 heme:nitrite ratio results in a decrease in absorbance at 545 and 575 nm (oxyHb decay) and an increase in absorbance at 500 and 630 nm (metHb growth) (Figure 2.2). These changes support the report that oxyHb reacts with nitrite to yield metHb and nitrate (46). The $t_{1/2}$ of this reaction was found to be 34.8±2.2 min (n=3) at 541 nm for 2.5 mM oxyHb, which is similar to the value of 36.9 min reported at pH 7.2 for 50 μM oxyHb with 200 μM nitrite (46).

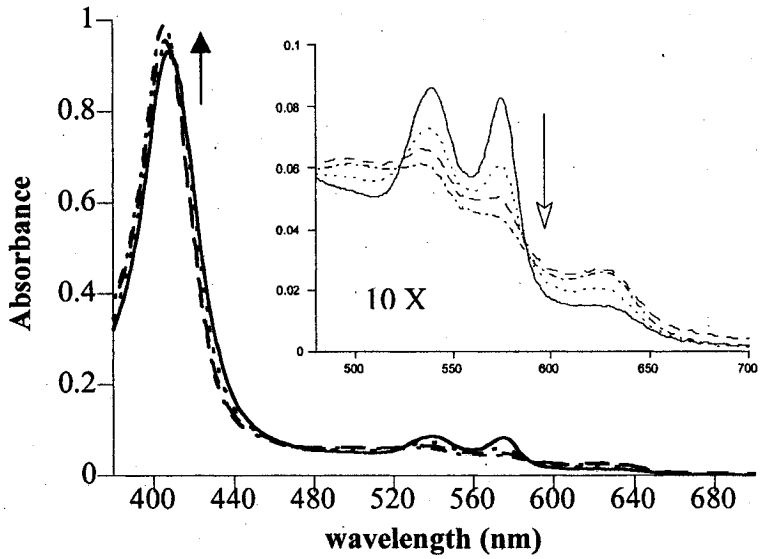

Figure 2.2. Effect of nitrite on the oxyHb UV/visible spectrum. Spectrum of 2.5 mM oxyHb before (—), and after incubation with 10 mM nitrite for 5 min (·····), 10 min (- - -) and 15 min (-·-·-). Spectra were recorded in 200 mM sodium phosphate buffer (pH 7.2) at room temperature in a FTIR-type cell with a 6-μm path length (n = 3).

2.3.4 UV/visible absorption spectra of oxyHb/nitrite incubations with CuZnSOD

CuZnSOD is present in RBCs at a concentration of 10 μM CuZnSOD dimer per 5 mM Hb (48). The incubation of 2.5 mM oxyHb containing 5 μM CuZnSOD with 10 mM nitrite gave the same results as the reaction without CuZSOD (Figure 2.1 versus 2.2). The half-time of the reaction was 35.2±3.2 min (n=3) which is similar to the value of 34.8±2.2 min (Section 2.3.3) without CuZnSOD. Since nitrite reacts with oxyHb to form metHb and nitrate in the presence and absence of CuZnSOD, the putative oxyHb-CuZnSOD encounter complex that promotes the formation of HbSNO in GSNO/oxyHb incubations (48) seems to have no effect on the nitrite/oxyHb reaction (48, 49).

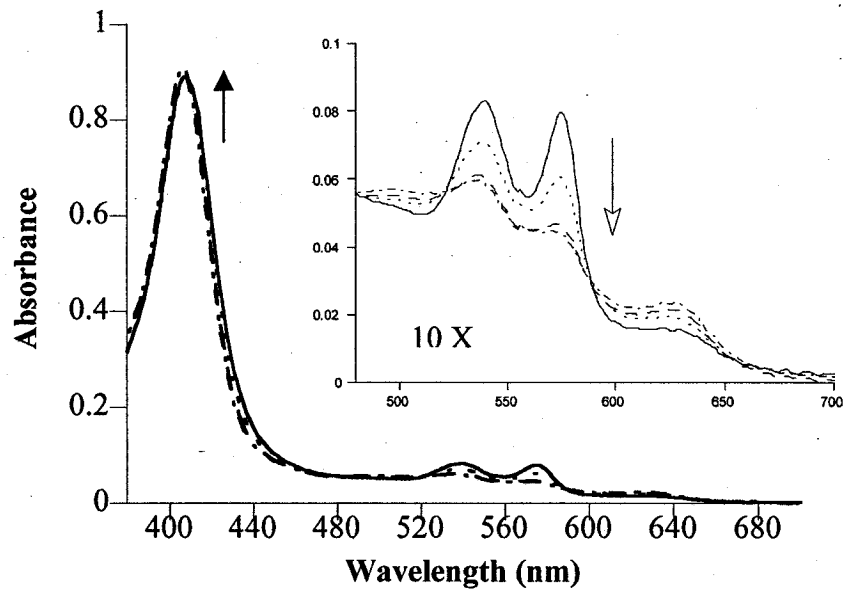

Figure 2.3. Effect of nitrite on the oxyHb UV/visible spectrum with 5 μM CuZnSOD. Spectrum of 2.5 mM oxyHb + 5 μM CuZnSOD before (—), and after incubation with 10 mM nitrite for 5 min (·····), 10 min (- - -), and 15 min (-·-·-). Spectra were recorded in 200 mM sodium phosphate buffer (pH 7.2) at room temperature in a FTIR-type cell with a 6-μm path length (n = 3).

2.3.5 UV/visible absorption spectra of metHb/nitrite incubations

The incubation of 2.5 mM metHb with nitrite at a 1:1 heme:nitrite ratio leads to a red shift of the Soret band to 409 nm and the appearance of two new bands at 543 and 573 nm in the visible region (Figure 2.4). Since these spectral changes are similar to those reported in the literature for 5.8 μM metHb (27), the concentration of metHb does not seem to influence the formation of $HbFe^{III}NO_2^-$. The ligation of NO_2^- to metHb occurs by the reversible displacement of the coordinated water molecule at the Fe^{III} heme center to give a $HbFe^{III}NO_2^-$ complex (27).

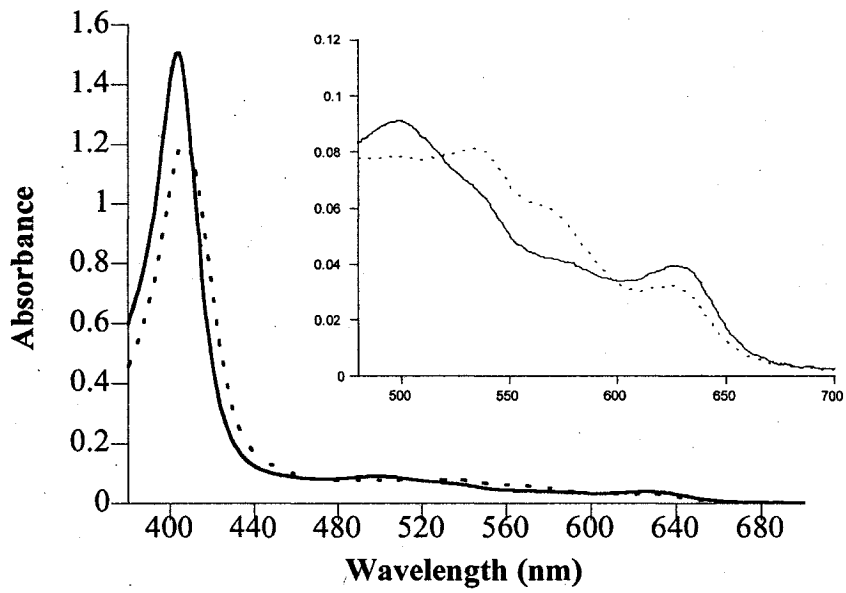

Figure 2.4 Effect of nitrite on the metHb UV/visible spectrum. Spectrum of 2.5 mM metHb before (—), and after incubation with 10 mM nitrite for 5 min (·····). Spectra were recorded in 200 mM sodium phosphate buffer (pH 7.2) at room temperature in a FTIR-type cell with a 6-μm path length (n = 3).

2.3.6 UV/visible absorption spectra of deoxyHb/nitrite incubations

The spectrum recorded during the reaction of deoxyHb with nitrite is shown in Figure 2.5. DeoxyHb shows a Soret band at 430 nm and a visible maximum at 555 nm

whereas the 5-min incubation of 3 mM deoxyHb with 12 mM nitrite has a blue-shifted Soret at 408 nm, and three visible bands at 545, 575, and 630 nm. The spectral changes indicate an alteration in the heme environment that could correlate with the reported observation of NO binding at the heme group to form nitrosylHb (48). The quaternary T-state of Hb switches to the R structure, the salt bridges between the C-terminal of the four subunits are broken, and the six-coordinate, low-spin iron moves into the heme plane. Also, the appearance of a band at 630 nm is an indication of the formation of metHb.

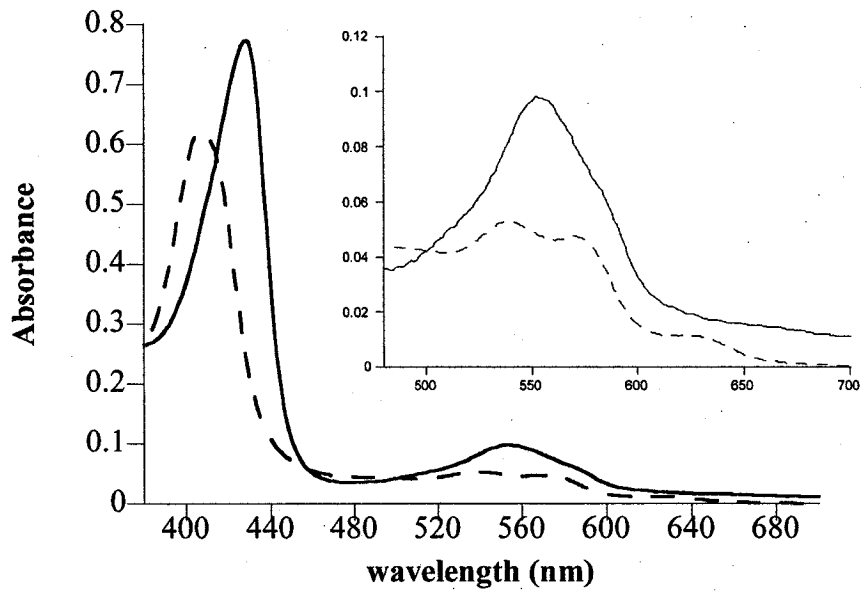

Figure 2.5. Effect of nitrite on the deoxyHb UV/visible spectrum. The spectrum of 3 mM deoxyHb before (—), and after incubation with 12 mM nitrite for 5 min (- - -). Spectra were recorded in 200 mM sodium phosphate buffer (pH 7.2) at room temperature in a FTIR-type cell with a 6-μm path length (n = 3).

The results presented above are in agreement with the literature reports that show nitrite reduction to NO by deoxyHb with the concurrent formation of metHb (12, 50). The NO formed is trapped by another deoxyHb to yield nitrosylHb (12). No spectral evidence was obtained here for nitrosylmetHb formation as predicted by some studies

(52, 53). NitrosylmetHb exhibits two visible bands at 540 and 565 nm, in contrast to the bands at 545 and 575 nm observed in the incubation of deoxyHb/nitrite (Figure 2.5) (48). The formation of nitrosylmetHb intermediate may be too rapid or its concentration too low to be observed by steady-state spectroscopic analysis.

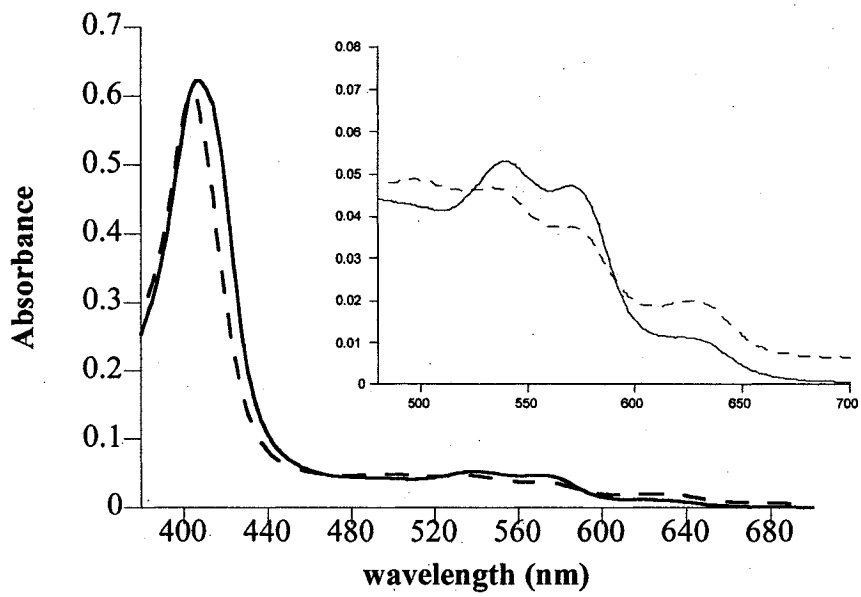

Figure 2.6. Effect of O_2 on the UV/visible spectrum of the deoxyHb/nitrite incubation. The spectrum of 5 min incubation of 3 mM deoxyHb + 12 mM nitrite before (—), and after the addition of air (- - -). Spectra were recorded in 200 mM sodium phosphate buffer (pH 7.2) at room temperature in a FTIR-type cell with a 6-μm path length (n = 3).

The effects of adding air to the deoxyHb/nitrite incubation are shown in Figure 2.6. This experiment was performed to assess if the transfer of the heme-bound NO to Cysβ93 occurs on reoxygenation as proposed by Stamler and coworkers (7). The spectrum shows a blue shift in the Soret band to 404 nm, a decrease in intensity of the bands at 545 and 575 nm, an increase in intensity of the 630-nm band and the appearance

of a new band at 500 nm. This is characteristic of the formation of metHb implying that O_2 reacts with the NO bound at the heme group to form metHb and nitrate:

$$HbFe^{II}\text{-}NO + O_2 \rightarrow HbFe^{III} + NO_3^- \qquad (2.9)$$

There is no evidence from the spectrum in Figure 2.6 for the formation of HbSNO since the heme absorption of oxyHbSNO produced via reoxygenation would be identical to that of oxyHb at 545 and 575 nm.

2.3.7 CD spectra of Hb/nitrite incubations

Above 300 nm, the optical activity of the heme group results from short- and long-distance interactions of the heme group with the protein matrix. Therefore, a simple rotation of the heme in the porphyrin plane changes the sign of the Soret CD band (58). Various other possible mechanisms contribute to the visible optical activity such as the mixing of $\pi \rightarrow \pi^*$ heme transitions with d $\rightarrow$ d iron transitions. Studies show that the CD bands in the Soret region of Hb are sensitive to the oxidation state of the heme, ligand and subunit interactions (58). The visible CD was used as a probe to determine the mechanism of reaction between nitrite and deoxyHb. Liganded ferrous Hb has a characteristic CD band at ~ 420 nm, which is distinct from that of deoxyHb (432 nm) and metHb (410 nm). In Figure 2.7, the Soret band of 3 mM deoxyHb was observed as an intense peak at 432 nm with a positive ellipticity of 25 $M^{-1}cm^{-1}$ and a negative signal at 414 nm with an ellipticity of 2.45 $M^{-1}cm^{1}$. These characteristics of the Soret band of tetrameric deoxyHb were previously reported by a number of investigators (58). In the

presence of equimolar nitrite, the Soret band blue shifts to 418 nm and the intensity decreases by 54%. This reflects the change in heme environment induced by the quaternary structure T → R transition and by ligand binding. These changes are in good agreement with those detected by UV/visible analysis (Section 2.3.6).

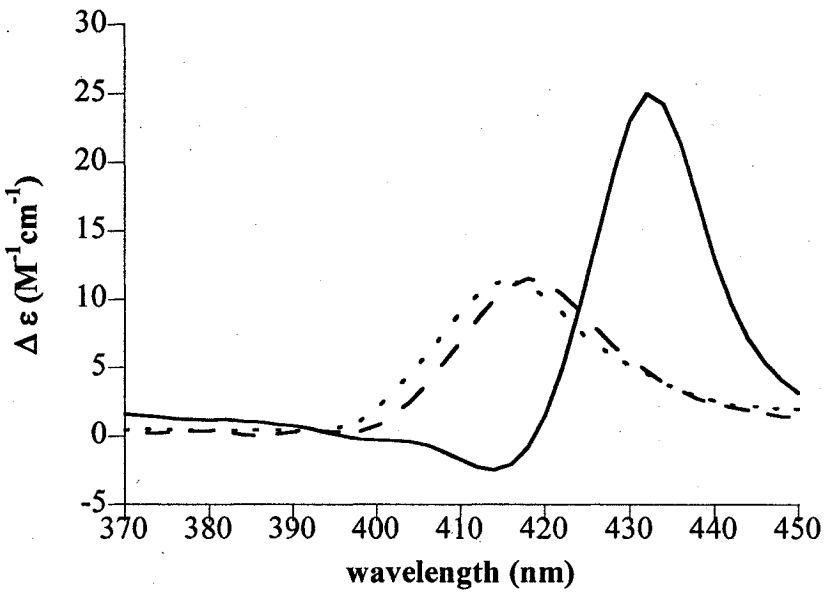

Figure 2.7. Effect of O_2 on the visible CD spectrum of the deoxyHb/nitrite incubation. The spectrum of 3 mM deoxyHb before (—), and after incubation with 12 mM nitrite for 5 min (- - -), after addition of air into the incubation (····). Spectra were recorded in 200 mM sodium phosphate buffer (pH 7.2) at room temperature in a FTIR-type cell with a 50-μm path length using a scan time of 20 nm/min and a bandwidth of 1 nm. Each spectrum is an average of 5 scans with a resolution of 0.2 nm and a response time of 2 s.

The addition of air to the deoxyHb/nitrite incubation results in a blue shift of the Soret band to 414 nm (Figure 2.7). This suggests oxidation of the iron to form metHb (58) in agreemment with the results obtained by UV/visible spectroscopy (Section 2.3.6).

2.4 Discussion

Concentrated (2.5 mM) Hb samples were found here to exhibit similar properties as those published for dilute samples. Specifically, the spectral changes and the rates of

reaction observed on the incubation of nitrite with concentrated Hb were similar to those reported for dilute (5—50 μM) Hb solutions.

The CuZnSOD-oxyHb complex has been shown to target NO from GSNO to Cysβ93 (28). Howerver, the presence of CuZnSOD during the reaction of oxyHb with nitrite had no detectable effect on the products (Figure 2.2 and 2.3). Thus any CuZnSOD-oxyHb complex formed had no effect on the nitrite/oxyHb reaction unlike its effect on the GSNO/oxyHb reaction (48).

We found that the reaction between nitrite and deoxyHb at equimolar nitrite:heme ratio forms nitrosylHb and metHb. On aeration, O_2 attacks the NO bound to the heme to form nitrate and metHb (59). HbSNO was not detected on aeration as proposed (eqs 2.4, 2.5 and 2.6). However, Gow and Stamler demonstrated the importance of the NO:Hb ratio in NO transfer from the heme to Cysβ93 (28). They proposed that the allosteric transition of Hb is involved in NO transfer since NO dissociation from the heme is 7-fold faster in the T-structure than in the fully bound R- state (54). Also, NO dissociation from β-heme is favored over the α-heme (60). Under our experimental conditions (heme:nitrite = 1:1), nitrosylHb is already in the R-state so that addition of oxygen does not induce the allosteric T→R transtion that reportedly induces NO transfer from the heme to Cysβ93 (28). In Chapters 3 and 4, the formation of HbSNO in nitrite/deoxyHb incubations upon oxygenation was investigated at a nitrite:heme ratio of 1:400 which is closer to physiological conditions. The determination of NO transfer to Cysβ93 under these conditions required a more sensitive method than visible spectroscopy, and the method developed for HbSNO analysis is discussed in the next chapter.

3.0 Hemoglobin *S*-nitrosation on oxygenation of nitrite/ deoxyhemoglobin incubations is inhibited by methemoglobin

3.1 Introduction

Recent experiments from a number of laboratories have established that RBCs provide NO vasodilator activity in a Hb-mediated, O_2-responsive manner (7, 61). The proposed O_2 sensing event is the well-documented R→T allosteric transition of Hb that occurs around its P_{50} (58, 61). How the allosteric transition of Hb is coupled to the release of NO vasoactivity from the RBC is still a matter of debate. Stamler and coworkers have proposed that in addition to its O_2/CO_2 cycle, Hb carries out an "NO cycle", binding NO in the lungs and releasing it in tissues (62). On oxygenation in the lungs, Hb undergoes its T→R transition and NO is partially transferred from the heme and intraerythrocytic GSNO to the thiol group of Cysβ93 forming a limited amount of HbSNO. Deoxygenation of Hb in the microvasculature is accompanied by the reverse R→T transition, which is promoted by Hb binding to the AE1 protein, in the RBC membrane. NO is transferred from Cysβ93 of HbSNO to thiols in AE1 and subsequently released from the RBC (63). Destabilization of the Cys–NO bond during HbSNO deoxygenation facilitates NO transfer to AE1 (7, 63).

More recently, Gladwin and coworkers (12) proposed that nitrite is the major storage form of NO bioactivity in the vasculature. Consistent with this view, they demonstrated that nitrite infusion results in vasodilation in humans (64) due to the allosterically regulated nitrite reductase activity of deoxyHb (12), which is most efficient at the P_{50} of Hb (61):

$$NO_2^- + \text{deoxyHb} + H^+ \rightarrow NO + \text{metHb} + OH^- \qquad (3.1)$$

Fe^{II} hemes bind NO tightly (65) so NO generated in RBCs by reaction (3.1) would be trapped by another deoxyHb molecule:

$$\text{deoxyHb} + NO \rightarrow \text{nitrosylHb} \qquad (3.2)$$

NitrosylHb is generally considered a dead-end for NO bioactivity and a scheme for NO release from the RBC has not been proposed by Gladwin and coworkers. However, Stamler and coworkers (28) demonstrated NO transfer from the heme to Cysβ93 on oxygenation of *partially* nitrosylated Hb:

$$\text{nitrosylHb} + O_2 \rightarrow \text{oxyHbSNO} + 1e^- + H^+ \qquad (3.3)$$

At low NO-to-heme ratios (~ 1:400) relevant to the physiological situation, 80% conversion of NO to HbSNO has been reported on oxygentation of anaerobic incubates containing deoxyHb and NO (28). Thus, reaction (3.3) provides a route for NO conversion to HbSNO *via* a nitrosylHb intermediate (7, 28, 66).

While the present experiments were in progress, Stamler and coworkers reported that oxygenation of nitrite/deoxyHb incubations also leads to HbSNO formation (53). Surprisingly, they reported that nitrite reacts immediately (within 10 s) with a large excess of deoxyHb to form a HbSNO precursor with a $Fe^{III}NO$ or $Fe^{II}NO^+$ heme (53). A transient nitrosylmetHb intermediate likely forms in Reaction 3.1 but the time scale (10

sec) of HbSNO formation reported by Stamler and coworkers (53) is considerably faster that expected based on the published bimolecular rate constants for nitrite reduction by excess deoxyHb (0.2–2.69 $M^{-1}s^{-1}$) (12, 45, 50).

Since the induction of "SNO synthase" activity on aeration of nitrite/deoxyHb incubations has already been reported (53), our goal now is to communicate that we have confirmed this important observation providing further support for the critical role proposed for HbSNO in blood flow (7, 67-70). Of particular relevance in light of previous results (28, 53) we have observed that metHb inhibits HbSNO formation, which suggests a regulatory role for metHb in hypoxic vasodilation. Furthermore, we used different methodology from Stamler and coworkers for HbSNO determination (53). The Saville assay for *S*-nitrosothiols (71) was modified to increase the sensitivity and decrease interference from the high Hb concentrations used in the incubations. Our results indicate that HbSNO is clearly produced on aeration of nitrite/deoxyHb incubations, the percent NO transfer from nitrite to Hb depends strongly on: (i) The initial nitrite/deoxyHb ratio, (ii) the preincubation time, (iii) the concentration of metHb present, and (iv) the presence of cyanide, a metHb ligand.

3.2 Materials and methods

3.2.1 Materials

Adult human Hb, sulfanilamide, *N*-(1-naphthyl)ethylenediamine, mercuric chloride, trichloroacetic acid (TCA), horse skeletal muscle apomyoglobin, *L*-methionyl-arginyl-phenylalanyl-alanine acetate (MRFA) and *L*-cysteine were purchased from Sigma.

Sodium nitrite, sodium tetraborate, ammonium hydroxide, and formic acid were obtained from Anachemia. Sodium dithionate ($Na_2S_2O_4$), sodium phosphate, potassium cyanide, and all solvents were from Fisher Scientific. Diethylenetriamine pentaacetic acid (DTPA) was from ICN Pharmaceuticals and *S*-nitroso-*L*-glutathione (GSNO) was obtained from Calbiochem. Sephadex G-25 was obtained from Amersham Biosciences and AccuBond^{II} C18 SPE (solid-phase extraction) 1 mL (100 mg) was from Agilent. Nanopure water (specific resistance, 18 MΩ-cm) obtained from a Millipore Simplicity water purification system was used to prepare all aqueous solutions.

3.2.2 Hb preparation

Lyophilized Hb (1 g) from the bottle was dissolved in 200 mM sodium phosphate buffer (pH 7.4) or 100 mM sodium tetraborate buffer (pH 9.2) containing 100 μM DTPA. The samples were centrifuged at 12,000 rpm for 2 min, and the supernatants were stored at 4°C prior to use. DeoxyHb was prepared in a glove box (MBraun, Model MB-OX-SE1) by treating the Hb supernatant (mainly metHb) with 50 mg sodium dithionite followed by desalting on a 2x5-cm Sephadex G-25 column equilibrated with 200 mM sodium phosphate buffer (pH 7.4) or 100 mM sodium tetraborate buffer (pH 9.2). OxyHb was formed by vortexing deoxyHb in air for 10 min. Hb concentrations were determined spectrophotometrically using the following extinction coefficients (ε, mM^{-1} cm^{-1}) per heme; ε_{541nm} = 13.5 and ε_{576nm} = 14.6 for oxyHb, and ε_{555nm} = 12.5 for deoxyHb (72).

3.2.3 CysNO preparation

One volume of 200 mM cysteine in 1 N HCl was incubated at room temperature in the dark with 1 volume of equimolar sodium nitrite in water for 5 min. The pH of the resultant CysNO solution was adjusted to 7.4 with 2 volumes of 1 M sodium phosphate buffer (pH 7.4)/100 μM DTPA (73).

3.2.4 HbSNO preparation

OxyHb in 100 mM tetraborate buffer (pH 9.2)/100 μM DTPA was exposed to 10-fold molar excess CysNO for 30 min at room temperature in the dark. A 10-μL aliquot was diluted with 1 mL of water, and 3 μL was injected into a capillary high-performance liquid chromatography HPLC/MS system (QTOF 2, Waters) to confirm HbSNO formation. The α- and β-globin subunits were separated on a 0.18x23.5-mm C_{18} column (Symmetry 300, 5 μm, Waters) with a linear gradient of 10 to 90% B over 18 min and 90% B for 10 min at a flow rate of 1 μL/min. Mobile phases A and B were 0.1% formic acid in water and acetonitrile (ACN), respectively. The pump output was split to direct 100 nL/min into the Z-spray ion source of the mass spectrometer. The source block temperature was 80°C and the voltage settings were as follows: 3.4 kV (capillary), 40 V (cone), 10 V (collision), -9.1 kV (ToF), and 2.2 kV (MCP). The scan range was m/z 50–2100, and data analysis was performed using MassLynx 4.0 software. Following confirmation of Hb *S*-nitrosation, the sample was desalted on a 2x20-cm G-25 column equilibrated with 200 mM sodium phosphate buffer (pH 7.4)/100 μM DTPA, and the HbSNO yield was determined by the modified Saville assay as described in section 3.2.7.

3.2.5 Preparation of nitrite/deoxyHb incubations

Stock solutions of 40 μM–12 mM sodium nitrite in water were degassed and placed in the glove box under N_2. DeoxyHb (400 μM or 3 mM) in 200 mM phosphate buffer (pH 7.4)/100 μM DTPA was incubated with sodium nitrite at 1:400, 1:40 and 1:1 (nitrite:heme) ratios for 15 min to 2 h in the glove box. The visible spectra of the incubations and the HbSNO yields were measured (section 3.2.6) prior to aeration. The samples were removed from the glove box, vortexed in air for 10 min, and the spectra and HbSNO yields were remeasured.

3.2.6 Visible absorption of equimolar nitrite/Hb incubations

A 10-μL aliquot was removed from an incubation containing equimolar nitrite and heme, and was loaded by syringe onto a 13x2-mm CaF_2 window of a dismountable FTIR-type cell (Harrick) in the glove box under N_2. The cell was immediately assembled using a 6-μm Teflon spacer (Harrick) and placed in a custom-made bracket in a Beckman DU 800 UV-visible spectrophotometer and the spectrum was recorded. Following oxygenation of the incubate, the spectrum was recorded in a similar manner but the cell was assembled outside the glovebox. Multicomponent analysis of the optical spectra was performed using a program available at www.1728.com/indexalg.htm and the previously recorded basis spectra of metHb, deoxyHb, nitrosylHb and oxyHb (49).

3.2.7 Modified Saville assay

The determination of low micromolar and submicromolar HbSNO in a millimolar Hb sample represents a challenging analytical problem. The methods used are based on

the well-known Saville assay for RSNOs (71, 73-75), which involves addition of mercuric chloride to cleave the S-NO bond. This results in the formation of nitrite, which is derivatized to an azo dye for colorimetric detection (Scheme 3.1), a fluorescent triazole for fluorescence detection (73, 75, 76) or reduced to NO for chemiluminescence detection (77, 78). The colorimetric method, the basis of the original Saville assay, has a limit of detection (LOD) > 1 μM (71, 79) whereas chemiluminescence methods can detect 1 nM HbSNO (67). In the present study, an LOD of 100 nM was required, so the colorimetric Saville assay was modified to increase the sensitivity and to decrease the multiple interferences from the high (250–400 μM) Hb concentrations used in the incubations (28, 53). The concentration of sulfanilamide, which traps the nitrite released from RSNO (Scheme 3.1), was increased two-fold to compete with Hb for free nitrite (71). Solid-phase extraction of the azo dye coupled with HPLC and mass spectrometric detection increased the sensitivity and removed the possible interferences. These modifications to the standard Saville assay decreased the LOD to ~ 50 nM a factor of 20 lower than that normally achieved using colorimetric detection.

3.2.8 Diazotization with the Griess reagent

The Griess reagent [20 μL of 15% sulfanilamide in 2.2 N HCl and 20 μL of 0.36% *N*-(1-naphthyl)ethylenediamine in 0.4 N HCl; Scheme 3.1], was added to 100-μL solutions of nitrite, GSNO, or HbSNO, and the samples were incubated at room temperature for 25 min. GSNO and HbSNO incubations were run with and without the addition of 10 μL of 70 mM $HgCl_2$ (in water) to cleave the S-N bond and generate free nitrite (71). To precipitate Hb, 40 μL of 142% (w/v) TCA was added, and after 5 min the

samples were centrifuged at 12,000 rpm for 2 min. The supernatants were loaded on an AccuBond^{II} Octadecyl C_{18} cartridge preconditioned with 1.0 mL of 50% (v/v) methanol/water, and washed with 5% ammonium hydroxide in water. The azo dye (Scheme 3.1) was eluted with 5% ammonium hydroxide in methanol and lyophilized with a Speed Vac (Savant, Model SC110) at 43°C. Following reconstitution in 1 M HCl, the samples were analyzed by HPLC/UV/MS.

3.2.9 HPLC/UV/MS of the azo dye

Analysis was carried out with an Agilent 1090 HPLC equipped with a diode-array detector set at 532 nm and interfaced to a ThermoFinnigan SSQ 7000 mass spectrometer. Samples (20 μL) in 1 M HCl were loaded onto a 4.6x150-mm C_{18} column (Eclipse XDB; 5 μm; Agilent) equilibrated with mobile phase A. Separation of the azo dye from the reagents was effected with a gradient of 10-30% B over 20 min at a flow rate of 1 mL/min where mobile phases A and B consisted of 0.5% formic acid in water and acetonitrile, respectively. The HPLC eluate was split and directly introduced into the ESI source of the mass spectrometer (Thermo Finnigan SSQ 7000) at a flow rate of 20-30 μL/min. A spray voltage of +4.0 kV, a capillary temperature of 250°C, and a sheath-gas pressure of 35 psi were maintained during the analysis. Mass calibration was carried out using horse skeletal muscle apomyoglobin and MRFA as external reference compounds. The mass accuracy and resolution of the instrument were 300 ppm and 600, respectively. Spectra were scanned over a range of 150-500 m/z at 3 s/scan, and quantitation of the azo dye was performed in single-ion monitoring (SIM) mode by measuring peak areas of the

MH^+ ion of the azo dye at m/z 370. Peak areas of samples without $HgCl_2$ were subtracted from those with $HgCl_2$ for GSNO and HbSNO quantification (Scheme 3.1).

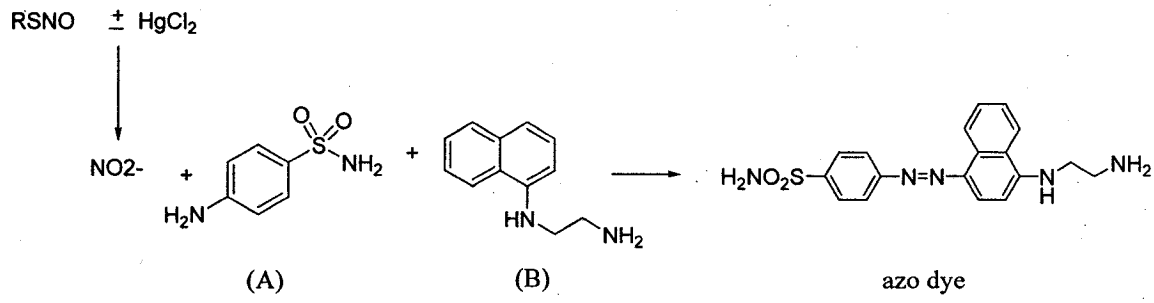

Scheme 3.1. The Saville assay. RSNOs (HbSNO or GSNO) were decomposed with mercuric chloride to yield NO_2^-, which is trapped with sulfanilamide (A) and converted on reaction with *N*-(1-naphthyl)ethylenediamine (B) to the azo dye. The latter has a visible absorption maximum at 532 nm and its MH^+ ion appears at m/z 370 in the ESI mass spectrum.

3.3 Results

3.3.1 Visible absorption spectra of equimolar nitrite/deoxyHb incubations

After 5 minutes incubation of 3 mM deoxyHb at nitrite:heme ratio of 1:1, the deoxyHb band at 555 nm disappeared and three new bands appeared at 545, 575 and 630 nm (Figure 3.1), indicating the formation of nitrosylHb and metHb (49, 72). Multicomponent analysis (49) revealed that 0% deoxyHb, 52% nitrosylHb and 48% metHb were present, consistent with nitrite reduction by one Fe^{II} heme (eq 3.1) and the trapping of the NO formed at a second Fe^{II} heme to give nitrosylHb (eq 3.2). Since equimolar nitrite and heme were present in the incubation, the maximum theoretical yield of nitrosylHb is 50% since two Fe^{II} hemes are required to form nitrosylHb from nitrite via reactions (3.1) and (3.2). Thus, the observed yield of 52% indicates full conversion of

NO_2^- to NO within 5 min as expected since a half-life of 31 s is expected for reaction (3.1) under the experimental conditions in Figure 3.1 based on the published bimolecular rate constant of 2.69 $M^{-1}s^{-1}$ (45).

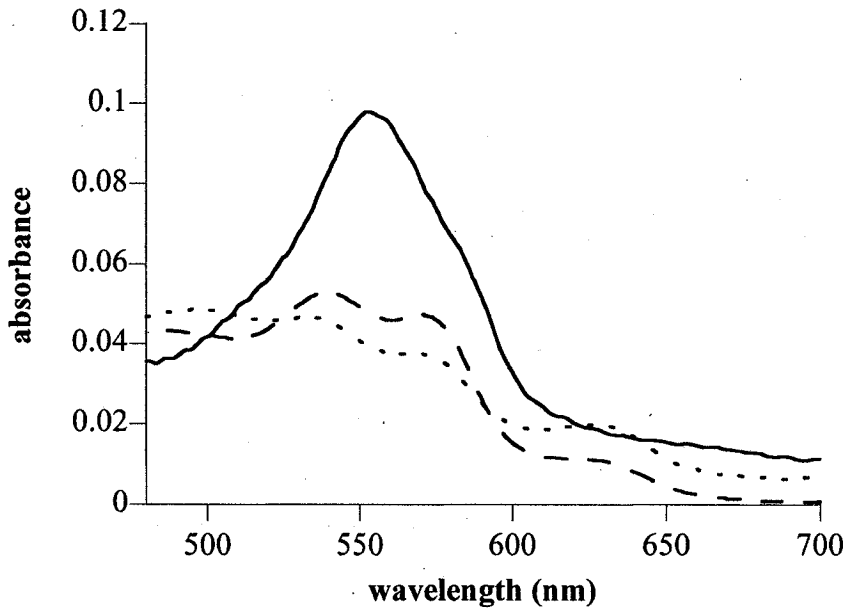

Figure 3.1. Effect of aeration on the visible absorption spectra of an equimolar nitrite/deoxyHb incubation. Spectrum of 3 mM deoxyHb before (—), and after incubation with 12 mM nitrite for 5 min (- - -), and after vortexing in air for 10 min (·····). All spectra were recorded in 200 mM sodium phosphate buffer (pH 7.4)/100μM DTPA at room temperature in a FTIR type cell with a 6-μm spacer.

Air was added to determine its effect on the spectrum. The nitrosylHb bands at 545 and 575 nm decreased in intensity while the band at 630 nm increased, and a band appeared at 500 nm (Figure 3.1). These spectral changes indicate the conversion of nitrosylHb to metHb on reaction of O_2 with the heme-bound NO (eq 3.4). Multicomponent analysis (49) revealed that 5% nitrosylHb and 95% metHb were present 20 min after aeration due to reaction (3.4), which has a reported rate constant of 2 x 10^{-4} s^{-1} (59).

$$\text{nitrosylHb} + O_2 \rightarrow \text{metHb} + NO_3^- \qquad (3.4)$$

Gow and Stamler (28) demonstrated efficient NO transfer from the heme to Cysβ93 (equation 3.3) upon oxygenation of NO/deoxyHb incubations at physiological (~1:400) but not at high (>1:4) NO:heme ratios. Absorption spectroscopy is not sufficiently sensitive to measure formation and decay of 0.25% nitrosylHb or to probe HbSNO formation. Hence, the Saville assay (71) was modified to provide a sensitive method to quantify HbSNO formed in the incubations.

3.3.2 Validation of the modified Saville assay

Typical MS and UV chromatograms of the azo dye obtained after nitrite derivatization with the Griess reagent are presented in Figure 3.2. The dye appears in the chromatogram at 14 min, and there was no interference from the excess Griess reagents, *N*-(1-naphthyl)ethylenediamine (retention time: 12.5 min, not shown) or sulfanilamide (retention time: 2.4 min, not shown), under our experimental conditions. Calibration curves were generated using known quantities of nitrite and GSNO. As illustrated in Figure 3.3, the nitrite and GSNO readings fall on the same line. A HbSNO standard was synthesized by oxyHb incubation with excess CysNO. ESI/MS analysis confirmed formation of HbSNO by β-globin *S*-nitrosation (80, 81) since the β-globin had a mass shift of +29 (*m/z* 15896) with respect to the native globin (*m/z* 15867) (Figure 3.4A) but the α-chain was unmodified. Using the modified Saville assay, we determined that the reaction of 10 μM oxyHb with 100 μM CysNO for 30 min yielded 2.30±0.05 μM

nitrosated Hb whereas the buffer and oxyHb alone contained no detectable HbSNO (Figure 3.4B). The negative value in this figure for the HbSNO concentrations in buffer and in the oxyHb sample alone are due to mercury binding to nitrite. HbSNO dilutions were prepared in the presence of excess oxyHb and analyzed by the modified Saville assay. The HbSNO concentrations fall on the GSNO and nitrite calibration curves (Figure 3.3), which demonstrates that GSNO standards can be used to determine HbSNO concentration in the presence of excess oxyHb.

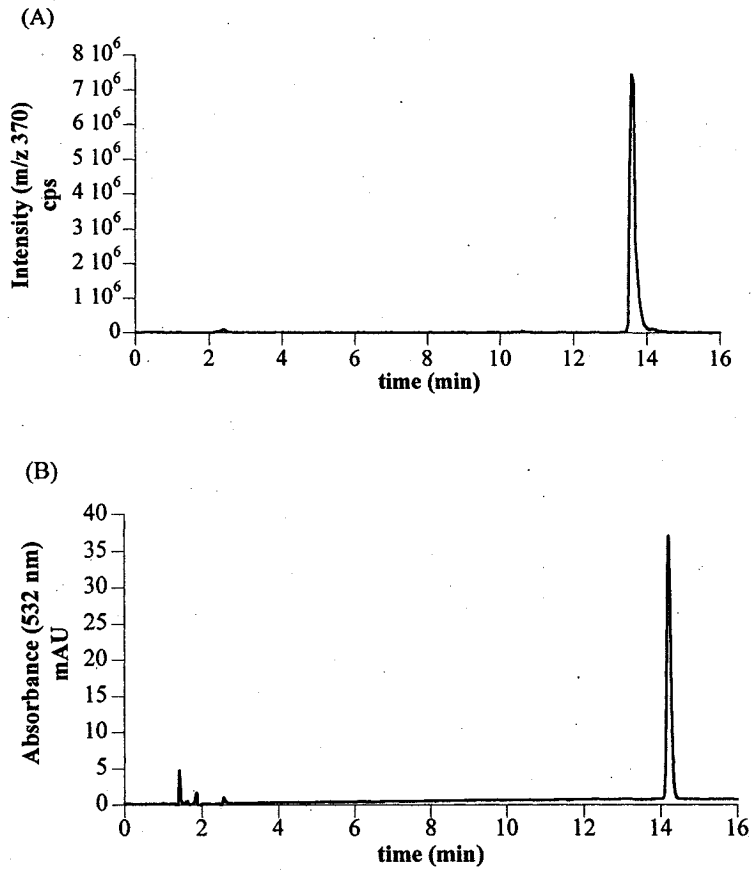

Figure 3.2. HPLC/UV/MS of nitrite derivatization. HPLC of the azo dye following derivatization of 20 μM nitrite with the Griess reagent (Scheme 3.1). (A) mass spectrometric detection with SIM at m/z 370; (B) UV detection at 532 nm.

The LOD for the modified Saville assay with HPLC/UV detection is 50 nM HbSNO.

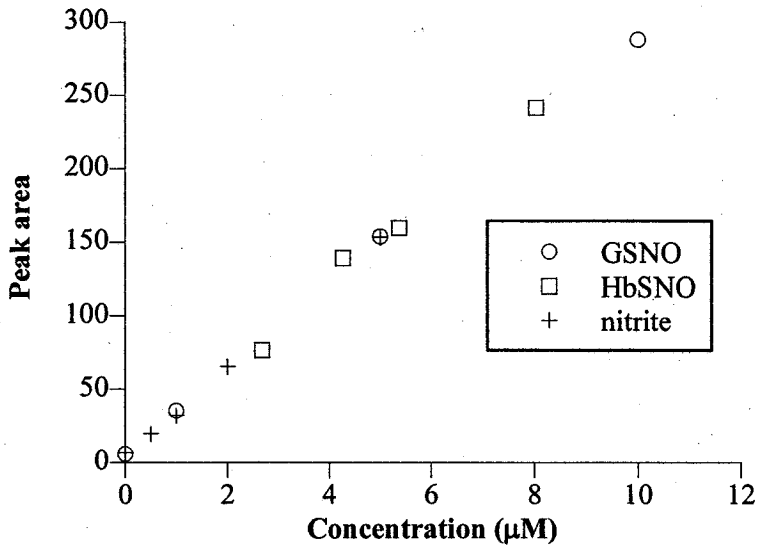

Figure 3.3. Nitrite, GSNO and HbSNO calibration curves. Calibration curve of 0.5—10 μM nitrite (+), GSNO (○), and 2.5 - 8.5 μM HbSNO in the presence of 60 μM oxyHb (□). The y-axis gives the peak areas of the azo dye analyzed by HPLC/UV at 532 nm (Figure 3.2.B).

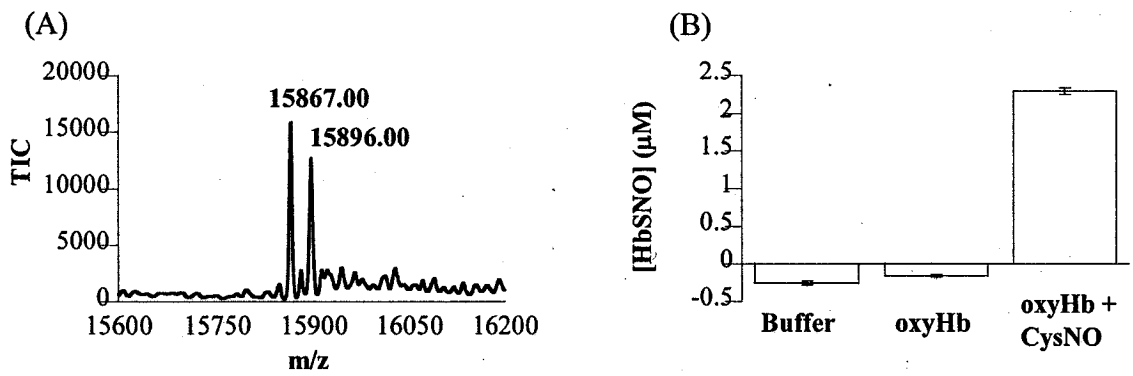

Figure 3.4. Qualitative and quantitative analysis of HbSNO formation. (A) ESI mass spectrum following incubation of 170 μM oxyHb with 1.7 mM CysNO at room temperature for 15 min. Prior to MS analysis, the sample was diluted 100-fold with water, and 3 μL was injected into the HPLC/MS as described in Section 3.2.4. (B) Quantitation of HbSNO. OxyHb (10 μM) was incubated ± 100 μM CysNO for 30 min at room temperature, and the HbSNO concentration was determined by the modified Saville assay (n = 3).

The coefficient of variation is 8.3 and 5.4% for intra- and interassay precision, respectively. The HbSNO standard was found to be stable at -80°C for >8 days. A similar LOD was obtained by Herold and Roch using a modified Saville assay with colorimetric detection (51), but their methodology used large sample volumes and low Hb concentrations (500 μL and 50 μM) compared to the method developed in the present study.

3.3.3 NO is transferred to Cysβ93 on oxygenation of nitrite/deoxyHb incubates

The HbSNO concentration was determined in nitrite/deoxyHb incubations (nitrite:heme 1:400) to establish the extent of nitrite-to-Cysβ93 NO transfer under physiological conditions.

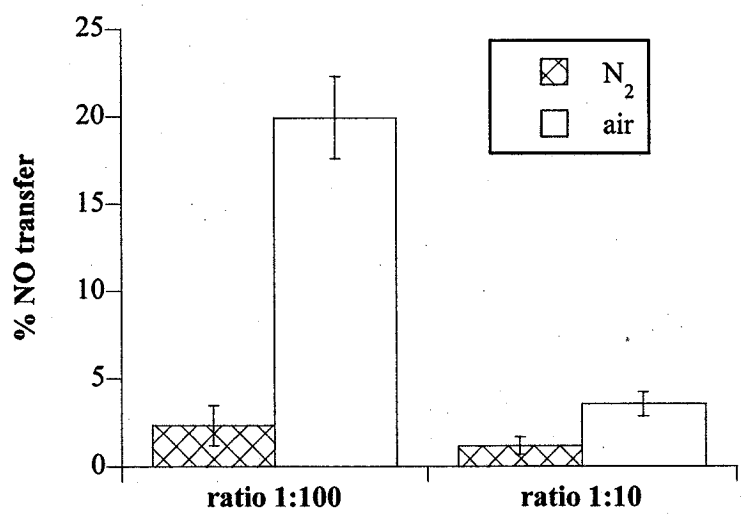

Figure 3.5. Formation of HbSNO in nitrite/deoxyHb incubations at two nitrite concentrations. DeoxyHb (363 μM) was incubated for 20 min at room temperature with 3.6 μM nitrite (1:400; nitrite:heme) or with 36 μM nitrite (1:40 nitrite:heme) in 200 mM sodium phosphate buffer (pH 7.4)/100 μM DTPA in a glove box under N_2 (☒). Samples were then vortexed in air for 10 min at room temperature (☐), and HbSNO concentrations were determined by the modified Saville assay (n = 3). The %NO transfer corresponds to the percent nitrite converted to HbSNO in the incubation.

The detection of 83 nM HbSNO in the anaerobic incubations reveals that only 2% of the nitrite was converted to HbSNO whereas the yield increased to 20% on oxygenation (Figure 3.5).

Gow and Stamler demonstrated that the efficiency of NO transfer to Cysβ93 on oxygenation of NO/deoxyHb incubations increases inversely with the NO:Hb ratio and was optimal when the NO concentration was close to physiological values (nanomolar range) (7, 28). Figure 3.5 reveals similar behavior in the nitrite/deoxyHb incubations since the transfer efficiency dropped to 4% when the nitrite:heme ratio was increased 10-fold.

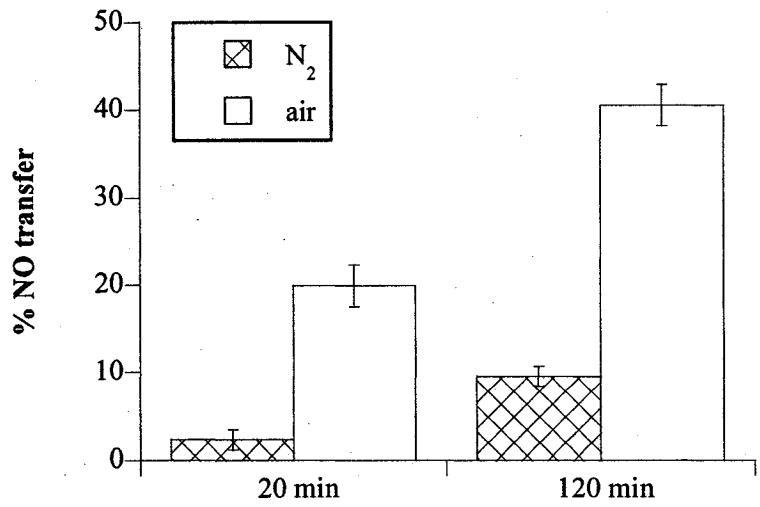

Figure 3.6. Formation of HbSNO in nitrite/deoxyHb incubations versus time. DeoxyHb (363 μM) was incubated for 20 min or 2 h at room temperature with 3.6 μM nitrite (1:400 nitrite:heme) in 200 mM sodium phosphate buffer (pH 7.4)/100 μM DTPA in a glove box under N_2 (☒). Samples were then vortexed in air for 10 min at room temperature (☐), and HbSNO concentrations were determined by the modified Saville (n = 3). The %NO transfer corresponds to the percent nitrite converted to HbSNO in the incubation.

Thus, the oxygen-induced conversion of nitrosylHb to HbSNO likely occurs by a similar mechanism whether NO gas or nitrite is initially added to deoxyHb. Figure 3.6 shows that nitrite incubation with deoxyHb for 2 h more than doubled the HbSNO yield compared to that observed after 20 min in both the anaerobic and aerobic samples.

Following oxygenation, 41% of the nitrite was converted to HbSNO after 2 h incubation versus 20% after 20 min incubation. Since the HbSNO yield increases with the length of anaerobic incubation, nitrite reduction by deoxyHb (eq 3.1) is likely the rate-limiting step in HbSNO formation and not a reaction that occurs on oxygenation.

3.3.4 Effects of metHb on NO transfer

Since metHb binds nitrite (K_d = 4.48 mM) (27), the Fe^{III} heme generated in reaction (3.1) may slow down the formation of HbSNO. This was confirmed by adding metHb to the incubation, which decreased the NO transfer yield in a dose-dependent manner from 15% to ~8% and ~3%, respectively (Figure 3.7).

The competitive effects of metHb generated *in situ* by reactions (3.1) and (3.4) can be inhibited by adding a strong ferric heme ligand. Thus, KCN was added to the incubations since CN^- binds more strongly (K_d = 3.3 nM) (82) than nitrite to metHb and is a poor ligand for deoxyHb (K_d = 1 M) (83). In sharp contrast to the effects of exogenous metHb, the presence of 4 μM KCN allowed 46% of the nitrite present to be converted to HbSNO (Figure 3.8).

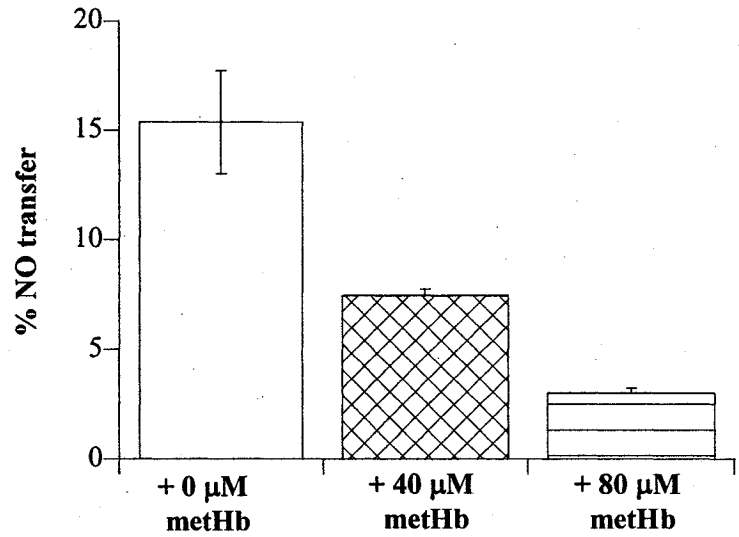

Figure 3.7. Effects of metHb on the formation of HbSNO following oxygenation of nitrite/deoxyHb incubations. DeoxyHb (363 μM) was incubated for 15 min at room temperature with 3.6 μM nitrite (1:400 nitrite:heme) and 0 (☐), 40 (☒) or 80 μM metHb (▤), and the samples were vortexed in air for 10 min. HbSNO concentrations were determined by the modified Saville assay (n = 3). The %NO transfer corresponds to the percent nitrite converted to HbSNO in the incubation.

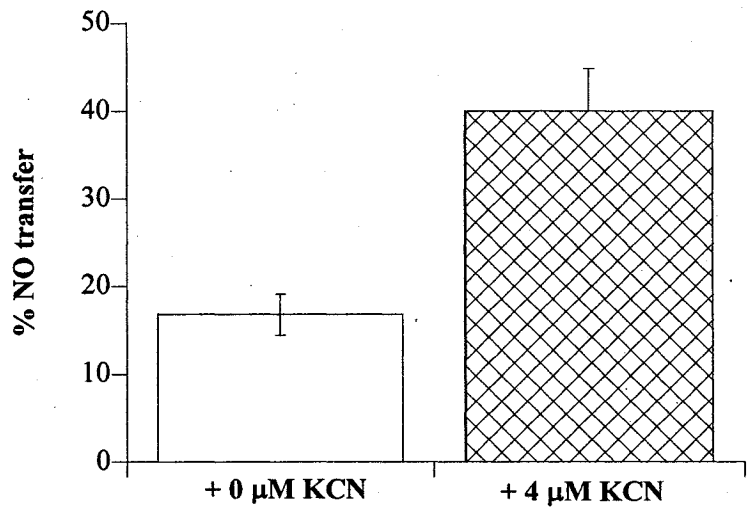

Figure 3.8. Effects of KCN on HbSNO formation following oxygenation of nitrite/deoxyHb incubations. DeoxyHb (363 μM) was incubated for 15 min at room temperature with 3.6μM nitrite (1:400 nitrite:heme) and 0 (☐) or 4 μM KCN (☒), and the samples were vortexed in air for 10 min. HbSNO concentrations were determined by the modified Saville assay (n = 3). The %NO transfer corresponds to the percent nitrite converted to HbSNO in the incubation.

3.4 Discussion

RBCs provide NO vasodilator activity in a Hb-mediated, O_2-responsive manner (7, 61). However, the mechanism(s) of NO storage within the RBC and the release of its vasoactivity to tissues are not well understood. The principal storage forms of NO considered to date are GSNO, nitrite, HbSNO, and nitrosylHb (5, 7, 49, 67). Cosby *et al.* reported that RBCs concentrate nitrite to 0.15—1.0 μM and have observed nitrite-induced vasodilation in humans associated with reduction of nitrite to NO (12). Here we demonstrated *in vitro* that the nitrite store can be converted to nitrosylHb and HbSNO under close to physiological conditions (nitrite:Hb ratio; 1:100).

NO released from nitrite on its reduction by excess deoxyHb (eq 3.2) is trapped as nitrosylHb and, following oxygenation, the heme-bound NO is transferred to Cysβ93 to form HbSNO. The rate of HbSNO production is controlled by the rate of nitrite reduction by deoxyHb, which has a bimolecular rate constant of 0.2—2.69 $M^{-1}s^{-1}$ at 25°C and pH 7 (12, 45, 50). Thus, with ~10 mM Fe^{II} heme in the RBC around the P_{50} of Hb (61), the half-life for nitrite reduction would be ~37–500 s based on the published bimolecular rate constants. Only 0.5–6% of *free* RBC nitrite would be converted to NO within 5 s, which may be sufficient to trigger the fast phase of hypoxic vasodilation given that very low NO levels (nanomolar range) are needed for vasodilation (7, 12).

Importantly, we show here that metHb is highly effective at inhibiting the conversion of nitrite to HbSNO (Figures 3.6 and 3.7). The NADH-cytochrome b_5 metHb reductase system of the RBC reduces metHb to deoxyHb so that normally ≤1% of Hb is present in the ferric form (47). However, 1% of the 5 mM Hb found in RBCs corresponds to 200 μM Fe^{III} heme, which is significantly higher than the concentration found to

inhibit NO transfer (Figure 3.7). MetHb concentrations may vary throughout the RBC to promote localized nitrite turnover, and we propose that nitrite scavenging by metHb may play a regulatory role *in vivo*. In this context, one of the effects of cyanide poisoning is an immediate and progressive sense of warmth induced by vasodilation (84). This could be due in part to a dramatic increase in HbSNO formation as seen in Figure 3.8 in the presence of 4 μM KCN.

Stamler and coworkers have proposed that nitrosylmetHb is a precursor to HbSNO (53). Our results suggest a metHb-independent pathway of Cysβ93 S-nitrosation since addition of the strong ferric heme ligand CN^-, which blocks Fe^{III} heme, increases the production of HbSNO. NO produced in nitrite/deoxyHb incubations with excess deoxyHb will most likely be in the nitrosylHb (K_d = 3.75 pM) (54, 85) form rather that the nitrosylmetHb (K_d = 0.2 mM) form (51). Herold and Roch examined oxygenation of nitrosylHb in the presence of low concentrations of metHb and found that addition of KCN to the incubations resulted in no change in HbSNO formation (51). This indicates that metHb is not involved in HbSNO formation from nitrosylHb which does not involve nitrite reduction.

Our results highlight differences between NO/deoxyHb (or nitrosylHb) and nitrite/deoxyHb as storage forms of NO. Oxygenation of the former leads to a transfer efficiency of 80% (28) versus the maximum of ~46% observed here (Figure 3.6). This can be attributed to $>10^7$-fold faster rate for the reaction of deoxyHb with NO ($6x10^7$ M^{-1} s^{-1}) (86) versus nitrite (0.2—2.69 M^{-1} s^{-1}) (45). Also, nitrite binds to metHb (154 $M^{-1}s^{-1}$) (27) 60—800 fold faster that it reacts with deoxyHb so that binding to the ferric heme additionally slows down nitrite reduction. Also, systematic studies carried out by Herold

and Roch on oxygenation of nitrosylHb revealed that the following factors can modify the HbSNO yield: heme:NO ratio, phosphate buffer concentration, and rate of NO addition, which makes comparisons between the various studies more difficult (51).

Stamler and coworkers demonstrated that 80% of HbSNO is associated with the RBC membrane under physiological conditions (63). This would allow rapid NO transfer from Cysβ93 to thiols in the major RBC membrane protein AE1 (87), and the release of NO vasoactivity from the RBC. Furthermore, since it binds deoxyHb (12), AE1 is likely a major site of nitrite reduction in the RBC membrane. These considerations suggest that other NO stores must be converted to HbSNO prior to release of NO vasoactivity from the RBC. GSNO, which is also present in the RBC, and which we have shown to be an efficient NO donor to Cysβ93 of oxyHb in the presence of CuZnSOD *in vitro* (48, 49), may also generate HbSNO in RBCs, imparting redundancy to the system.

In summary, we have confirmed that oxygenation drives the formation of HbSNO from nitrite. NO produced by the proposed nitrite reductase activity of deoxyHb, which is maximal at the P_{50} of Hb (61), is converted to HbSNO via a nitrosylHb intermediate. MetHb may play a regulatory role, limiting the amount of free non-Hb-bound nitrite within the RBC to prevent hypotension.

4.0 Mechanistic insights into NO transfer in hemoglobin from the ferrous heme to Cysβ93, a life-saving switch

4.1 Introduction

Several *in vivo* studies have shown that HbSNO and nitrosylHb concentrations change with oxygen saturation. For example, a gain in O_2 increases the HbSNO concentration and decreases the nitrosylHb concentration (68, 69, 88, 89). These results have been associated with the O_2-induced transfer of NO from the heme of nitrosylHb to the Cysβ93 but the detailed mechanism of the NO switch has not yet been elucidated. Gow and Stamler have demonstrated that HbSNO is also formed on oxygenation of partially nitrosylated Hb *in vitro* and the HbSNO yield increases to 80% at close to physiological ratios of NO to Hb (28). An important role has been proposed for the T→R allosteric transition of Hb (47) since Cysβ93 is brought into close proximity with the β-heme in the R-structure, which should promote NO transfer from the heme to the thiol. This NO switch also requires NO/NO^+ redox cycling because NO is bound to the Fe^{II} hemes whereas NO^+ binds to the Cysβ93 thiolates. The electron acceptor in the redox cycling may be a ferric heme, trace metal impurity, oxygen, or another organic acceptor such as nicotinamide adenine dinucleotide (90).

Previous studies point to oxygen as the electron acceptor (28, 90), and the mechanisms proposed involve a $HbSN^{\cdot}$-OH (eqs 4.1 and 4.2) (91) or a NO^+ intermediate (eqs 4.3 and 4.4) (92):

$$HbSH + NO^{\cdot} \rightarrow HbSN^{\cdot}\text{-}OH \qquad (4.1)$$

$$HbSN^{\cdot}\text{-}OH + O_2 \rightarrow HbSN{=}O + O_2^{\cdot -} + H^+ \qquad (4.2)$$

$$NO + O_2 \rightarrow NO^+ + O_2^{\cdot-} \quad (4.3)$$

$$NO^+ + HbSH \rightarrow HbSNO + H^+ \quad (4.4)$$

HbSNO and superoxide ($O_2^{\cdot-}$) are generated in both mechanisms. In Chapter 3, we have shown that HbSNO can be formed by the reaction of nitrite with deoxyHb followed by oxygenation. This reaction was further examined here to elucidate the mechanism of the NO switch. The effects of replacing oxygen with carbon monoxide (CO), and of adding CuZnSOD, catalase, or hydrogen peroxide were investigated.

4.2 Materials and methods

4.2.1 Materials

Human Hb, sulfanilamide, *N*-(1-naphthyl)ethylenediamine, mercuric chloride, catalase and trichloroacetic acid (TCA) were purchased from Sigma. Sodium nitrite and formic acid were obtained from Anachemia. Sodium dithionate ($Na_2S_2O_4$), sodium phosphate salts and all solvents were obtained from Fisher Scientific. Diethylenetriamine pentaacetic acid (DTPA) was obtained from ICN Pharmaceuticals. *S*-nitroso-*L*-glutathione (GSNO) was obtained from Calbiochem. Hydrogen peroxide was obtained from APC. CuZnSOD was obtained from Roche. Nanopure water (specific resistance, 18 MΩ-cm) obtained from a Millipore Simplicity water purification system was used to prepare all H_2O solutions. Nitrogen and carbon monoxide gas were obtained from Praxair. Sephadex G-25 was obtained from Pharmacia. AccuBond^{II} Octadecyl (C18) SPE (solid phase extraction) (100 mg) was obtained from Agilent.

4.2.2 Hb Preparation

Lyophilized metHb from the bottle was dissolved in 200 mM phosphate buffer (pH 7.4) ± 100 μM DTPA. The chelating agent DTPA was used in all incubations except when CuZnSOD and catalase were present. DeoxyHb was prepared a the glove box (MBraun, Model MB-OX-SE1) by treating metHb with 50 mg sodium dithionite followed by desalting on a Sephadex G-25 column. DeoxyHb concentration was determined spectrophotometrically using ε_{555nm} = 12.5 mM^{-1} cm^{-1} per heme group (72).

4.2.3 Reaction of nitrite with deoxyHb followed by O_2 or CO

A stock solution of 40 μM $NaNO_2$ in water was prepared, degassed under nitrogen, and placed in the glove box. DeoxyHb (400 μM) in 200 mM phosphate buffer (pH 7.4) with or witout 100 μM DTPA was incubated with $NaNO_2$ at a heme to nitrite ratio of 400:1 for 15 min inside the glove box. Where indicated, 3.2 μM CuZnSOD, 0.4 μM catalase or 40—400 μM hydrogen peroxide was added to the incubation. The sample was removed from the glove box, unsealed, vortexed in air, or under carbon monoxide atmosphere (carbon monoxide from a cylinder was added by syringe) for 10 min, and the HbSNO yield was measured using the modified Saville assay (Section 4.2.4).

4.2.4 Diazotization with the Griess reagent

GSNO and HbSNO solutions (100 μL) were incubated with 40 μL of the Griess reagent (20 μL of 15% sulfanilamide in 2.2 N HCl and 20 μL of 0.36% *N*-(1-naphthyl)ethylenediamine in 0.4 N HCl) for 25 min wit or without 10 μL of 70 mM $HgCl_2$ in water. To precipitate the proteins, 40 μL of 142% (w/v) TCA was added, and

after 5 min the samples were centrifuged at 12,000 rpm for 2 min. The supernatants were loaded on an AccuBond^{II} Octadecyl C_{18} cartridge preconditioned with 1.0 mL of 50% methanol/water, and washed with 5% ammonium hydroxide in water. The azo dye was eluted with 5% ammonium hydroxide in methanol and lyophilized by Speed Vac (Savant, Model SC110) at 43°C. Following reconstitution in 1 M HCl, the samples were analyzed by HPLC/UV.

4.2.5 HPLC/UV of the azo dye

Analysis was carried out with Agilent 1100 HPLC equipped with a diode-array detector set at 532 nm (10 mm cell pathlength). Samples (20 μL) in 1 M HCl were loaded onto a 4.6x150-mm C_{18} column (Eclipse XDB; 5 μm; Agilent) equilibrated with mobile phase A. Separation of the azo dye from the reagents was effected with a gradient of 10—30% B over 20 min at a flow rate of 1 mL/min where mobile phases A and B consisted of 0.5% formic acid in water and in acetonitrile, respectively. Peak areas of samples without $HgCl_2$ were subtracted from those with $HgCl_2$ for GSNO and HbSNO quantification

4.3 Results

4.3.1 Effect of carbon monoxide on NO transfer

In Chapter 3, the importance of oxygen for HbSNO formation in nitrite/deoxyHb incubations was demonstrated. Under anaerobic conditions the HbSNO yield is only 2.3% based on the NO_2^- concentration while oxygenation of the incubation increases the HbSNO yield to 15%. This result reveals an important role for oxygen in the NO transfer.

Previous studies have proposed that the allosteric T → R transition of Hb promotes NO transfer from the heme to Cysβ93,(7, 12, 28, 67, 68, 88) because the thiol is brought into close proximity to the heme in the R structure. Oxygen is known to promote the T → R transition of Hb but other ligands also have this property. When deoxyHb combines with CO, it forms carboxyHb, which is bright red. CO binding promotes the T → R allosteric transition and the Hb binding affinity for CO is 300 times greater than its affinity for oxygen (47, 93). To demonstrate the importance of the allosteric transition on NO transfer, the effect of replacing O_2 with CO was investigated. Figure 4.1 shows that HbSNO yield decreases from 15 to 4% when O_2 is replaced by CO although CO promotes the T→R transition of Hb. This result indicates an additional role for oxygen in the NO transfer.

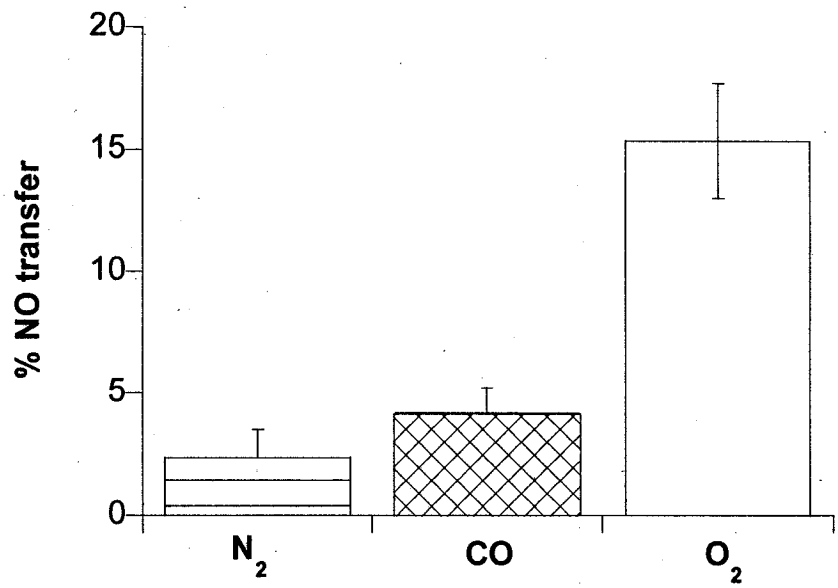

Figure 4.1. Effects of O_2 and CO on the formation of HbSNO in nitrite/deoxyHb incubations. DeoxyHb (363 μM) in 200 mM phosphate buffer (pH 7.4)/100 μM DTPA was incubated with 3.6 μM nitrite for 15 min inside the glove box. The sample was removed from the glove box and vortexed in air or CO was added by a syringe for 10 min at room temperature. HbSNO concentrations were determined by the modified Saville assay (n = 3). The %NO transfer corresponds to the percent nitrite converted to HbSNO in the incubation.

4.3.2 Effect of catalase and CuZnSOD on NO transfer

NO transfer between the Fe^{II} heme and Cysβ93 requires the allosteric transition of Hb but also NO/NO^+ redox cycling. As discussed in Section 4.1, oxygen has been proposed to act as the electron acceptor in this cycling (eq 4.5) (28, 90).

$$HbFe^{II}NO + O_2 \rightarrow HbSNO + O_2^{\cdot-} \qquad (4.5)$$

S-nitrosothiol and superoxide are generated in reaction 4.5. Superoxide can act both as an oxidant (by accepting electrons) or as a reductant (by donating electrons). However, superoxide is not particularly reactive in biological systems and does not cause much oxidative damage by itself. However, it is a precursor to other oxidizing agents such as hydrogen peroxide, peroxynitrite, and other highly reactive molecules. Thus, superoxide and superoxide-derived species can cause damage to Hb and compete with the formation of HbSNO (94). Under biological conditions, the main reaction of superoxide is to react with itself to produce hydrogen peroxide and oxygen, a reaction known as dismutation. Superoxide dismutation can be spontaneous or can be catalyzed by the enzyme, superoxide dismutase.

Figure 4.2 shows the effect of CuZnSOD on NO transfer. When added to the deoxyHb/nitrite incubation, CuZnSOD increases the HbSNO yield from 15% to 38%. CuZnSOD is ån extremely efficient enzyme; it catalyzes the dismutation of superoxide nearly as fast as the two can diffuse together spontaneously in solution. The mechanism of superoxide turnover by CuZnSOD is as follows:

$$Cu^{2+}ZnSOD + O_2^{\cdot-} \rightarrow Cu^{1+}ZnSOD + O_2 \quad (4.6)$$

$$Cu^{1+}ZnSOD + O_2^{\cdot-} + 2H^+ \rightarrow Cu^{2+}ZnSOD + H_2O_2 \quad (4.7)$$

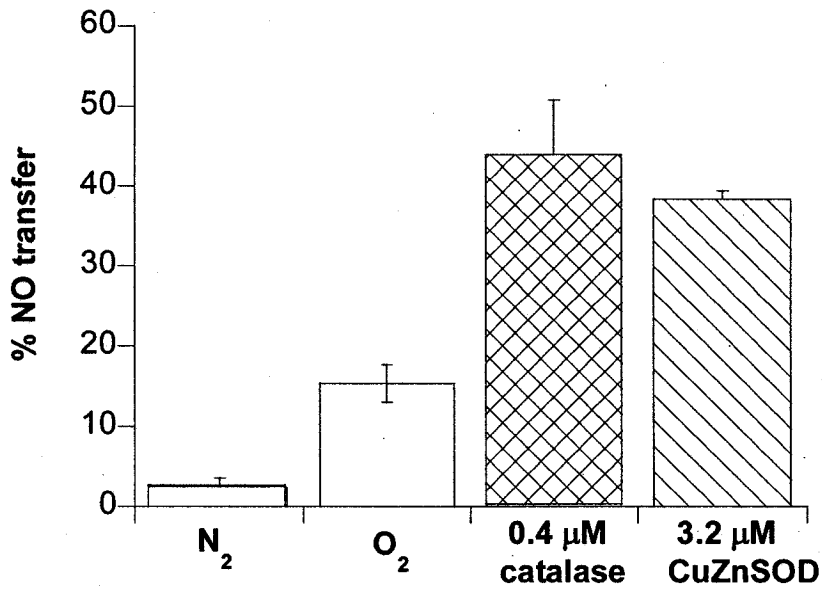

Figure 4.2. Effects of CuZnSOD and catalase on the formation of HbSNO following oxygenation of nitrite/deoxyHb incubations. DeoxyHb (363 µM) was incubated for 15 min at room temperature with 3.6 µM nitrite in 200 mM phosphate buffer (pH 7.4) inside the glove box and 3.2 µM CuZnSOD or 0.4 µM catalase were added. Oxygen was added to the solution for 10 min by vortexing in air at room temperature. HbSNO concentrations were determined by the modified Saville assay (n = 3). The %NO transfer corresponds to the percent nitrite converted to HbSNO in the incubation.

Hydrogen peroxide is known to have many side effects on Hb such as those described in Section 4.3.3 below. Catalase has one of the highest turnover rates of all enzymes (95); one molecule of catalase can convert 6 million molecules of hydrogen peroxide to water and oxygen per minute by the following mechanism (eqs 4.8 and 4.9):

$$H_2O_2 + Fe^{III}\text{-}E \rightarrow H_2O + O{=}Fe^{V}\text{-}E \quad (4.8)$$

$$H_2O_2 + O{=}Fe^{V}\text{-}E \rightarrow H_2O + Fe^{III}\text{-}E + O_2 \quad (4.9)$$

The addition of catalase to the deoxyHb/nitrite incubation increases the HbSNO yield transfer from 15% to 44% (Figure 4.2).

4.3.3 Effect of hydrogen peroxide on NO transfer

H_2O_2 is known to oxidize Hb which can generate potentially cytotoxic products such as the ferryl heme (Fe^{IV}), metHb, hemichromes, and free heme or iron (96). Addition of 40 μM and 400 μM hydrogen peroxide to the incubation decreased the HbSNO yield from 15% to 6% and 0%, respectively (Figure 4.3).

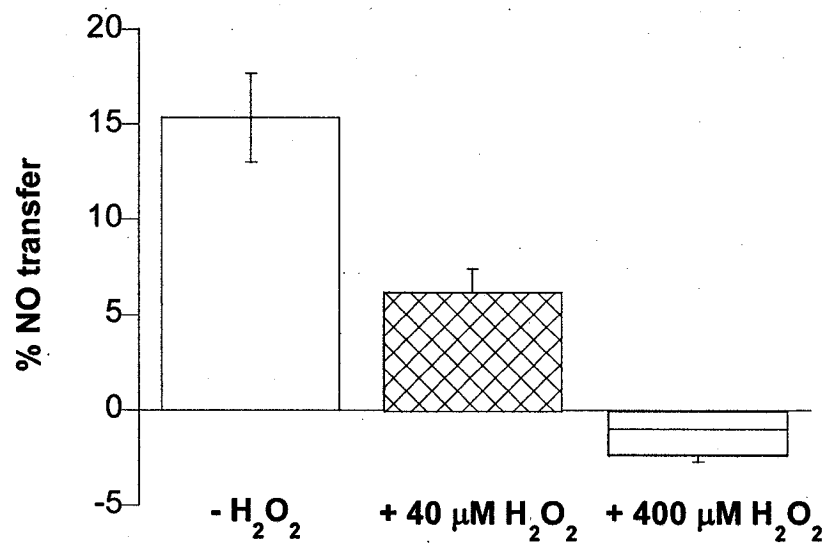

Figure 4.3. Effects of hydrogen peroxide on the formation of HbSNO following oxygenation of nitrite/deoxyHb incubations. DeoxyHb (363 μM) was incubated for 15 min at room temperature with 3.6 μM nitrite in 200 mM phosphate buffer (pH 7.4) inside the glove box and 0, 40 or 400 μM of hydrogen peroxide was added. Oxygen was added in the solution for 10min by vortexing in air at room temperature. HbSNO concentrations were determined by the modified Saville assay (n = 3). The %NO transfer corresponds to the percent nitrite converted to HbSNO in the incubation.

4.4 Discussion

The mechanism of HbSNO formation on oxygenation of deoxyHb/nitrite incubations is still under investigation. Nitrosation of biological thiols is believed to be mediated by N_2O_3, metal nitrosyl complexes, and peroxynitrite. Several pathways for HbSNO formation from nitrosylHb have been proposed. One pathway involves ·NO dissociation from partially heme nitrosylated Hb and its subsequent reaction with O_2 to form N_2O_3, which is known to nitrosate thiols (51). In this mechanism a high local concentration of NO is needed:

$$HbFe^{II}NO \rightarrow HbFe^{II} + NO\cdot \quad (4.10)$$

$$2\,NO + O_2 \rightarrow 2\,NO_2 \quad (4.11)$$

$$NO_2 + NO \rightarrow N_2O_3 \quad (4.12)$$

$$HbSH + N_2O_3 \rightarrow HbSNO \quad (4.13)$$

Other groups have postulated that nitrosylmetHb is the precursor to HbSNO (53, 97). NO^+ is proposed to dissociate from the heme of $HbFe^{II}NO^+$ and transfer to Cysβ93:

$$HbFe^{III}NO \rightleftharpoons HbFe^{II}NO^+ \quad (4.14)$$

$$HbFe^{II}NO^+ + O_2 \rightarrow \text{oxyHbSNO} \quad (4.15)$$

Our results are more consistent with a mechanism where oxygen acts both to promote the T→R transition of Hb and as electron acceptor to yield HbSNO and superoxide (eq 4.16 to 4.18) (28, 91, 92).

$$HbFe^{II}NO + O_2 \rightarrow HbFe^{II}NO^+ + O_2^{\cdot-} \quad (4.16)$$

$$HbFe^{II}NO^+ \rightleftharpoons oxyHb + NO^+ \quad (4.17)$$

$$NO^+ + oxyHbSH \rightarrow oxyHbSNO + H^+ \quad (4.18)$$

Superoxide generated in reaction 4.16 could start a cascade of oxidative reactions that lead to RBC-induced oxidative stress (94). Superoxide and hydrogen peroxide can promote hemichrome formation and heme oxidative degradation. Such reactions will compete with HbSNO formation as suggested by Figure 4.2 and 4.3.

Our results show the importance of antioxidant proteins in RBCs. Catalase and CuZnSOD are present in high concentrations in human RBCs and form a crucial part of the cellular antioxidant defense mechanism by protecting cells against the harmful effects of hydrogen peroxide and superoxide, respectively. The presence of CuZnSOD or catalase in the deoxyHb/nitrite incubation doubled the HbSNO yield. This increase in NO transfer is attributed to the suppression of side reactions of superoxide and hydrogen peroxide and also superoxide removal should drive NO transfer (eq 4.5). Consistent with reactive oxygen species (ROS) inducing side reactions, the addition of hydrogen peroxide to the deoxyHb/nitrite incubations decreased the HbSNO yield, confirming the negative effect of oxidative stress on NO transfer.

The results obtained in this study corroborate *in vivo* experiments which demonstrate that oxidative stress decreases nitrite-induced vasodilation (98). Attenuation of HbSNO levels by ROS as demonstrated in Figures 4.2 and 4.3 could be particularly detrimental during activity. Acute exercise training has been observed to increase plasma SOD activity and nitrite levels (98) which may be correlated to increased NO release

from RBCs by HbSNO. CuZnSOD may play multiple roles in vasorelaxation by protecting Hb from superoxide and ROS damage, and by increasing HbSNO formation from RBC NO_2^-. We have previously demonstrated that CuZnSOD promotes HbSNO formation via targeting of NO from GSNO to Cysβ93 of oxyHb (48).

5.0 Evaluation of sequential extraction and quantification of vasodilators in interstitial fluid dialysates

5.1 Introduction

The mechanism by which blood flow is regulated locally at the muscle-vascular interface to match oxygen delivery to the metabolic demands of tissues is not precisely known, especially during exercise. This is of importance in understanding the pathophysiological basis for impaired oxygen and nutrient supply in cardiovascular diseases. The putative mediators of muscle vasodilation during exercise, including adenosine, NO, prostaglandins, and EETs, are produced in endothelial cells in response to shear stress (1, 30). They are thought to increase and maintain blood flow during exercise but no single factor has been identified to constitute the primary metabolic regulator. Single or combined vasodilator blockade studies offer the potential to uncover synergistic interactions and compensatory responses amongst several substances in the regulation of exercise hyperemia. To date, most studies have reported only blood flow or alternatively the concentration of a single vasodilator during blockade interventions or vasodilator infusions (31, 99, 100). Measurements of multiple vasodilator concentrations in biological fluids during exercise could provide more insight into their mechanisms of action and interaction.

Microdialysis is a relatively new (*in vivo*) sampling method that is gaining popularity in muscle blood flow studies (101). This technique allows the quantitation of vasodilator concentrations close to their site of action (e.g., between the skeletal muscle and the endothelium-smooth muscle layer of vessels). However, because of the small

volumes of the microdialysate (5-100 μL), quantitation of more than one analyte per sample is challenging. In this study, we have developed a sequential extraction method that allows the separation of nitrite (an indicator of NOS activity), adenosine, and EETs from 50 μL of artificial interstitial fluid. After extraction, nitrite and EETs were analyzed by HPLC/fluorescence to achieve high sensitivity. Adenosine was analyzed by HPLC/MS/MS in order to achieve both high sensitivity and selectivity. The methodology was applied in the analysis of human microdialysates collected during knee extension exercises from five volunteers. Nitrite and adenosine were detected but EETs were below the level of detection. Approaches to extend the methodology for determination of analytes in biological fluids obtained from blockade and infusion experiments designed to uncover mechanisms of biochemical control of blood flow are discussed.

5.2 Materials and methods

5.2.1 Materials

Sodium nitrite, sodium tetraborate and formic acid (FA) were obtained from Anachemia. Adenosine, 2-chloroadenosine, 11,12-epoxyeicosatrienoic acid (11,12-EET), 14,15-epoxyeicosatrienoic acid (14,15-EET), 2,3-diaminonaphthalene (DAN), sodium citrate ($C_6H_5Na_3O_7$), magnesium chloride ($MgCl_2$), sodium sulfate (Na_2SO_4), calcium chloride ($CaCl_2$), and ammonium acetate were purchased from Sigma. 2′-O-(*N*-methylanthraniloyl) guanosine 3′,5′-cyclic monophosphate salt (MGCM), and 2-(2,3-naphthalimino)ethyl trifluoromethanesulfonate (NeOTF) were purchased from Molecular Probes Inc. Sodium acetate was obtained from Baker. *N,N* diisopropylethylamine,

hydrochloric acid, sodium chloride (NaCl), potassium chloride (KCl), dibasic sodium phosphate (Na_2HPO_4), sodium bicarbonate ($NaHCO_3$), acetonitrile (ACN) and methanol (MeOH, HPLC grade) were obtained from Fisher. Ethyl acetate was obtained from BDH. C_{18} cartridges were obtained from Agilent (Accubond C_{18}, 100 mg). Nanopure water (specific resistance, 18 MΩ-cm) obtained from a Millipore Simplicity water purification system was further purified on a strong anion-exchange cartridge (SAX, Agilent, 100 mg).

5.2.2 Artificial interstitial fluid

Interstitial fluid is mostly blood plasma minus most of the proteins. Microdialysis probes with 20 kDa cut-off are used to collect the interstitial fluid and remove large molecules. The microdialysate analyzed in this study contained small molecules and electrolytes. Artificial interstitial fluid with a pH of 7.4 was prepared to mimic the human muscle dialysate by dissolving in 1 L of water with the following salts at the final concentrations given: 0.1 M NaCl, 4.0 mM KCl, 1.0 mM Na_2HPO_4, 0.5 mM Na_2SO_4, 2.5 mM $CaCl_2$, 7.0 mM CH_3COONa, 31 mM $NaHCO_3$, 0.3 mM $C_6H_5Na_3O_7$, and 1.0 mM $MgCl_2$ (102, 103).

5.2.3 Analyte extraction method

A standard solution was prepared by spiking the artificial interstitial fluid (40 μL) with known concentrations of EETs, nitrite, and adenosine. A 50-μL aliquot of 100 mM tetraborate buffer (pH 9.2) was added to the standard solution and the interstitial fluid microdialysates (Section 5.2.2), extraction with 400 μL of ethyl acetate was carried out

twice, and the organic layer was analyzed for EETs. The aqueous fraction was loaded onto a C_{18} cartridge pre-conditioned with 2 mL of methanol followed by 4 mL of water. Nitrite, which is not retained on the cartridge, was collected by elution from the C_{18} with 800 µL of water and then adenosine was collected by elution with 1 mL of 20% ACN.

5.2.4 EET analysis by HPLC/fluorescence

The ethyl acetate fraction containing EETs was evaporated to dryness under a stream of nitrogen and reconstituted with 136 µL of anhydrous ACN to which was added 5 µL of 10 µM tridecanoic acid as an internal standard (IS) to correct for derivatization and fluorescence detection (104). Derivatization of the carboxylate groups was performed by the method of Yue *et al.* (104) with minor modifications. Briefly, 4 µL of diisopropylethylamine and 10 µL of NeOTF (4 mg/mL) was added to the EET extract and incubated for 30 min at 4°C in the dark in a dessicooler. The reaction mixture was evaporated under nitrogen, reconstituted in 40 µL of ACN, and 10 µL was injected onto a Eclipse C_{18} XDS column (150x4.6-mm; 5 µm) connected to a HPLC (Agilent 1100) equipped with a fluorescence detector (HP 1046A) set at excitation and emission wavelengths of 260 and 396 nm, respectively, with a gain of 9. The sample was eluted at a flow rate of 1.0 mL/min with a gradient of 50-65% B for 10 min, 65 to 100% B for 20 min, and 100% B for 20 min. Mobile phases A and B consisted of 0.5% formic acid in water and ACN, respectively.

5.2.5 Nitrite analysis by HPLC/fluorescence

The nitrite extracted from the C_{18} cartridge (800 µL) was mixed with 20 µL of 360 µM DAN in 0.62 N HCl to form 2,3-naphthotriazole (NAT), a highly fluorescent compound (105, 106). After 15 min incubation at room temperature in the dark, 10 µL of 2.8 N NaOH was added to quench the reaction. The mixture was evaporated to dryness on a Savant Speed Vac (Model SC110) at 43°C and reconstituted with 35 µL of water, 10 µL of 0.62 N HCl and 5 µL of 2.8 M NaOH containing 100 µM MGCM as internal standard to correct for fluctuations in the fluorescence detector or sample volume. NAT analysis was carried out on the HPLC/fluorescence system described above using excitation and emission wavelengths of 376 and 415 nm, respectively, and a gain of 12. A 15-µL aliquot was injected onto the Eclipse C_{18} XDB column (150x4.6-mm; 5 µm) and eluted at a flow rate of 1 mL/min with a gradient of 20-70% B in 10 min, 70 to 90% B in 5 min, and 90% B for 2 min. Mobile phase A consisted of 15 mM ammonium acetate (pH 6.8) with 30% (v/v) MeOH, and mobile phase B consisted of 100% MeOH.

5.2.6 Adenosine analysis by HPLC/MS/MS

The eluate containing adenosine was evaporated to dryness on the Speed Vac at room temperature and reconstituted in 35 µL of mobile phase with 10 µL of 20 µM 2-chloroadenosine as IS to correct for MS/MS detection fluctuations. Adenosine in a 10-µL aliquot was separated on an ODS Hypersil column (100x4.6mm; 5µm) at a flow rate of 1.5 mL/min. The mobile phase consisted of 20 mM ammonium acetate (pH 6.0) with 5.0% (v/v) ACN and the eluate was monitored by UV (260 nm) and ESI-MS/MS on a Waters Quattro Micro mass spectrometer operating in positive-ion mode. Adenosine and

the IS were detected and quantitated in the multiple reaction monitoring (MRM) mode (adenosine, m/z 268 → 136; 2-chloroadenosine m/z 302 → 170) with capillary, cone, and collision voltages of 3.5 kV, 22 V, and 25 V, respectively. The Z-spray ESI source and desolvation temperatures were 120°C and 350°C, respectively.

5.2.7 Method validation

The artificial interstitial fluid was spiked with each standard to establish the accuracy and precision of the analysis. The LOD is reported as the lowest analyte concentration giving a signal-to-noise ratio > 3 in the artificial interstitial fluid. Precision is expressed as the relative standard deviation (%RSD) of the measured values. Intra-day precision and accuracy were determined using a solution of 2.5 μM nitrite, 2.5 μM adenosine and 0.5 μM 11,12-EET, and 0.5 μM 14,15-EET, and analyzing three replicates on the same day. Inter-day variability was determined by analyzing the same solution on three consecutive days.

5.2.8 Sample collection by microdialysis

Five healthy and physically active young males participated in the study, which was approved by the Ethical Committee of Copenhagen (KF 11-140/03) and conformed to the Declaration of Helsinki. All subjects gave their informed consent to participate. The mean age was 24 years (range 22–28 years), height 183 cm (range 170–190 cm) and weight 76 kg (range 70–100 kg). The participants were all involved in different sporting activities, had no previous history of cardiorespiratory disease or muscle injury nor took any form of medication for over 2 months prior to the experiment. The subjects were

asked not to participate in any kind of heavy exercise during the week before the experiment. After anaesthetizing the skin with 1% lidocaine (0.1 mL), a microdialysis fiber was inserted into the mid-portion of the vastus lateralis of the quadricep muscle group. The dialysis probe consisted of a 4-cm semipermeable dialysis membrane (20 kDa cut-off) attached at both ends to hollow nylon tubes (CMA/Microdialysis, Stockholm, Sweden). The probes (Figure 5.1) were perfused (inflow) at a rate of 5 μL/min with Ringer's acetate solution (pH 5.6) containing 0.5 mM lactate and 3 mM glucose. The dialysate (outflow) was collected at rest and during 15 min of exercise at 25 and 40 Watts (W) intensity. Each exercise period was separated by a 45-min recovery period. The dialysate samples 1 to 100 μL were collected in capped microvials (CMA/Microdialysis, Stockholm, Sweden) and immediately frozen at -80°C until analysis. The microdialysis volumes obtained from skeletal muscle tissue during rest and exercise differed by < 5% from the expected values based on inflow rates.

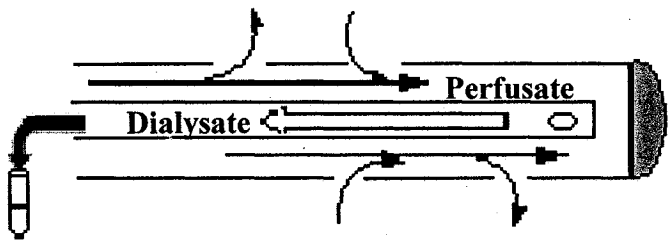

Figure 5.1. Schematic diagram of microdialysis. This method was used here for the collection of interstitial fluid from muscle tissue (for more details: http://www.microdialysis.se/www/md_pic_int.htm).

5.2.9 Exercise study

All experiments were performed in the morning and the microdialysis probe was inserted as described above. The subjects rested in a supine posture for 90 min to ensure a

time delay between fiber insertion and sampling. A period of ≥ 100 min in the resting state was previously found (33) to be sufficient to minimize any tissue response to the insertion trauma. Following this rest period, the subjects were moved to a seated upright position in a custom-built ergometer (Figure 5.2), that is routinely used for dynamic knee extension exercises (107). Subjects then performed dynamic extension from 90° of knee flexion to 170° of knee extension at 25 W for 15 min at a cadence matched to a metronome set to 60 contractions per min, with passive recoil of the leg to the starting position. After a 45-min recovery period, the same exercise was repeated at 40 W for 15 min.

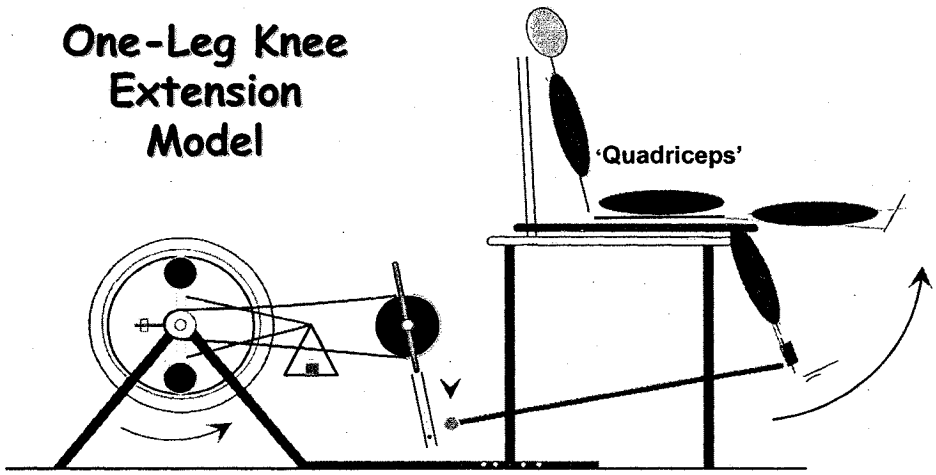

Figure 5.2. Schematic of the exercise device for performing dynamic knee extension exercises. This device isolates the use of the quadricep femoris muscles from other muscle groups (adapted from (107)).

5.3 Results and Discussion

5.3.1 Extraction optimization

Liquid-liquid extraction is a rapid method for the separation of complex chemical mixtures. Due to the large difference in polarity of the three analytes of interest, liquid-liquid extraction was selected as a starting point. Non polar EETs are highly soluble in organic solvents, and following evaluation of different solvents, the best recovery and separation of the fatty acids from adenosine and nitrite was obtained with ethyl acetate. The influence of varying pH was also examined (Figure 5.3) to minimize the co-extraction with EETs of nitrite or adenosine. Only 25% nitrite was retained in the aqueous fraction at pH 5.0, which was due to the partial loss of nitrite via its conversion to NO gas under acidic conditions (eq 5.1) (108, 109). Nitrite is essentially fully ionized ($pK_a = 3.4$) at pH 7.0 and 9.2, and is retained in the aqueous fraction (Figure 5.3).

$$3NO_2^- + 3H^+ \rightarrow 3HNO_2 \rightarrow HNO_3 + 2\,NO_{(g)} + H_2O \qquad (5.1)$$

The extraction efficiencies of adenosine and EETs were similar at the three pHs investigated. At the optimal pH of 9.2, the aqueous fraction contained 99% of the adenosine and 90% of the nitrite, whereas 93% of 11,12-EET and 84% of 14,15-EET were present in the organic fraction. Nitrite and adenosine were present together in the aqueous fraction following liquid-liquid extraction with all the organic solvents tested. Thus, SPE, in which the solution is passed through a solid phase such as C_{18} on silica, was used to separate these analytes. Nitrite was not retained on the C_{18} cartridge due to its

ionic nature and was ~100% recovered using water as the eluent. Adenosine was retained on the cartridge and required 20% ACN for elution. After liquid-liquid extraction and SPE, 93% of the adenosine was recovered, which is an excellent recovery for a two-step procedure.

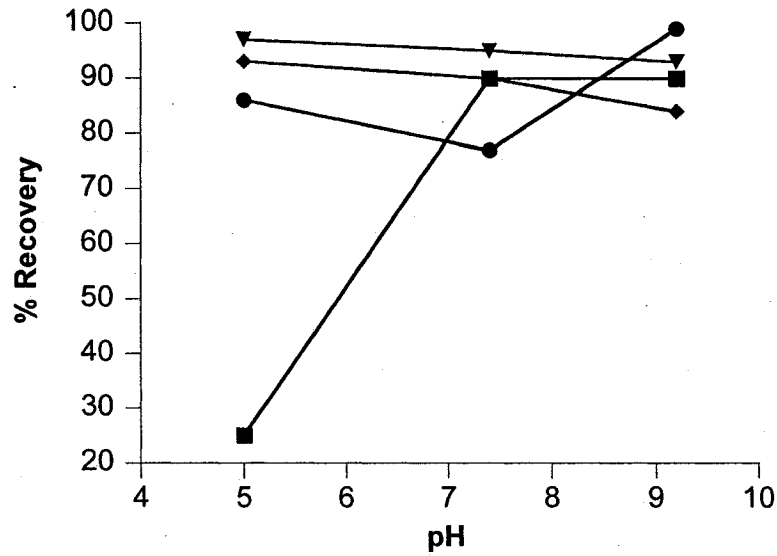

Figure 5.3. Percent analyte recovery from the aqueous (−■− nitrite, −●− adenosine) and organic (−♦ 14,15-EET, −▼− 11,12-EET) fractions during liquid-liquid extraction at pH 5.0, 7.4, and 9.2. Ethyl acetate (800 µL) was added to 100 µL of a solution containing 2.5 µM nitrite, 2.5 µM adenosine, 0.5 µM 11,12-EET, and 0.5 µM 14,15-EET in water (pH 5.0), 100 mM phosphate buffer (pH7.4), and 100 mM borate buffer (pH 9.2). Analyte recovery was determined by calculating the ratios of peak areas for each analyte before and after liquid-liquid extraction after correcting for dilution.

5.3.2 EET analysis in the artificial samples

After extraction by ethyl acetate, 11,12-EET and 14,15-EET were analyzed by HPLC/fluorescence. This method is used by many laboratories for the determination of EETs at low concentration in biological samples and cell cultures (42, 104, 110). To our knowledge, very few groups have detected EETs in human samples (111, 112) and no measurements in interstitial fluids have been reported. The extraction, separation, and

detection steps were optimized for sensitivity. A typical chromatogram of the standards (Figure 5.4.A) demonstrates that the two EETs were separated using an ACN gradient. The retention time was 27.5 min for 11,12-EET and 26.8 min for 14,15-EET with no apparent interference peaks. Excellent linearity was observed for plots of peak area versus EET concentration over the range 10—500 nM ($R^2 > 0.997$; data not shown), and the LOD for both compounds was 10 nM, which is similar to the LOD found in the literature (42, 104, 110). The complete accuracy and precision values of the assays are summarized in Table 5.1; for 11,12-EET, the intra-day and inter-day precision values are 1.64% and 2.75%, and the accuracy values are 92.6% and 90.6%, respectively. For 14,15-EET, the intra-day and inter-day precision values are 0.98% and 5.08%, and the accuracy values are 83.8% and 89.4%, respectively. These results indicate that the method is precise and accurate for both EETs.

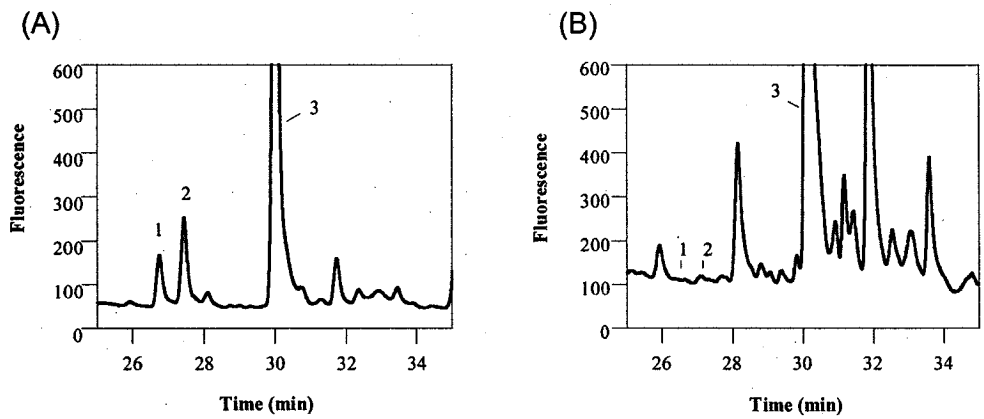

Figure 5.4. EET analysis by HPLC/fluorescence. (A) Chromatogram of 0.25 μM EET standard in artificial interstitial fluid with 1.25 μM tridecanoic acid as IS. (B) Chromatogram of interstitial fluid from subject #1 during exercise at 40 W with 1.25 μM tridecanoic acid as IS. Peak 1: 14,15-EET; peak 2: 11,12-EET; peak 3: tridecanoic acid (IS). The HPLC and derivatization methods are described in the Materials and Methods section.

5.3.3 Nitrite analysis in the artificial samples

Endogenous NO formation by endothelial NOS is measured via the determination of its oxidation product, nitrite (109). Following SPE, nitrite was reacted with DAN to form highly fluorescent NAT that was analyzed by HPLC/fluorescence (105, 106). Figure 5.5.A shows a typical HPLC chromatogram of a nitrite standard where NAT appears at 6.8 min without any interference. The nitrite calibration curve based on peak areas was linear over the range 15 nM—5 μM ($R^2 > 0.99$; data not shown) with a LOD of 5 nM at a signal-to-noise ratio of 3 and a gain setting of 12 on the fluorescence detector. This LOD is better that the 10 nM found in the literature (105, 106). Inter-day and intra-day reproducibility was determined using artificial interstitial fluid spiked with 2.5 μM nitrite. The intra-day and inter-day accuracy values are 103.4% and 99.5%, and the precision values are 10% and 7.92%, respectively.

Reported nitrite concentrations in human fluids vary considerably from undetectable to micromolar (109, 113). The spread in values can be attributed in part to differences in sample preparation, to problems inherent to the analytical procedure used, and to interferences. The major interferences are nitrite scavenging by protein, and contamination of the water and equipment. The lower reproducibility found for nitrite compared to the other analytes in this study (RSD values, Table 5.1) is attributed to the presence of trace nitrite in the Milli Q water, and on the glassware, plasticware, and pipette tips. These interferences make high reproducibility hard to achieve (106, 114), but purification of the Milli Q water on a strong anion-exchange column decreased the LOD and improved the reproducibility. Also, the microdialysis technique can help to overcome

the protein scavenging problem in the microdialysates since a 20-kDa cut-off membrane was used.

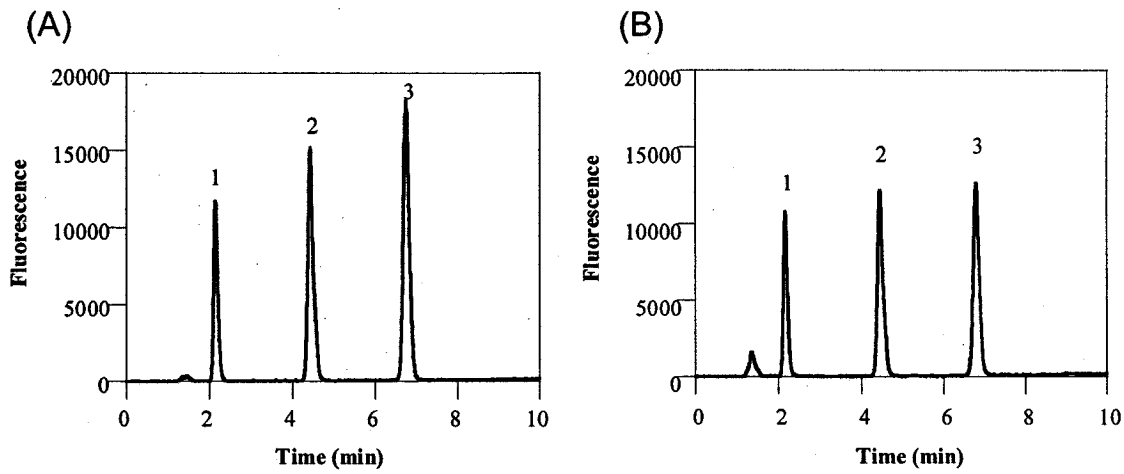

Figure 5.5. HPLC/fluorescence analysis of nitrite following its conversion to NAT. (A) Chromatogram of 2.5 μM nitrite standard in artificial interstitial fluid. (B) Nitrite present in interstitial fluid of subject #1 during exercise at 25 W. MGCM (10 μM) was added as IS to all samples. Peak 1: MGCM (IS); peak 2: DAN; peak 3: NAT. The HPLC and derivatization methods are described in the Materials and Methods section.

5.3.4 Adenosine analysis in artificial sample

Adenosine was eluted from the SPE column in the 20% ACN fraction and was detected by HPLC/UV/MS/MS. Many measurements by HPLC/UV of adenosine concentration in biological fluids have been reported (31, 115-118). It is difficult to quantify adenosine in interstitial fluid by its UV-absorption due to the presence of components with similar polarity and absorption spectra, but the selectivity of HPLC/MS/MS overcomes the interferences in human interstitial fluid samples. The adenosine MH^+ ion at m/z 268 ion fragments by loss of the sugar moiety giving the protonated adenine group at m/z 136 (Figure 5.6.A).

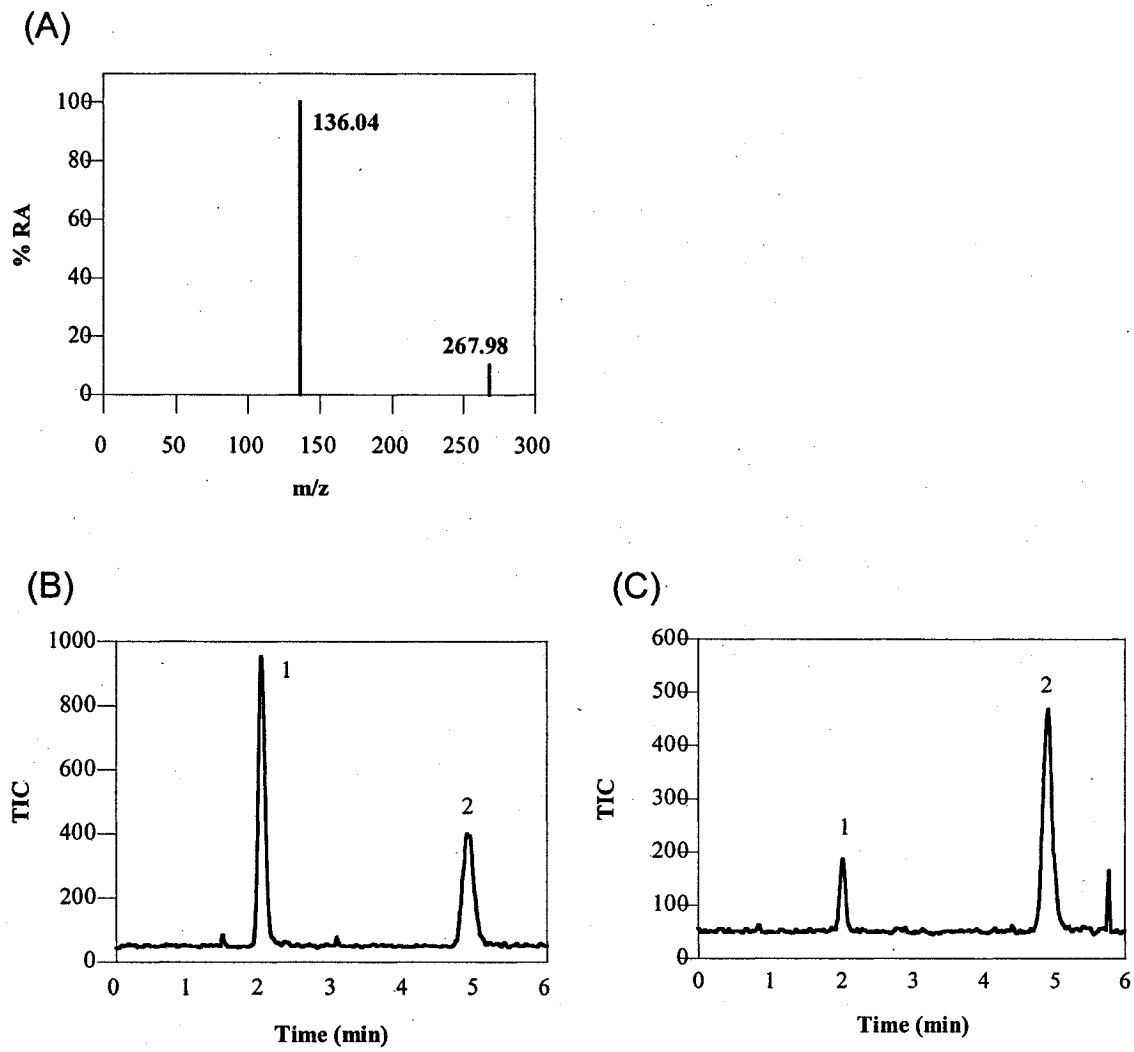

Figure 5.6. HPLC/ESI/MS/MS analysis of adenosine. (A) ESI MS/MS of 5 μM adenosine in water at a cone voltage of 22 V and collision energy of 20 eV. (B) HPLC/ESI/MS/MS elution profile of 2.5 μM adenosine standard in artificial interstitial fluid with 4.5 μM 2-chloroadenosine as IS. (C) Analysis of adenosine present in the interstitial fluid from subject #2 at rest with 4.5 μM 2-chloroadenosine as IS. Samples in (B) and (C) were analyzed in MRM mode using the transitions m/z 268 → 136 for adenosine, and m/z 302 → 170 for 2-chloroadenosine. Peak 1: adenosine; peak 2: 2-chloroadenosine (IS). The HPLC/MS/MS conditions are described in the Materials and Methods section.

The MRM chromatogram of a standard containing adenosine and 2-chloroadenosine is shown in Figure 5.6.B. The retention times of adenosine and 2-chloroadenosine on the ODS Hypersil column are 2.0 and 4.9 min, respectively, and the LOD of 10 nM is 20

times more sensitive than that reported for the commonly used HPLC/UV methods. Adenosine shows a linear calibration curve over a range of 10 nM—5 μM ($R^2 > 0.99$; data not shown), the intra-day and inter-day accuracy values are 92.6% and 92.3%, and the precision values expressed as RSDs are 1.58% and 3.63% (Table 5.1), respectively.

Table 5.1 Intra-day and inter-day reproducibility in the determination of adenosine, nitrite, and EETs in artificial interstitial fluid[a]

		Concentration spiked (μM)	Concentration measured (μM)	RSD (%)	Accuracy (%)
Intra-assay (n=3)	nitrite	2.50	2.58	10.0	103.4
	adenosine	2.50	2.32	1.58	92.6
	11,12-EET	0.50	0.46	1.64	92.6
	14,15-EET	0.50	0.42	0.98	83.8
Inter-assay (n=3)	nitrite	2.50	2.49	7.92	99.5
	adenosine	2.50	2.31	3.63	92.3
	11,12-EET	0.50	0.45	2.75	90.6
	14,15-EET	0.50	0.45	5.08	89.4

[a] Analytes were determined as described in Section 5.2.3 to 5.2.6. The composition of the artificial interstitial fluid is discussed in Section 5.2.2.

5.3.5 Human interstitial fluid analysis

The extraction and detection methods developed were applied in the analysis of human interstitial microdialysates collected during knee extension exercise as described in Section 5.2.8 and 5.2.9. EETs were not detected in the microdialysates at the different exercise intensity levels (Figure 5.4.B) indicating that the EET concentration in the dialysates from human interstitial fluid is <10 nM. The low sample volume obtained by microdialysis (100 to 1 μL) does not allow pre-concentration as with urine or plasma (1-

10 mL). Thus, more sensitive methods will have to be developed to detect EETs in interstitial fluid. Also, protein binding properties of EETs and %recovery of EETs by the microdialysis probe will have to be investigated to understand the very low concentration of EETs in the microdialysates of interstitial fluids. Concentrations of 79±16, 416±126, and 943±241 nM adenosine were detected in the samples from individuals performing 0 W (at rest), 25 W and 40 W exercise, respectively (Figure 5.6.C and 5.7.B).

The level of adenosine increases over 10-fold with exercise intensity, and the current results are consistent with those found in the literature (31-33). Significantly, individual differences expressed as RSD values vary from 20% to 30% compared to the intra-day RSD of only 1.58% for the adenosine standard (Table 5.1) Thus, the large variation in adenosine levels between the 5 subjects is likely physiological, and related to blood flow heterogeneity and differential vasodilator influences (119).

The levels of nitrite, the oxidation product of NO, also increase with exercise intensity. Concentrations of nitrite at 0 W, 25 W and 40 W exercise were 0.37±0.13, 2.17±0.32, and 4.67±0.30 μM, respectively (Figure 5.5.B and 5.7.A). Individual differences expressed as RSD values vary from 6% (40 W) to 35% (0 W) in comparison to the intra-day precision of 10% for the standard (Table 5.1), indicating that variation between the 5 subjects is only significant at rest. In summary, our data reveal that NO and adenosine are clearly involved in maintaining increased blood flow during exercise since their levels increase over 10-fold with exercise intensity.

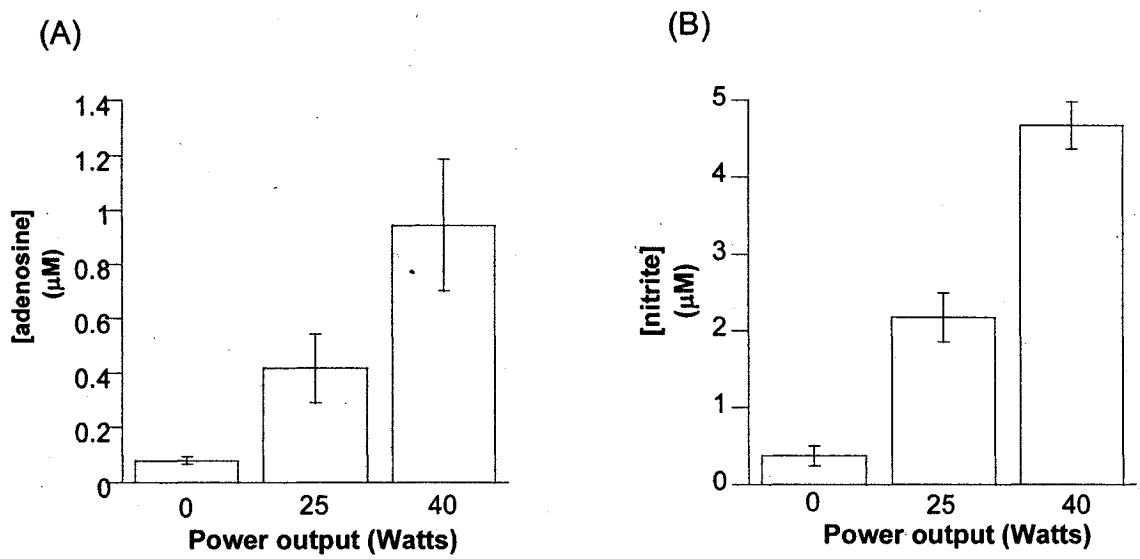

Figure 5.7. Concentrations of (A) adenosine and (B) nitrite in human skeletal muscle interstitial fluid. Microdialysates were collected from 5 subjects at 0 W, and while performing 25 and 40 W dynamic knee extensor exercises (see Figure 5.2).

5.4 Conclusions

A sequential extraction method to separately isolate nitrite, adenosine, and EETs with high recovery from human interstitial fluid was developed. Methods to quantitate each analyte with LODs comparable to or lower that those reported previously are described. The results reveal that the EET levels in human interstitial fluid dialysate are below the LOD (< 10 nM), and that nitrite and adenosine levels increase over 10-fold with exercise intensity. Further applications of this technology will allow us and others to establish interactions among the different mediators of tissue blood flow.

6.0 Effects of combined inhibition of nitric oxide and prostaglandin production on blood flow, nitrite, and adenosine levels in interstitial fluid microdialysates

6.1 Introduction

Possible mediators of muscle vasodilation during exercise such as adenosine, NO, PGs, and EETs are produced in the endothelium cell in response to shear stress. However their relative importance in regulating exercise-induced muscle blood flow in humans is not fully understood. Several studies have demonstrated that during exercise blood flow levels remain the same with the blockade of NO (32), PG (120), or EETs (121) alone. This suggests a redundancy mechanism where the compromised synthesis of one vasodilator can be compensated for by the enhanced formation of other vasodilators (122).

Redundant, synergistic interactions and compensatory responses amongst several vasodilator substances remain under investigation. Combined blockades of vasodilator formation may provide a better understanding of the interactions between various vasodilators and their mechanisms of action (30, 122). Previous studies have shown that combined blockade of NO and EETs formation (121) or blockade of NO and PG (99) considerably reduce muscle blood flow during exercise, suggesting interaction between these specific vasodilators (30, 99, 121). Measurement of multiple vasodilator concentrations in biological fluids during these experiments is critical in establishing their relative importance.

The purpose of this study was to determine the influence of the combined local inhibition of PG and NO formation on the levels of adenosine and nitrite in interstitial fluid as well as the pH of this fluid during exercise. The hypothesis was that the nitrite concentration would be reduced by NOS inhibition and that the adenosine concentration would increase to compensate. Inhibitors of PG and NO, indomethacin and *L*-NAME, were locally infused into the vastus lateralis muscle and the vasodilator concentrations were measured in the region of blockade and in two additional regions of the vastus lateralis muscle at 1 and 4 cm from the inhibition infusion site. In addition, muscle blood flow in the same regions was measured to investigate the heterogeneity of the blockage and the reciprocal changes in the vasodilator concentrations.

6.2 Materials and methods

6.2.1 Human experiments

6.2.1.1 Exercise study protocol

This protocol was performed at the Copenhagen Muscle Research Centre with the same volunteers as in Section 5.2.8. Briefly, following the Seldinger technique, a catheter was placed in the femoral vein of the right leg for infusion of indocyanine green (ICG). In addition, three 4-cm microdialysis catheters (CMA 60; 20 kDa molecular cut off, 0.5-mm outer diameter; CMA/Microdialysis, Stockholm, Sweden) were inserted in the vastus lateralis muscle, 1-cm depth and parallel to the muscle fibers. The catheters were placed at three different positions (1 and 4 cm away from the first catheter placed in the middle of the muscle). Probes for blood-flow measurements (Section 6.2.1.4) were positioned on

the surface of the leg directly over the microdialysis catheters. After placement of the microdialysis probes, the subjects rested for 2 h.

The subjects were seated in an upright position in a custom-built ergometer that is used routinely for dynamic knee-extension exercises (107). Blood-flow measurements and microdyalysate collections were performed at rest and during exercise, which consisted of knee flexion from 90° to 170° for 15 min at 25 W and followed by 15 min at 40 W at a cadence matched to a metronome set to 60 contractions per min (Figure 5.2). After 30-min recovery, *L*-NAME and indomethacin were infused for 60 min (Section 6.2.1.3). Blood flow was measured and microdialysates were collected under the same exercise levels as without the blockade.

6.2.1.2 Microdialysis

After inserting the catheters, they were constantly perfused at a rate of 2 μL/min with a Ringer's acetate solution (pH 5.6) containing 0.5 mmol/L lactate and 3 mmol/L glucose. The dialysate samples were collected in capped microvials (CMA/Microdialysis, Stockholm, Sweden) and immediately frozen at -80 °C until analysis. Neither during rest nor exercise did the microdialysis volumes obtained from skeletal muscle tissue differ by more than 5% from the expected values based on the pre-set infusion rates (123).

6.2.1.3 Local pharmacological inhibition of NO and PGs

Cyclooxygenase and NOS were inhibited using indomethacin and *L*-NAME, respectively. A saline solution containing 100 mg/mL of indomethacin and 10 mg/mL of *L*-NAME was infused into the vastus lateralis muscle via the middle microdialysis

catheter at a rate of 2 μL/min. The doses used for the infusion were based on previous experiments with whole body (systemic) infusion of the same substances (99), and pilot studies that ensured 100% local blockade of PG release in the infusion fiber, 90% in the fiber at 1 cm, and 50% in the fiber at 4 cm from the infusion probe.

6.2.1.4 Blood flow measurements

Muscle blood flow was measured using near-infrared spectroscopy (NIRS) and ICG as a tracer. The method has been previously validated for blood flow measurements during exercise in humans (123) and is described in previous report (119). Briefly, blood flow was measured using 2 NIRO 300 (Hamamatsu Photonics) spectrophotometers with dual-channel laser diodes during ICG injection. Light attenuation in muscle was measured at 6 Hz immediately after venous bolus injection of ICG. Changes in tissue ICG concentration were determined by measuring light attenuation at 775, 813, 850, and 913nm, and analyzed using an algorithm incorporating the modified Beer-Lambert Law (123).

6.2.2 Biochemical analysis

6.2.2.1 Materials

In addition to the materials listed in Section 5.2.1, indomethacin was obtained from Confortid, Alpharma (Denmark) and *L*-NAME was obtained from Clinalfa, Laufelfingen (Switzerland).

6.2.2.2 Extraction method and analysis of nitrite and adenosine

Nitrite and adenosine were extracted from interstitial fluid samples as described in Section 5.2.3. Nitrite levels were determined by HPLC/fluorescence and adenosine concentrations were quantitatively analyzed with reverse-phase HPLC/MS/MS. The methods used are described in Sections 5.2.5 and 5.2.6, respectively.

6.3 Results

6.3.1 Muscle blood flow without and with the blockade of NO and PG

The blood flow index (119) increased significantly from rest to exercise at 20 watts and further increased with exercise at 40 watts both without and with local inhibition of NO and PG production (Figure 6.1).

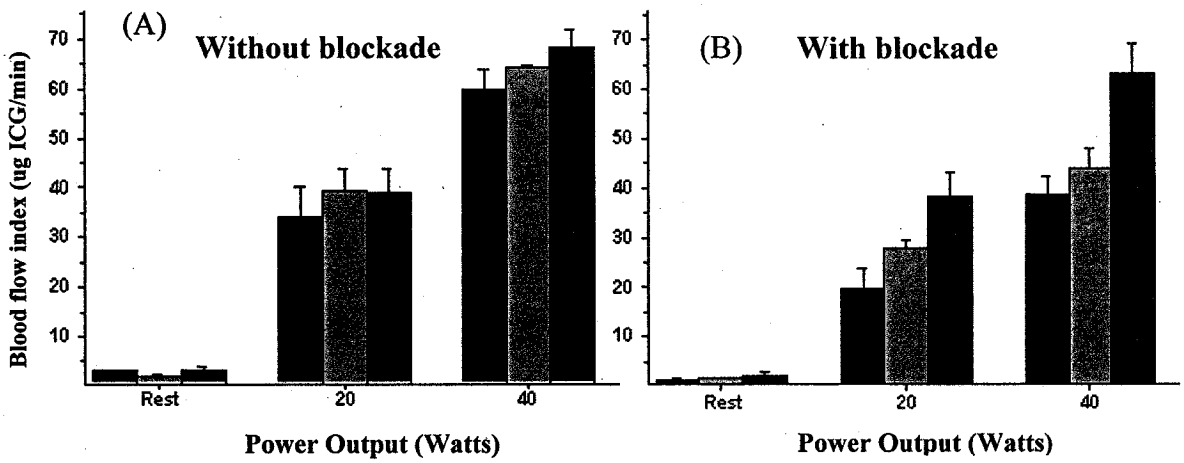

Figure 6.1. Microvascular blood flow at rest and during knee-extension exercise. The blood-flow index (μg ICG/min) was recorded at rest, 25 and 40 W of knee-extension at the infuse probe (▬), 1-cm probe (▬), and 4-cm probe (▬). (A) Without blockade, (B) with NO and PGs blockade.

The blood flow index was similar in the three muscle regions without blockade, but inhibition of NO and PGs decreased blood flow in the infusion region and to a lesser

extent in the region 1-cm from the infusion site. No change in blood flow was detected in the region 4-cm from the infusion site compare to the control (Figure 6.1) (119).

6.3.2 Nitrite and adenosine levels in interstitial fluid microdialysates

Adenosine levels at rest were similar both without and with the combined blockade at the different probe positions. The adenosine concentration increased with increasing exercise intensity but the level was similar without and with the combined blockade and at the different probe positions (Figure 6.2).

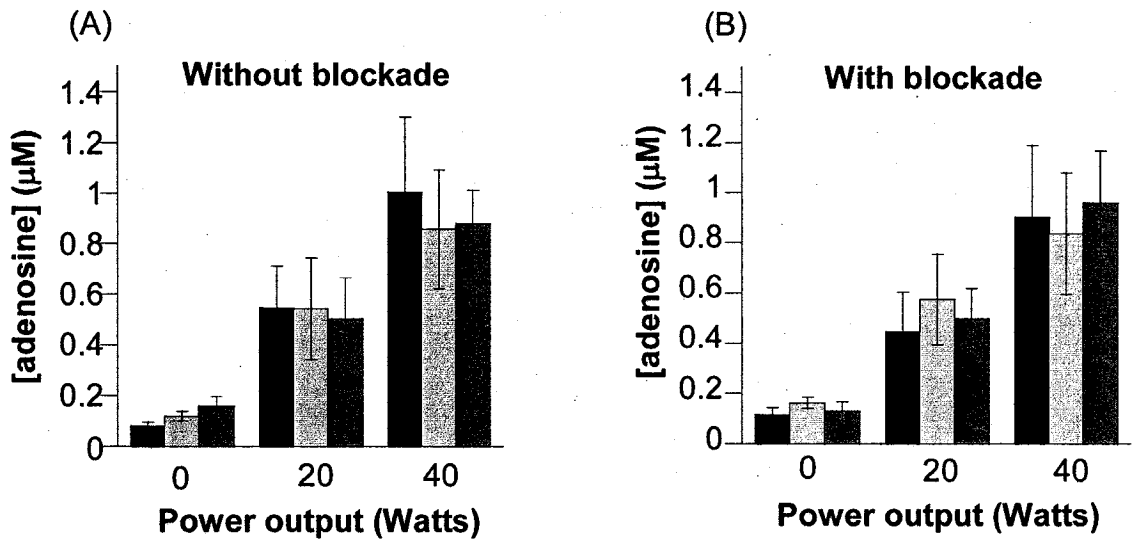

Figure 6.2. Adenosine levels (n=4) in human skeletal muscle interstitial fluid. Microdialysates were taken at 0 W, 25 and 40 W of dynamic knee extensor exercise at the infuse probe (▬), 1-cm probe (▬), and 4-cm probe (▬). (A) Without blockade (B) With NO and PG blockade.

The nitrite level increased with exercise intensity with and without the blockade (Figure 6.3). The nitrite concentration was smaller with blockade at the infuse probe and at the 1-cm probe at 20 and 40 W. However, the nitrite levels remained the same at rest and at 4-cm probe at each level of exercise with and without blockade. (Figure 6.3).

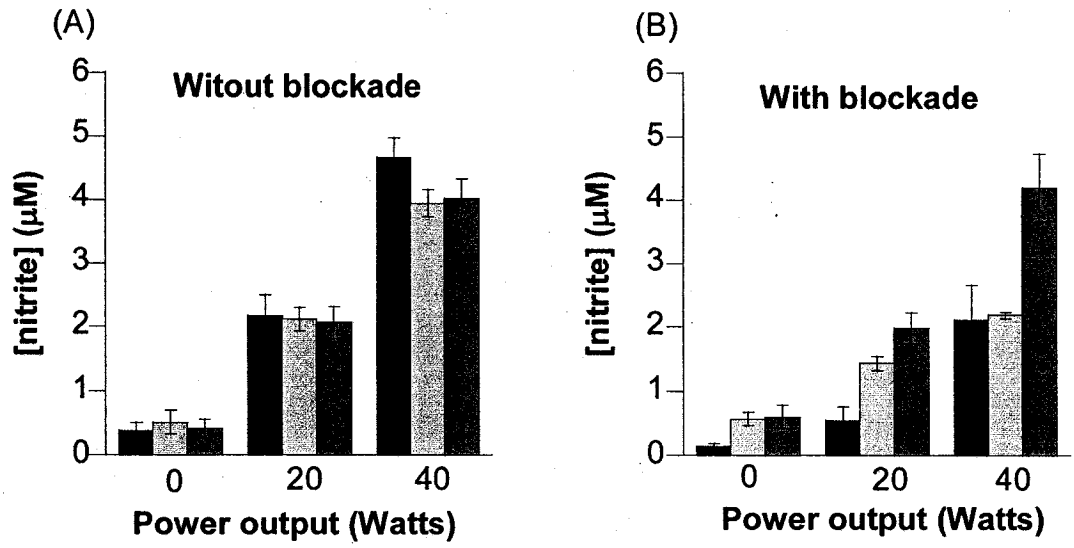

Figure 6.3. Nitrite levels (n=5) in human skeletal muscle interstitial fluid. Microdialysates were taken at rest, 25 and 40 W dynamic knee-extensor exercise at the infuse probe (▬), 1-cm probe (▬), and 4-cm probe (▬). (A) Without blockade. (B) with NO and PG blockade.

6.4 Discussion

In the present study we tested the association between local blood flow and local concentrations of two important vasodilators, nitrite and adenosine, in response to local blockade of NO and PG. Our hypothesis was that the nitrite concentration would be reduced and adenosine concentration compensatory increased in the muscle in response to blockade. The results partly support this hypothesis since the nitrite concentration was clearly reduced at the site of blockade (Figure 6.3). However, the results failed to support any redundancy between nitrite and adenosine in the control of local blood flow in human skeletal muscle since adenosine levels were largely insensitive to the blockade (Figure 6.2).

The increase in nitrite and adenosine levels in interstitial fluid as well as in blood flow with increased of exercise level support the previous demonstration that NO and adenosine are involved in exercise-induced muscle blood flow (12, 30, 31, 33).

The combined local inhibition of NO and PG administered directly into the vastus latealis muscle elicited highly localized reduction in NO concentration during exercise (Figure 6.2) that correlates with the microvascular blood-flow measurements (Figure 6.1) (119). However, the adenosine concentration is not affected by the localized blockade because it remained homogenous between the three probe regions (Figure 6.3).

The nitrite levels and blood flow follow the same pattern with and without the combined blockade of NO and PG production. The decreased blood flow and nitrite levels observed during blockade at rest and during exercise are attributed to inhibition of NO formation. Partial blockade was observed because the nitrite concentration was not totally abolished, which is consistent with the report of 67% NOS activity observed during infusion of *L*-NAME (124).

The insensitivity of adenosine levels to the blockade could arise for two reasons. First, adenosine is not involved in a redundancy mechanism, such that when NO and PG formation is blocked, adenosine does not compensate for the diminution in these vasodilators. Second, previous studies have demonstrated that adenosine-induced vasodilation in humans is mediated by endothelial release of NO (125), which facilitates adenosine production via the activation of 5'-nucleotidase (125, 126). Hence, similar level of adenosine in the control and during blockade may be due to two opposing mechanisms: the lowering of adenosine concentrations due to NOS inhibition and their

augmentation due to a compensatory response, resulting in similar adenosine levels with and without the blockade.

7.0 General conclusions and suggestions for further study

7.1 Chapters 2, 3 and 4

In Chapters 2, 3 and 4, we have determined that the reaction rate and final products formed in the reaction of nitrite with Hb are similar in concentrated and dilute Hb solutions. We demonstrated that the reaction of oxyHb with nitrite was similar in the presence and absence of CuZnSOD, in contrast to the reaction of GSNO with oxyHb where CuZnSOD plays an important role (48, 49). We have confirmed that nitrosylHb is formed in the reaction of deoxyHb with nitrite. Following oxygenation, HbSNO is formed only at low, but physiologically relevant, nitrite to heme ratios (1:400). The HbSNO yield in nitrite/deoxyHb incubations is lower than in NO/deoxyHb incubations (28) due to the slow rate of nitrite reduction by deoxyHb compared to the fast reaction of NO with deoxyHb. The metHb formed in nitrite/deoxyHb incubations can bind nitrite and decrease the HbSNO yield. Also, we have demonstrated that the HbSNO yield is lower in presence of hydrogen peroxide (and probably other ROS) whereas the presence of antioxidant enzymes in the deoxyHb/nitrite incubation promotes NO transfer from heme to Cysβ93. We have shown that NO transfer not only requires that Hb undergo its T→R allosteric transition but that oxygen be present, presumably as an oxidant.

7.2 Chapters 5 and 6

We have developed methodologies combining liquid-liquid and solid-phase extraction that allow sequential isolation of nitrite, adenosine and EETs from standard mixtures and from biological samples. HPLC/fluorescence methods were optimized to analyze nitrite and EETs with good sensitivity. A HPLC/UV/MS/MS method was

developed to detect adenosine with good sensitivity and selectivity. The methodology was applied to the analysis of nitrite, adenosine and EETs in artificial interstitial fluid and from human samples to determine interactions among different mediators of tissue blood flow. Adenosine and nitrite were quantified in the human interstitial fluid samples but EETs were not detected. We found that nitrite and adenosine levels increased with exercise intensity confirming that NO and adenosine are involved in exercise-induced increases in muscle blood flow. NO and PG blockage attenuated nitrite levels relative to the controls. This correlates with the reported partial inhibition of NOS activity by *L*-NAME. Also, we found that adenosine levels do not change with NO and PG blockade, which suggests that the adenosine level is not altered by a redundancy mechanism. Alternatively, adenosine decreased on NOS inhibition but was increased by an unknown redundancy mechanism, which resulted in no net change.

7.3 Suggestions for future work

(1) With regard to heme ligation, previous research (127) has shown that the quaternary structure of human nitrosylHb can be switched from the R to the T state by the potent allosteric effector, 2,3-diphosphoglycerate (2,3-DPG). The effects of this allosteric effector on the reaction of nitrite with deoxyHb and on HbSNO yields are of interest and should be elucidated.

(2) In RBCs, the fraction of oxyHb can drop from 85% to 33% in a few minutes so the utilization of different forms of Hb *in vitro* would be more representative of *in vivo* conditions. Thus, products formed from the reactions of nitrite with oxyHb, deoxyHb and metHb in different proportions should to be investigated.

(3) The mechanism of NO transfer proposed in Chapter 4 involves the production of superoxide. The confirmation of superoxide production and the effect of its addition (as a superoxide salt) on the HbSNO yield should be investigated. A detection method for superoxide using a trap such as hydroethidium has to be developed (128-131).

(4) GSH is present at 10 mM level in RBCs. The effect of GSH on the HbSNO yields should be investigated to determine if intermolecular NO transfer from the heme to GSH competes with the intramolecular NO transfer from the heme to Cysβ93 of Hb.

(5) The detection of EETs in human interstitial fluid dialysates was not possible using the HPLC/fluorescence and HPLC/MS/MS methods developed here. A more sensitive method should be tested to detect EETs in human interstitial fluid. ELISA kits are very sensitive and can be used to measure dihydroepoxyeicosatrienoic acids (DHETs) with EETs levels at pg/ml (132). The effect of protein binding on EETs recovery in the microdialysate should be investigated.

(6) To establish if adenosine acts as a compensatory vasodilator during exercise, adenosine concentrations in interstitial fluid following single blockade of PG and EETs, or triple blockade of NOS, PG, and EET should be measured using the methodology developed here.

8.0 References

1. Saltin B, Radegran G, Koskolou MD, Roach RC. *Skeletal muscle blood flow in humans and its regulation during exercise.* Acta Physiol Scand **1998;** 162: 421-36.

2. Buehler PW, Alayash AI. *Redox biology of blood revisited: the role of red blood cells in maintaining circulatory reductive capacity.* Antioxid Redox Signal **2005;** 7: 1755-60.

3. Crawford JH, Isbell TS, Huang Z, Shiva S, Chacko BK, Schechter AN, Darley-Usmar VM, Kerby JD, Lang JD, Jr., Kraus D, Ho C, Gladwin MT, Patel RP. *Hypoxia, red blood cells, and nitrite regulate NO-dependent hypoxic vasodilation.* Blood **2006;** 107: 566-74.

4. Gladwin MT. *Hemoglobin as a nitrite reductase regulating red cell-dependent hypoxic vasodilation.* Am J Respir Cell Mol Biol **2005;** 32: 363-6.

5. Gladwin MT, Crawford JH, Patel RP. *The biochemistry of nitric oxide, nitrite, and hemoglobin: role in blood flow regulation.* Free Radic. Biol. Med. **2004;** 36: 707-17.

6. Nelson D, Cox MM. *Lehninger Principles of Biochemistry*: **2000**; Worth Publishers, New York; Chapter 7: 210-220.

7. Singel DJ, Stamler JS. *Chemical physiology of blood flow regulation by red blood cells: the role of nitric oxide and S-nitrosohemoglobin.* Annu. Rev. Physiol. **2005;** 67: 99-145.

8. Hakim TS, Sugimori K, Camporesi EM, Anderson G. *Half-life of nitric oxide in aqueous solutions with and without haemoglobin.* Physiol Meas **1996;** 17: 267-77.

9. Gladwin MT, Schechter AN, Kim-Shapiro DB, Patel RP, Hogg N, Shiva S, Cannon RO, 3rd, Kelm M, Wink DA, Espey MG, Oldfield EH, Pluta RM, Freeman BA, Lancaster JR, Jr., Feelisch M, Lundberg JO. *The emerging biology of the nitrite anion.* Nat Chem Biol **2005;** 1: 308-14.

10. Smith CC, Stanyer L, Betteridge DJ. *Evaluation of methods for the extraction of nitrite and nitrate in biological fluids employing high-performance anion-exchange liquid chromatography for their determination.* J Chromatogr B Analyt Technol Biomed Life Sci **2002;** 779: 201-9.

11. Tsikas D, Rossa S, Sandmann J, Frolich JC. *High-performance liquid chromatographic analysis of nitrite and nitrate in human plasma as S-nitroso-N-acetylcysteine with ultraviolet absorbance detection.* J Chromatogr B Biomed Sci Appl **1999;** 724: 199-201.

12. Cosby K, Partovi KS, Crawford JH, Patel RP, Reiter CD, Martyr S, Yang BK, Waclawiw MA, Zalos G, Xu X, Huang KT, Shields H, Kim-Shapiro DB, Schechter AN, Cannon RO, 3rd, Gladwin MT. *Nitrite reduction to nitric oxide by deoxyhemoglobin vasodilates the human circulation.* Nat. Med. **2003;** 9: 1498-505.

13. Dejam A, Hunter CJ, Pelletier MM, Hsu LL, Machado RF, Shiva S, Power GG, Kelm M, Gladwin MT, Schechter AN. *Erythrocytes are the major intravascular storage sites of nitrite in human blood.* Blood **2005;** 106: 734-9.

14. Dejam A, Hunter CJ, Schechter AN, Gladwin MT. *Emerging role of nitrite in human biology*. Blood Cells Mol Dis **2004;** 32: 423-9.

15. Gladwin MT, Schechter AN. *NO contest: nitrite versus S-nitroso-hemoglobin.* Circ Res **2004;** 94: 851-5.

16. Bortle WH. *Kirk-Othmer Encyclopepia of Chemical Technology*: Sodium Nitrite **2001**; John Wiley and Sons, Inc.,

17. Bjorne HH, Petersson J, Phillipson M, Weitzberg E, Holm L, Lundberg JO. *Nitrite in saliva increases gastric mucosal blood flow and mucus thickness*. J Clin Invest **2004;** 113: 106-14.

18. Bryan NS, Fernandez BO, Bauer SM, Garcia-Saura MF, Milsom AB, Rassaf T, Maloney RE, Bharti A, Rodriguez J, Feelisch M. *Nitrite is a signaling molecule and regulator of gene expression in mammalian tissues*. Nat Chem Biol **2005;** 1: 290-7.

19. Benjamin N, O'Driscoll F, Dougall H, Duncan C, Smith L, Golden M, McKenzie H. *Stomach NO synthesis*. Nature **1994;** 368: 502.

20. McKnight GM, Smith LM, Drummond RS, Duncan CW, Golden M, Benjamin N. *Chemical synthesis of nitric oxide in the stomach from dietary nitrate in humans.* Gut **1997;** 40: 211-4.

21. Pique JM, Whittle BJ, Esplugues JV. *The vasodilator role of endogenous nitric oxide in the rat gastric microcirculation.* Eur J Pharmacol **1989;** 174: 293-6.

22. Li H, Samouilov A, Liu X, Zweier JL. *Characterization of the magnitude and kinetics of xanthine oxidase-catalyzed nitrite reduction. Evaluation of its role in nitric oxide generation in anoxic tissues*. J Biol Chem **2001;** 276: 24482-9.

23. Godber BL, Doel JJ, Sapkota GP, Blake DR, Stevens CR, Eisenthal R, Harrison R. *Reduction of nitrite to nitric oxide catalyzed by xanthine oxidoreductase.* J Biol Chem **2000;** 275: 7757-63.

24. Webb A, Bond R, McLean P, Uppal R, Benjamin N, Ahluwalia A. *Reduction of nitrite to nitric oxide during ischemia protects against myocardial ischemia-reperfusion damage.* Proc Natl Acad Sci U S A **2004;** 101: 13683-8.

25. Gamgee A. *Researches on the Blood. On the Action of Nitrites on Blood.* Philosophical Transactions of the Royal Society of London **1868;** 158: 589-625.

26. Meier R. *Methemoglobin formation. VII. Nitrite.* Archiv fuer Experimentelle Pathologie und Pharmakologie **1926;** 110: 241-264.

27. Wanat A, Gdula-Argasinska J, Rutkowska-Zbik D, Witko M, Stochel G, van Eldik R. *Nitrite binding to metmyoglobin and methemoglobin in comparison to nitric oxide binding.* J. Biol. Inorg. Chem. **2002;** 7: 165-76.

28. Gow AJ, Stamler JS. *Reactions between nitric oxide and haemoglobin under physiological conditions.* Nature **1998;** 391: 169-73.

29. http://en.wikipedia.org/wiki/Endothelium

30. Boushel R. *Metabolic control of muscle blood flow during exercise in humans.* Can J Appl Physiol **2003;** 28: 754-73.

31. Hellsten Y, Maclean D, Radegran G, Saltin B, Bangsbo J. *Adenosine concentrations in the interstitium of resting and contracting human skeletal muscle.* Circulation **1998;** 98: 6-8.

32. Frandsen U, Bangsbo J, Langberg H, Saltin B, Hellsten Y. *Inhibition of nitric oxide synthesis by systemic N(G)-monomethyl-L-arginine administration in*

humans: effects on interstitial adenosine, prostacyclin and potassium concentrations in resting and contracting skeletal muscle. J Vasc Res **2000;** 37: 297-302.

33. Langberg H, Bjorn C, Boushel R, Hellsten Y, Kjaer M. *Exercise-induced increase in interstitial bradykinin and adenosine concentrations in skeletal muscle and peritendinous tissue in humans.* J Physiol **2002;** 542: 977-83.

34. Vos IH, Joles JA, Rabelink TJ. *The role of nitric oxide in renal transplantation.* Semin Nephrol **2004;** 24: 379-88.

35. Mariotto S, Menegazzi M, Suzuki H. *Biochemical aspects of nitric oxide.* Curr Pharm Des **2004;** 10: 1627-45.

36. Xu WM, Liu LZ. *Nitric oxide: from a mysterious labile factor to the molecule of the Nobel Prize. Recent progress in nitric oxide research.* Cell Res **1998;** 8: 251-8.

37. Ferlito S. *Physiological, metabolic, neuroendocrine and pharmacological regulation of nitric oxide in humans.* Minerva Cardioangiol **2000;** 48: 169-76.

38. http://www.cvphysiology.com/

39. Zhu Y, Schieber EB, McGiff JC, Balazy M. *Identification of arachidonate P-450 metabolites in human platelet phospholipids.* Hypertension **1995;** 25: 854-9.

40. Spector AA, Norris AW. *Action of epoxyeicosatrienoic acids (EETs) on cellular function.* Am J Physiol Cell Physiol **2006;** In Press:

41. Larsen BT, Gutterman DD, Hatoum OA. *Emerging role of epoxyeicosatrienoic acids in coronary vascular function.* Eur J Clin Invest **2006;** 36: 293-300.

42. Maier KG, Henderson L, Narayanan J, Alonso-Galicia M, Falck JR, Roman RJ. *Fluorescent HPLC assay for 20-HETE and other P-450 metabolites of arachidonic acid.* Am J Physiol Heart Circ Physiol **2000;** 279: H863-71.

43. Boushel R, Langberg H, Risum N, Kjaer M. *Regulation of blood flow by prostaglandins.* Curr Vasc Pharmacol **2004;** 2: 191-7.

44. Bennett A. *Prostaglandins: their release, biological effects and relationships to pain and inflammation.* Cephalalgia **1986;** 6 Suppl 4: 17-20.

45. Doyle MP, Pickering RA, DeWeert TM, Hoekstra JW, Pater D. *Kinetics and mechanism of the oxidation of human deoxyhemoglobin by nitrites.* J. Biol. Chem. **1981;** 256: 12393-8.

46. Rodkey FL. *A mechanism for the conversion of oxyhemoglobin to methemoglobin by nitrite.* Clin Chem **1976;** 22: 1986-90.

47. Antonini E, Brunori M. *Hemoglobin and myoglobin in their reactions with ligands*: **1971**; North-Holland, Amterdam; 276.

48. Romeo AA, Capobianco JA, English AM. *Superoxide dismutase targets NO from GSNO to Cysbeta93 of oxyhemoglobin in concentrated but not dilute solutions of the protein.* J. Am. Chem. Soc. **2003;** 125: 14370-8.

49. Romeo AA, Capobianco JA, English AM. *Heme nitrosylation of deoxyhemoglobin by s-nitrosoglutathione requires copper.* J. Biol. Chem. **2002;** 277: 24135-41.

50. Huang KT, Keszler A, Patel N, Patel RP, Gladwin MT, Kim-Shapiro DB, Hogg N. *The reaction between nitrite and deoxyhemoglobin. Reassessment of reaction kinetics and stoichiometry.* J. Biol. Chem. **2005;** 280: 31126-31.

51. Herold S, Rock G. *Reactions of deoxy-, oxy-, and methemoglobin with nitrogen monoxide. Mechanistic studies of the S-nitrosothiol formation under different mixing conditions*. J. Biol. Chem. **2003;** 278: 6623-34.

52. Nagababu E, Ramasamy S, Abernethy DR, Rifkind JM. *Active nitric oxide produced in the red cell under hypoxic conditions by deoxyhemoglobin-mediated nitrite reduction.* J. Biol. Chem. **2003;** 278: 46349-56.

53. Angelo M, Singel DJ, Stamler JS. *An S-nitrosothiol (SNO) synthase function of hemoglobin that utilizes nitrite as a substrate.* Proc. Natl. Acad. Sci. U S A **2006;** 103: 8366-71.

54. Sharma VS, Ranney HM. *The dissociation of NO from nitrosylhemoglobin.* J. Biol. Chem. **1978;** 253: 6467-72.

55. Kim-Shapiro DB, Gladwin MT, Patel RP, Hogg N. *The reaction between nitrite and hemoglobin: the role of nitrite in hemoglobin-mediated hypoxic vasodilation.* J Inorg Biochem **2005;** 99: 237-46.

56. Marklund S, Marklund G. *Involvement of the superoxide anion radical in the autoxidation of pyrogallol and a convenient assay for superoxide dismutase.* Eur J Biochem **1974;** 47: 469-74.

57. Sampath V, Zhao XJ, Caughey WS. *Characterization of interactions of nitric oxide with human hemoglobin A by infrared spectroscopy.* Biochem Biophys Res Commun **1994;** 198: 281-7.

58. Everse J, Vandegriff KD, Winslow RM. *Hemoglobins Part C: Biophysical Methods*: Methods in Enzymology **1994**; Academic Press, California; 232: 247-266.

59. Herold S, Rock G. *Mechanistic studies of the oxygen-mediated oxidation of nitrosylhemoglobin.* Biochemistry **2005;** 44: 6223-31.

60. Taketa F, Antholine WE, Chen JY. *Chain nonequivalence in binding of nitric oxide to hemoglobin.* J Biol Chem **1978;** 253: 5448-51.

61. Huang Z, Shiva S, Kim-Shapiro DB, Patel RP, Ringwood LA, Irby CE, Huang KT, Ho C, Hogg N, Schechter AN, Gladwin MT. *Enzymatic function of hemoglobin as a nitrite reductase that produces NO under allosteric control.* J. Clin. Invest. **2005;** 115: 2099-2107.

62. Stamler JS, Jia L, Eu JP, McMahon TJ, Demchenko IT, Bonaventura J, Gernert K, Piantadosi CA. *Blood flow regulation by S-nitrosohemoglobin in the physiological oxygen gradient.* Science **1997;** 276: 2034-2037.

63. Pawloski JR, Hess DT, Stamler JS. *Export by red blood cells of nitric oxide bioactivity.* Nature **2001;** 409: 622-6.

64. Cosby K, Partovi KS, Crawford JH, Patel RP, Reiter CD, Martyr S, Yang BK, Waclawiw MA, Zalos G, Xu X, Huang KT, Shields H, Kim-Shapiro DB, Schechter AN, Cannon RO, 3rd, Gladwin MT. *Nitrite reduction to nitric oxide by deoxyhemoglobin vasodilates the human circulation.* Nat Med **2003;** 9: 1498-505.

65. Ford PC, Lorkovic IM. *Mechanistic aspects of the reactions of nitric oxide with transition-metal complexes.* Chem. Rev. **2002;** 102: 993-1018.

66. Luchsinger BP, Rich EN, Yan Y, Williams EM, Stamler JS, Singel DJ. *Assessments of the chemistry and vasodilatory activity of nitrite with hemoglobin under physiologically relevant conditions.* J. Inorg. Biochem. **2005;** 99: 912-21.

67. Jia L, Bonaventura C, Bonaventura J, Stamler JS. *S-nitrosohaemoglobin: a dynamic activity of blood involved in vascular control.* Nature **1996;** 380: 221-6.

68. McMahon TJ, Moon RE, Luschinger BP, Carraway MS, Stone AE, Stolp BW, Gow AJ, Pawloski JR, Watke P, Singel DJ, Piantadosi CA, Stamler JS. *Nitric oxide in the human respiratory cycle.* Nat. Med. **2002;** 8: 711-7.

69. Doctor A, Platt R, Sheram ML, Eischeid A, McMahon T, Maxey T, Doherty J, Axelrod M, Kline J, Gurka M, Gow A, Gaston B. *Hemoglobin conformation couples erythrocyte S-nitrosothiol content to O2 gradients.* Proc. Natl. Acad. Sci. U S A **2005;** 102: 5709-14.

70. Zhang Y, Hogg N. *S-nitrosohemoglobin: a biochemical perspective.* Free Radic. Biol. Med. **2004;** 36: 947-58.

71. Saville B. *A scheme for the Colorimetric Determination of Microgram Amounts of Thiols.* **1958;** 83: 670-672.

72. Romeo AA, Capobianco JA, English AM. *Superoxide dismutase targets NO from GSNO to Cysbeta93 of oxyhemoglobin in concentrated but not dilute solutions of the protein.* J Am Chem Soc **2003;** 125: 14370-8.

73. Jourd'heuil D, Gray L, Grisham MB. *S-nitrosothiol formation in blood of lipopolysaccharide-treated rats.* Biochem. Biophys. Res. Commun. **2000;** 273: 22-6.

74. Goldman RK, Vlessis AA, Trunkey DD. *Nitrosothiol quantification in human plasma.* Anal. Biochem. **1998;** 259: 98-103.

75. Cook JA, Kim SY, Teague D, Krishna MC, Pacelli R, Mitchell JB, Vodovotz Y, Nims RW, Christodoulou D, Miles AM, Grisham MB, Wink DA. *Convenient*

colorimetric and fluorometric assays for S-nitrosothiols. Anal. Biochem. **1996;** 238: 150-8.

76. Park JK, Kostka P. *Fluorometric detection of biological S-nitrosothiols*. Anal. Biochem. **1997;** 249: 61-6.

77. Gladwin MT, Shelhamer JH, Schechter AN, Pease-Fye ME, Waclawiw MA, Panza JA, Ognibene FP, Cannon RO, 3rd. *Role of circulating nitrite and S-nitrosohemoglobin in the regulation of regional blood flow in humans*. Proc. Natl. Acad. Sci. U S A **2000;** 97: 11482-7.

78. Gladwin MT, Ognibene FP, Pannell LK, Nichols JS, Pease-Fye ME, Shelhamer JH, Schechter AN. *Relative role of heme nitrosylation and beta-cysteine 93 nitrosation in the transport and metabolism of nitric oxide by hemoglobin in the human circulation*. Proc. Natl. Acad. Sci. U S A **2000;** 97: 9943-8.

79. Granger DL, Taintor RR, Boockvar KS, Hibbs JB, Jr. *Measurement of nitrate and nitrite in biological samples using nitrate reductase and Griess reaction*. Methods Enzymol. **1996;** 268: 142-51.

80. Ferranti P, Malorni A, Mamone G, Sannolo N, Marino G. *Characterisation of S-nitrosohaemoglobin by mass spectrometry*. FEBS Lett. **1997;** 400: 19-24.

81. Mamone G, Sannolo N, Malorni A, Ferranti P. *In vitro formation of S-nitrosohemoglobin in red cells by inducible nitric oxide synthase*. FEBS Lett. **1999;** 462: 241-5.

82. Boffi A, Ilari A, Spagnuolo C, Chiancone E. *Unusual affinity of cyanide for ferrous and ferric Scapharca inaequivalvis homodimeric hemoglobin. Equilibria and kinetics of the reaction*. Biochemistry **1996;** 35: 8068-74.

83. Brunori M, Antonini G, Castagnola M, Bellelli A. *Cooperative cyanide dissociation from ferrous hemoglobin.* J. Biol. Chem. **1992;** 267: 2258-63.

84. Landry DW, Oliver JA. *The pathogenesis of vasodilatory shock.* N. Engl. J. Med. **2001;** 345: 588-95.

85. Gow AJ, Luchsinger BP, Pawloski JR, Singel DJ, Stamler JS. *The oxyhemoglobin reaction of nitric oxide.* Proc. Natl. Acad. Sci. U S A **1999;** 96: 9027-32.

86. Cassoly R, Gibson Q. *Conformation, co-operativity and ligand binding in human hemoglobin.* J. Mol. Biol. **1975;** 91: 301-13.

87. Walder JA, Chatterjee R, Steck TL, Low PS, Musso GF, Kaiser ET, Rogers PH, Arnone A. *The interaction of hemoglobin with the cytoplasmic domain of band 3 of the human erythrocyte membrane.* J. Biol. Chem. **1984;** 259: 10238-46.

88. McMahon TJ, Exton Stone A, Bonaventura J, Singel DJ, Solomon Stamler J. *Functional coupling of oxygen binding and vasoactivity in S-nitrosohemoglobin.* J Biol Chem **2000;** 275: 16738-45.

89. Pawloski JR, Hess DT, Stamler JS. *Impaired vasodilation by red blood cells in sickle cell disease.* Proc Natl Acad Sci U S A **2005;** 102: 2531-6.

90. Lundberg JO, Weitzberg E. *NO generation from nitrite and its role in vascular control.* Arterioscler Thromb Vasc Biol **2005;** 25: 915-22.

91. Gow A, Buerk, D., Ischiropoulos H. *A novel reaction mechanism for the formation of S-nitrosothiol in vivo.* Journal of Biological chemistry **1997;** 272: 2841-2845.

92. Stamler JS, Singel DJ, Loscalzo J. *Biochemistry of nitric oxide and its redox-activated forms.* Science **1992;** 258: 1898-902.

93. Sharma VS, Schmidt MR, Ranney HM. *Dissociation of CO from carboxyhemoglobin.* J Biol Chem **1976;** 251: 4267-72.

94. Winterbourn CC, McGrath BM, Carrell RW. *Reactions involving superoxide and normal and unstable haemoglobins.* Biochem J **1976;** 155: 493-502.

95. http://www.callutheran.edu/Academic_Programs/Departments/BioDev/omm/catalase/frames/cattx.htm

96. D'Agnillo F, Alayash AI. *Interactions of hemoglobin with hydrogen peroxide alters thiol levels and course of endothelial cell death.* Am J Physiol Heart Circ Physiol **2000;** 279: H1880-9.

97. Nagababu E, Ramasamy S, Rifkind JM. *S-Nitrosohemoglobin: A mechanism for its formation in conjunction with nitrite reduction by deoxyhemoglobin.* Nitric Oxide **2006;** 15: 20-29.

98. Edwards DG, Schofield RS, Lennon SL, Pierce GL, Nichols WW, Braith RW. *Effect of exercise training on endothelial function in men with coronary artery disease.* Am J Cardiol **2004;** 93: 617-20.

99. Boushel R, Langberg H, Gemmer C, Olesen J, Crameri R, Scheede C, Sander M, Kjaer M. *Combined inhibition of nitric oxide and prostaglandins reduces human skeletal muscle blood flow during exercise.* J Physiol **2002;** 543: 691-8.

100. Fichtlscherer S, Dimmeler S, Breuer S, Busse R, Zeiher AM, Fleming I. *Inhibition of cytochrome P450 2C9 improves endothelium-dependent, nitric oxide-mediated vasodilatation in patients with coronary artery disease.* Circulation **2004;** 109: 178-83.

101. Bito L, Davson H, Levin E, Murray M, Snider N. *The concentrations of free amino acids and other electrolytes in cerebrospinal fluid, in vivo dialysate of brain, and blood plasma of the dog.* J Neurochem **1966;** 13: 1057-67.

102. Stopford W, Turner J, Cappellini D, Brock T. *Bioaccessibility testing of cobalt compounds.* J Environ Monit **2003;** 5: 675-80.

103. Moss OR. *Simulants of lung interstitial fluid.* Health Phys **1979;** 36: 447-8.

104. Yue H, Strauss KI, Borenstein MR, Barbe MF, Rossi LJ, Jansen SA. *Determination of bioactive eicosanoids in brain tissue by a sensitive reversed-phase liquid chromatographic method with fluorescence detection.* J Chromatogr B Analyt Technol Biomed Life Sci **2004;** 803: 267-77.

105. Gharavi N, El-Kadi AO. *Measurement of nitric oxide in murine Hepatoma Hepa1c1c7 cells by reversed phase HPLC with fluorescence detection.* J Pharm Pharm Sci **2003;** 6: 302-7.

106. Li H, Meininger CJ, Wu G. *Rapid determination of nitrite by reversed-phase high-performance liquid chromatography with fluorescence detection.* J Chromatogr B Biomed Sci Appl **2000;** 746: 199-207.

107. Andersen P, Saltin B. *Maximal perfusion of skeletal muscle in man.* J Physiol **1985;** 366: 233-49.

108. Takenaka N, Suzue T, Ohira K, Morikawa T, Bandow H, Maeda Y. *Natural denitrification in drying process of dew.* Environ. Sci. Technol. **1999;** 33: 1444-1447.

109. Jobgen WS, Jobgen SC, Li H, Meininger CJ, Wu G. *Analysis of nitrite and nitrate in biological samples using high-performance liquid chromatography.* J Chromatogr B Analyt Technol Biomed Life Sci **2006;** in Press:

110. Nithipatikom K, Pratt PF, Campbell WB. *Determination of EETs using microbore liquid chromatography with fluorescence detection.* Am J Physiol Heart Circ Physiol **2000;** 279: H857-62.

111. Kiss L, Schutte H, Mayer K, Grimm H, Padberg W, Seeger W, Grimminger F. *Synthesis of arachidonic acid-derived lipoxygenase and cytochrome P450 products in the intact human lung vasculature.* Am J Respir Crit Care Med **2000;** 161: 1917-23.

112. Catella F, Lawson JA, Fitzgerald DJ, FitzGerald GA. *Endogenous biosynthesis of arachidonic acid epoxides in humans: increased formation in pregnancy-induced hypertension.* Proc Natl Acad Sci U S A **1990;** 87: 5893-7.

113. Moorcroft MJ, Davis J, Compton RG. *Detection and determination of nitrate and nitrite: a review.* Talanta **2001;** 54: 785-803.

114. Makela S, Yazdanpanah M, Adatia I, Ellis G. *Disposable surgical gloves and Pasteur (Transfer) pipettes as potential sources of contamination in nitrite and nitrate assays.* Clin Chem **1997;** 43: 2418-20.

115. Tullson PC, Whitlock DM, Terjung RL. *Adenine nucleotide degradation in slow-twitch red muscle.* Am J Physiol **1990;** 258: C258-65.

116. Tullson PC, Terjung RL. *Adenine nucleotide degradation in striated muscle.* Int J Sports Med **1990;** 11 Suppl 2: S47-55.

117. Wynants J, Van Belle H. *Single-run high-performance liquid chromatography of nucleotides, nucleosides, and major purine bases and its application to different tissue extracts*. Anal Biochem **1985;** 144: 258-66.

118. Hellsten Y, Frandsen U. *Adenosine formation in contracting primary rat skeletal muscle cells and endothelial cells in culture*. J Physiol **1997;** 504 (Pt 3): 695-704.

119. Kalliokoski KK, Langberg H, Ryberg AK, Scheede-Bergdahl C, Doessing S, Kjaer A, Kjaer M, Boushel R. *Nitric oxide and prostaglandins influence local skeletal muscle blood flow during exercise in humans: coupling between local substrate uptake and blood flow*. Am J Physiol Regul Integr Comp Physiol **2006;** 291: R803-9.

120. Shoemaker JK, Naylor HL, Pozeg ZI, Hughson RL. *Failure of prostaglandins to modulate the time course of blood flow during dynamic forearm exercise in humans*. J Appl Physiol **1996;** 81: 1516-21.

121. Hillig T, Krustrup P, Fleming I, Osada T, Saltin B, Hellsten Y. *Cytochrome P450 2C9 plays an important role in the regulation of exercise-induced skeletal muscle blood flow and oxygen uptake in humans*. J Physiol **2003;** 546: 307-14.

122. Boushel R, Kjaer M. *Redundancy reflects versatility of blood flow regulation mechanisms*. J Physiol **2004;** 557: 346.

123. Boushel R, Langberg H, Olesen J, Nowak M, Simonsen L, Bulow J, Kjaer M. *Regional blood flow during exercise in humans measured by near-infrared spectroscopy and indocyanine green*. J Appl Physiol **2000;** 89: 1868-78.

124. Frandsenn U, Bangsbo J, Sander M, Hoffner L, Betak A, Saltin B, Hellsten Y. *Exercise-induced hyperaemia and leg oxygen uptake are not altered during*

effective inhibition of nitric oxide synthase with N(G)-nitro-L-arginine methyl ester in humans. J Physiol **2001;** 531: 257-64.

125. Smits P, Williams SB, Lipson DE, Banitt P, Rongen GA, Creager MA. *Endothelial release of nitric oxide contributes to the vasodilator effect of adenosine in humans*. Circulation **1995;** 92: 2135-41.

126. Obata T, Sato T, Yamanaka Y, Arita M. *NO and cGMP facilitate adenosine production in rat hearts via activation of ecto-5'-nucleotidase*. Pflugers Arch **1998;** 436: 984-90.

127. Deem S, Gladwin MT, Berg JT, Kerr ME, Swenson ER. *Effects of S-nitrosation of hemoglobin on hypoxic pulmonary vasoconstriction and nitric oxide flux*. Am J Respir Crit Care Med **2001;** 163: 1164-70.

128. Fink B, Laude K, McCann L, Doughan A, Harrison DG, Dikalov S. *Detection of intracellular superoxide formation in endothelial cells and intact tissues using dihydroethidium and an HPLC-based assay*. Am J Physiol Cell Physiol **2004;** 287: C895-902.

129. Papapostolou I, Patsoukis N, Georgiou CD. *The fluorescence detection of superoxide radical using hydroethidine could be complicated by the presence of heme proteins*. Anal Biochem **2004;** 332: 290-8.

130. Zhao H, Joseph J, Fales HM, Sokoloski EA, Levine RL, Vasquez-Vivar J, Kalyanaraman B. *Detection and characterization of the product of hydroethidine and intracellular superoxide by HPLC and limitations of fluorescence*. Proc Natl Acad Sci U S A **2005;** 102: 5727-32.

131. Zhao H, Kalivendi S, Zhang H, Joseph J, Nithipatikom K, Vasquez-Vivar J, Kalyanaraman B. *Superoxide reacts with hydroethidine but forms a fluorescent product that is distinctly different from ethidium: potential implications in intracellular fluorescence detection of superoxide.* Free Radic Biol Med **2003;** 34: 1359-68.

132. http://www.freepatentsonline.com/6440682.html